ELECTRICALLY ENERGIZED SHOCK TUBES

UNIVERSITY OF OKLAHOMA RESEARCH INSTITUTE
NORMAN, OKLAHOMA

ELECTRICALLY ENERGIZED SHOCK TUBES

RICHARD G. FOWLER,
UNIVERSITY OF OKLAHOMA
NORMAN, OKLAHOMA

1963

TECHNICAL REPORT NO. 19
ONR CONTRACT NONR 862(02)
PROJECT NR 061-087
UNIVERSITY OF OKLAHOMA
RESEARCH INSTITUTE
NORMAN, OKLAHOMA

A FINAL REPORT TO

THE U. S. OFFICE OF NAVAL RESEARCH

FLUID MECHANICS BRANCH

Project N9 onr 97700

PREFACE

The extent and duration of the project on fluid mechanics of plasmas at the University of Oklahoma demands that the work done and ideas gained be reviewed and recorded to prevent waste, if nothing more. Beginning as it did with an obscure physical phenomenon and passing to an engineering tool, many early ideas and statements need some final rectification, and many engineering results exist, neither of which will ever be reported unless this book is written.

Because of the increasing volume of activity of a similar sort in other laboratories, use will be made of such published results as are available to me to render the subject dealt with more complete than a simple report on our own project efforts would require. Since, however, the final report character of this document is paramount, our results will necessarily be allowed to "upstage" the many fine contributions of others, and I solicit the charity of anyone who feels that I have not credited his work with the importance it deserves in relation to our own work. Furthermore the treatment, dealing as it does with work which is still unfinished, is spotty and incomplete. For all these manifold defects I also apologize.

R. G. Fowler
University of Oklahoma
1962

TABLE OF CONTENTS

		Page
CHAPTER I	NATURE AND HISTORY OF ELECTRICAL DRIVEN SHOCK WAVES	1
CHAPTER II	EQUIPMENT AND DIAGNOSTIC TECHNIQUES	4
	2-1 General Remarks	4
	2-2 Apparatus for Flow Production	4
	2-3 Other Techniques for Plasma Flow Production	17
CHAPTER III	ELECTRICAL BEHAVIOR OF GASES IN THE DRIVER DISCHARGE	38
	3-1 Empirical Relations	38
	3-2 Theory of the Driver Discharge	39
	3-3 Energy Input Efficiencies	52
	3-4 Maxwell-Boltzman Averages of Gas Properties	52
	3-5 Non-Linear Situations	52
CHAPTER IV	ELECTRON DRIVEN PLASMA SHOCK WAVES	59
	4-1 Experimental Results - General Considerations	59
	4-2 Experimental Studies on the Delayed Wave	61
	4-3 Experimental Studies on the Prompt Shock Waves	67
	4-4 Electron and Gas Temperature Changes	69
	4-5 Theory of Electron Driven Shock Waves	73
	4-6 Theory of the Delayed Flow	81
	4-7 Blast Wave Theory	82
	4-8 Electron Driven Expansion of Planetary Nebulae	83
	4-9 Rarefaction Shocks	84
CHAPTER V	BREAKDOWN WAVES, PRECURSORS AND ELECTRON FLUID DYNAMICS	85
	5-1 Breakdown Waves	85
	5-2 Heat Conduction and Precursors	89
CHAPTER VI	RADIATION STUDIES	93
	6-1 General Observations	93
	6-2 Qualitative Spectral Observations	93

TABLE OF CONTENTS

		Page
	6-3 Half-Widths and Ion Concentrations	96
	6-4 Electron Recombination and the Radiation Law	101
	6-5 Opacity of Hydrogen Discharges	106
	6-6 Dissociative Recombination	106
CHAPTER VII	INTERACTIONS	111
	7-1 Zone to Zone Transitions of Waves	111
	7-2 Reflected Shocks	114
	7-3 Boundary Layer Effects	115
CHAPTER VIII	DIFFUSION, AND MAGNETIC INSULATION IN THE ELECTRICAL SHOCK TUBE	117
	8-1 Diffusion Cooling	117
	8-2 Magnetic Insulation	118
	8-3 Reduction of Effective Degrees of Freedom	121
	8-4 Experimental Studies of Diffusion	122
CHAPTER IX	IDEAL ELECTRICAL SHOCK TUBE DESIGN	126
	9-1 Design Problems	126
	9-2 Details of a Practical Segmented Shock Tube	126
	9-3 Design Considerations	128
	9-4 Experimental Behavior	133
CHAPTER X	ELECTRICAL PROPERTIES OF THE FLOWING PLASMA	135
	10-1 Experimental Observations on Conduction to Probes	135
	10-2 Concepts Involved in the Formulation of a Theory of Transient Conduction to Probes	138
	10-3 Critique	142
	10-4 Boundary Layer - Sheath Effects	143
	10-5 Electrostatic Probes and the Shock	144
CHAPTER XI	MISCELLANEOUS OBSERVATIONS	146
	11-1 MHD Studies	146
	11-2 Pinch Studies	148
	11-3 Plasma Flow Around Models	149
	11-4 Exploding Wires	150
	11-5 Electrode Driven Shocks	150
ACKNOWLEDGEMENT		151
BIBLIOGRAPHY		152
APPENDIX I	MOLECULAR AVERAGES	156
APPENDIX II	SHOCK AND CONTACT SURFACE VELOCITIES	161
APPENDIX III	BALMER CONTINUUM EMISSION DATA	166
APPENDIX IV	ENERGY REQUIREMENTS OF GASES AT 1 MM HG	169

ERRATTA

ERRATTA

Page

2 ... Paragraph 2 - line 3: Change "Chapter 2" to "Chapter 4".
Paragraph 3 - line 7: "Rayliegh" should be "Rayleigh".

5 ... Paragraph 3 - line 1 should read: "Numbers such as are given in Table I are not unique because the internal ...

13 ... Paragraph 3 - add sentence at the end of paragraph: "They are quite suitable for researches where efficiency is not a factor."
Paragraph 5 - line 7: "plate" should be "plane".

15 ... Figure 6: Abscissa is $\theta/2$.

17 ... Page is missing; see end of erratta section.

22 ... Paragraph 4 line 1: "for" should be changed to "with".

27 ... Paragraph 4 - line 1: Change the first sentence to read: "Thus, if V_λ ..."

29 ... Fig. 15. Capacitor is .005 μfd.

33 ... Fig. 18. Tube No. 5842 = 417A.

40 ... Fig. 21a: Change in Figure Caption: "No" to "N_o".
Fig. 21b: Change in Figure Caption: "No" to "N_o".

41 ... Fig. 21c: Change 10^5 at top of left column to 10^7.
Change in Figure Caption: "No" to "N_o".
Fig. 21d: Change in Figure Caption: "No" to "N_o".

43 ... Second Equation should read:

$$E = \frac{k\,T_e\,b}{e\,a}\left(e^{-\theta x} - 1\right), \text{ with } \theta^2 = \frac{4\pi e^2\,D_e\,a}{k\,T_e\,D_+}\,.$$

Third Equation should read:

$$\left(\frac{\partial E}{\partial x}\right)_0 = -\,4\pi e\,a = -\sqrt{\frac{4\pi k\,T_e\,D_e}{D_+\,a}}\;b.$$

Fifth Equation should read:

$$2\pi k\,D\sqrt{\frac{4\pi e^2\,D_+}{k\,T_e\,D_e}}\;n_e^{3/2}.$$

44 ... Fig. 22: "10^{12}" should be "10^{-12}": "σ" should be "σ_i".
Paragraph 2 - line 15: "sill" should be "still".
Second Equation should read:

$$\frac{4e\,(p\,D_+)}{(\sigma_i\,v_e\,N_o)}\left(\frac{\pi N_o \epsilon}{k\,T_+}\right)^{\frac{1}{2}}\left(\frac{\alpha}{p^{3/2}R}\right)^{\frac{1}{2}}$$

45 ... Fig. 23: Figure Curves should be labelled: "$T_+ = 300^\circ K$, $T_+ = 1000^\circ K$, $T_+ = 3000^\circ K$.

46 ... Fig. 24: Change "(T_p)transitions" to "(γp) transitional".
Change "α transitions" to "α transitional".

48 ... Seventh Equation should read:

$$i^2 = \frac{e^2 D_e}{k\,T_e}\left[(e\,V_i + 3/2\,k\,T_e)\overline{\sigma_i\,v_e}\,N + \frac{m^2}{M}\overline{\sigma_m\,v_e^3}\,N\right]$$

ERRATTA (continued)

Page

76 ... $\frac{\partial}{\partial t}\left[1/2\ MNV^2 + 3/2\ p + \alpha Ne\ V_i\right]$

$$+ \frac{\partial}{\partial x}\left[1/2\ MNV^3 + (3/2\ P + \alpha Ne\ V_i)\ V\right] = 0.$$

77 ... Third Equation: Change "$\alpha_2 N_2 eVi$" to "$\alpha_2 N_2 eV_i$".

78 ... First line "concluding" should be changed to "including".
Fourth Equation: Replace "α" with "β".

79 ... Paragraph 2 - line 2 and 3 should read: "but this seems an excellent assumption since the rarefaction is accompanied by a cooling which should make the response time to adjustment"...
Fourth line above Table VII: "$Z = (eV_i/MV^2) \ll 1/2$".

80 ... Second Equation should read:

$$\theta^{1/2} - \theta^{3/10}\ (\beta + 4)^{1/5} - \sqrt{\frac{3+\beta}{15}} = 0$$

81 ... Fig. 42: $\frac{V}{\alpha C}$ should be changed to $\frac{U_s}{y\ C_4}$.

Fig. 42 Caption: "C in Meters/sec" should be changed to "C_4 in Meters/sec".

82 ... Fig. 43 Caption:

$$K = \sqrt{\frac{(1+\alpha)k\ T_4}{M}}, \quad a_o = \sqrt{\frac{\gamma\ k\ T_1}{M}}.$$

Next to last equation should read:

$$R = \frac{2^{1/2}}{\pi^{1/4}}\left(\frac{\gamma+1}{2}\right)^{1/2}\left(\frac{W}{\rho_o}\right)^{1/4} t^{1/2}$$

Last Equation should read:

$$R = \left(\frac{5}{2}\right)^{2/5}\left(\frac{3}{4\pi}\right)^{1/5}\left(\frac{\gamma+1}{2}\right)^{2/5}\left(\frac{W}{\rho_o}\right)^{1/5} t^{2/5}$$

84 ... In the second equation change "P" to "p".
In the last equation change "P" to "p" and "N" to "n".
In the last line change "N" to "n" and "cm-1" to "cm-3".

87 ... The fifth equation should read:

$$m \propto N_1 V_1^3 = mnv^3 + 5nvkT_2 + 2 \propto N_1 eV_i V_1$$

Sixth equation: Change "T_e" to "T_2".
Eighth equation: Change "N" to "N_1".

89 ... Change "T_e" to "T_2" everywhere.
Addendum Note: The small amount of energy used by the wave is a second order effect. E_+ & E_- are maintained from outside.

91 ... Fig. 46 ordinate correction: Last number should be 10^4.

100 ... Fig. 49: Between -10 and 0 cm curves are for n and I; between 0 and 25 cm upper curves are for n^2 and I, lower curve is for n. All ordinates are arbitrary.

ERRATTA (continued)

Page

103 ... First Equation should read:

$$\vartheta_\lambda = \frac{e^4 h^2 V_i^2 n_+ n_e}{\pi c^2 m \lambda^2}\left(\frac{1}{6\pi mkT}\right)^{3/2} e^{-\frac{h\lambda}{ckT}} e^{\frac{e V_i}{4 kT}}$$

107 ... Fig. 52: Change labels to Ln I_o/I; $K_\nu/N_H^2 \times 10^{-42}$.
109 ... Lower paragraph - line 1: Change "complete" to "compete".
120 ... First Equation should read: "$D_{+\perp}$ = ".
124 ... Fig. 59 Caption: "Tube width 16.5 mm".
Fig. 60 Caption: "Tube width 50 mm".
127 ... Fig. 62: μ has been left out following all numbers.
133 ... Change the first equation to read:

$$\tau = \frac{2\ell_E}{U_s}$$

Change the second equation to read:

$$\frac{L}{R} > \frac{\ell_E}{U_s}$$

136 ... Paragraph 3 - line 6: Change "Sakuntale" to "Sakuntala".
Paragraph 3 - line 7: Change "pressure p" to "density ρ".
138 ... Paragraph 2 - line 3 should read: "suring the plasma resistance with probes (of copper) of"
139 ... Paragraph 2 - line 3: Change "deviation" to "duration".
Paragraph 2 - line 4: Delete square root sign around $2r/V_2$,
140 ... Equation 2: Change "n_o" to "n_+"..
141 ... Equation 5 should read:

$$\frac{1}{y}\frac{\partial\varphi}{\partial y} y\frac{\partial\varphi}{\partial y} + \frac{\partial^2\varphi}{\partial x^2} - \frac{\lambda}{2}|x|\left(\frac{V_2 B}{c} - \frac{\partial\varphi}{\partial x}\right) = 0.$$

Line following equation 5 should read: "If $\varphi = +\frac{V_2 B}{c} x + YX, \ldots$"
Equation 7 should read:

$$X'' - \frac{\lambda}{2}|x|X' - \mu^2 X = 0$$

Equation 8 should read:

$$R = \frac{k T}{2 D_+ \eta_+ e^2 n_+}\left(\frac{1}{2r} - \frac{\ell n 2}{\pi a}\right)$$

146 ... Fig. 71 Caption: Shocks without and with transverse field. Driver operated at 4860V and 5.5 mm Hg.
152 ... Bibliography: Ref. 1: Change Am. to Ann,
Ref. 2: Change Am. to Ann.
Ref. 3: Change Am. to Ann.
Ref. 7 Change Soo. to Soc.
Ref. 8: Change from page 26 (1944) to 236 (1946)

ERRATTA (continued)

Page

153 ... Bibliography: Ref. 56: Change M. L. Goldman to M. A. Goldman.

154 ... Bibliography: Ref. 66 should read: R. G. Fowler, G. W. Paxton, and H. G. Hughes, Phys. Fluids 4, 234 (1961).

Ref. 67: Change date from (1933) to(1958).

Ref. 105 should read: H. Hoffmann and O. Theimer, Ap. J. 127, 477 (1958).

APPENDIX 1: All curves are per electron per mm Hg.

Curves on p. 157 and 158 are wholly erroneous due to computer program error.

Curves on p. 159 for helium, hydrogen and methane require change of ordinates from 10^8 to 10^9, and 10^9 to 10^{10}.

a strongly fringing magnetic field produced by discharging capacitors in sequence through the sections of the solenoid lying just behind the slug. At a suitable injection speed the moving magnetic front seizes and propels the plasma at the characteristic speed of the line, driving a shock ahead of it if gas is present in the tube originally.

2-4 Test Equipment. Wave speed cameras have been the most useful devices in these studies, because they provide so much information in a single photograph that they make excellent survey instruments. Their essential difficulty is that being only one dimensional in space they are limited in scope of vision when applied to a shock wave with a wide front, and provide confused information when three dimensional motions are present in such a front. Coupled however with Kerr cell photographs, a fairly complete picture can be achieved.

The single space dimension is usually placed as nearly perpendicular as possible to the wave front to be observed, and is defined by a slit having this direction. The slit in some instances is at the face of the tube itself, in others is formed by imaging the tube on a slit.

One species of wave speed camera uses a plane rotating mirror, the image being formed by an entrance lens upon a circular film holder centered at the mirror. Preferably the axis of the mirror and film holder would coincide, but then the probability of a picture would be reduced to ½, so it is customary to use at least a two sided mirror, and a four sided mirror increases the chances of a favorable orientation still further, especially if there is enough light to illuminate two adjacent faces, and form comparison pictures. E. B. Turner has constructed a four-faced mirror on a polished 1" stellite cube, which can be rotated by an air turbine at sufficient speed to provide a writing rate of 4 mm/μsec on the image plane. This particular instrument has an effective aperture of F:13, and the flow under study is imaged on a built-in slit by an auxilliary lens.

A second species uses a concave mirror. Unlike the rotating plane mirror, which can either be operated synchronously or asynchronously with respect to the wave pattern to be photographed, the rotating concave mirror requires synchronization to form the image in the vicinity of its optic axis. Otherwise severe abberration results. A six-inch concave rotatable mirror of one meter focal length was chosen at the University of Oklahoma as the basis for construction of an F:8 high precision wave speed camera. An aberration-free focal area about 4 cm wide and centered about the optic axis was available as the mirror image swept across the film. Subsequent experience showed that a smaller mirror of the same F-number would have been more advantageous in some respects. To register pictures entirely in this area, a synchronized trigger circuit was constructed to initiate the spark discharge. Synchronization of the rotating mirror with the electrical discharge was done by creating a reference pulse from the mirror which

CHAPTER I

NATURE AND HISTORY OF ELECTRICALLY DRIVEN SHOCK WAVES

Acoustical effects have been immemorially associated with spark discharges in thunder and lightning. Scientifically, however, the earliest association was probable that of Toeppler, (1) who used (1850) the light of spark discharges to make visible their accompanying weak shock waves.

The investigation of spark discharges has been intensively carried on, yielding information on breakdown of the gas, and on the nature of the emitted radiation, temperatures and ion concentrations in the discharge, and the changes which occur in these quantities in time. If the breakdown of the dielectric be the phase of the discharge to which the term "spark" is restricted, then it is reasonable to say that a rather complete understanding of the spark is available. On the other hand, if the entire discharge is included in the term, much has remained obscure until the last decade. It is sometimes stated that the discharge after the disruption of the dielectric is simply to be regarded as an arc at high current. Our investigations have led us to the conclusion that this description is wrong when applied to the open spark; that the entire discharge has a unique character, and that a complete understanding of it cannot be achieved until the fluid flow processes present in the discharge have been considered.

The earliest recorded laboratory observation of the fluid flow processes which we now recognize as accompanying intense electrical discharges was made by Hertz (2) in 1878. In most subsequent discharge experiments, however, a closed system was characteristically employed, no avenue was available for fluid expansion, and hence no flow effects were observed.

Still, many studies of low pressure spark discharges have been made for an equally diverse number of reasons. The transient state of the discharge has long been recognized as an interval in which nature reveals the character of her processes more completely than at any other time. In 1835 Wheatstone determined with rotating mirror and induction coil that the luminosity in the spark moved as a front down the tube, traveling with a speed of upwards of 8×10^7 cm/sec. Von Zahn (3) could detect no Doppler shift in these fronts and concluded that there was no mass motion of the gas. J. J. Thomson (4) devised an ingenious rotating mirror method for measuring the time interval of passage of the luminosity between two points of the discharge tube, finding thus that it moved with one-third the speed of light and was independent of the nature of the gas and of the electrodes.

Beams (5) made improvements in the rotating mirror technique and demonstrated that the luminous fronts did indeed have velocities of the order observed by Thomson. He found that the fronts traveled from the free potential electrode to ground, regardless of the sign of the charge on the free electrode. He found that this speed was also independent of polarity, increased with decreasing pressure, and increased somewhat with increasing potential difference. Altering the composition of the tube wall made a definite change in the velocity. Further experiments (6) with a cathode ray oscillograph showed that some sort of electrical pulse was indeed propagated through the tube with speeds nearly identical with those of the luminous fronts. No evidence was obtained that the luminosity wave was cospatial with the potential wave. A reflected wave was observed which traveled at higher speed than the initial wave, probably because of the ionized gas through which it was returning.

This phenomenon has never been elucidated theoretically, may be related indirectly to the electron drive theory which will be described in Chapter 2, and certainly is the manifestation of an important process in the breakdown of the electric shock tube.

In 1944, Rayleigh (7) made the observation that the luminosity of an electrodeless discharge overflowed into side avenues out of the exciting field, and persisted as it flowed for times up to 10^{-5} second. Zanstra (8) 1946, suggested that recombination of outflowing ions produced in the discharge could account for the long duration of the supposed afterflow, but Lee (9) 1949, showed that the luminosity in the Rayliegh experiment was ejected in bursts, or fronts, whose space distribution could only be explained by assuming a continuing excitation of the gas during the expansion. Goldstein (10) 1948, and Compton (11) 1951, showed that the process could be observed in any pulsed discharge of sufficient energy, that it moved with speeds in the range of, but above, the acoustical speeds, and that it was subject to the reflections that would be expected of a wave motion. This first led us to the conclusion that shock wave motion was present, although the suggestion had been made in 1947 that the expansion of spark columns as observed by Craggs (12) at velocities more rapid than diffusion would permit might imply the presence of shock waves. An extensive investigation of the phenomenon was then undertaken with the support of the United States Office of Naval Research. It was found that the expansion of the excited gas during and after the discharge of electrical energy into the gas is in general completely analogous to the expansion of any compressed fluid upon the abrupt release of pressure.

Such an expansion comprises three main processes. First, a moving interface exists between the flowing gas originally external to the discharge, and the as yet undisturbed stationary gas also originally external to the discharge. This interface is known as a "shock wave" and moves with a speed many fold greater than the speed of sound in the stationary gas, and roughly 30% greater than the speed of the flowing gas behind the interface.

The second process is a moving interface between the flowing gas originally internal to the discharge and the flowing gas originally external to it. This interface is known as a "contact surface", and moves with the flow velocity of the gases, which is the same on either side of the interface. Pressure is also constant across this interface

The expanding gas originally internal to the discharge can be looked upon as a gaseous piston which drives the external gas ahead of it. The contact interface is the head of this piston. When viscous heat transfer effects are negligible, the speed of flow of the gas will be constant all the way from the shock interface, past the contact interface and up to the foot of the third process, the rarefaction wave This region is spoken of as a plateau.

The rarefaction wave is the region of pressure transition between the flowing gas originally interior to the discharge, and the as yet undisturbed, stationary gas orginally internal to the discharge. Normally it is a gradual transition region in the flow.

The rarefaction undergoes a complex motion. The velocity of the foot of the rarefaction is composed of a velocity equal to that which sound would have in the expanded, flowing, internal gas (directed inwardly, or away from the flow direction) combined vectorially with the outwardly directed flow velocity of the expanding internal gas. The motion of the head of the rarefaction wave is a motion at sound speed into the unexpanded, undisturbed internal gas directed away from the flow direction. At intermediate points the wave moves with an appropriate linear combination of the local sound velocity and flow velocity.

Deviations from this simple theory are naturally to be expected, and in fact are observed. They will be discussed in subsequent chapters. The most significant peculiarity is that there can be a phase, early in the flow, during which the electron pressure drives an otherwise very cold gas in a non-equilibrium flow.

The electric shock tube has proved to be a tool of value in preparing plasmas and studying them. By giving motion to the plasma it offers an extra degree of freedom for diagnosis. It possesses not just one, but two moving plasma regions (the shocked gas and the driver) of differing properties, and if it is desired the whole system can be brought to rest for further study by compression against an obstacle, while its state can be inferred by measurement of the various velocity parameters.

CHAPTER II

EQUIPMENT AND DIAGNOSTIC TECHNIQUES

2-1 General Remarks. The studies which have been made on electrically driven shock waves have been made in a variety of apparatus, and have employed a variety of techniques of observation for the significant parameters. Production of plasma flow has been achieved by impulsive Joulean heating; by continuous Joulean heating; by mechanical compression; and by Amperean forces in various configurations. Observations have depended on the composition and spatial-temporal configurations of the light produced; the pressures generated; the conductivities measurable: the emfs that can be induced; on the reflectivities, absorbabilities, and transmissivities of various radiations. Quantities which have been inferred from these observations with varying degrees of success are wave speeds. flow speeds, wave thicknesses, c_p/c_v; temperatures, pressures, densities; ion concentrations,electron concentrations; opacities; ionization, diffusion, and recombination coefficients.

2-2 Apparatus for Flow Production. Energy is necessary in large quantities, and quickly, to produce interesting flowing plasmas. High voltage capacitors, high current inductors. massive flywheels coupled to generators, compressed gases, or even high explosives can be used and have been used to supply the needed energy. Many of the conclusions of the research seem applicable to nuclear explosions if one wishes to regard nuclear material as outside the class of high explosives. The principal attention here will be devoted to the electrical generation of plasma flow.

Capacitor energy storage is the most widely used form. It involves selection of a suitable capacitor, switch, and method for coupling the energy into the gas. Suitability of the components is a systems problem, and varies still with the phenomenon which is under investigation. Achievement of an optimization of the electron drive phase of the flow, for example, demands that the electric field in the driven plasma be maintained as large as possible for as long as possible. Optimization of the thermal flow, on the other hand, requires that power be the adjusted and maximized variable. The way of achieving these conditions in turn varies with the mode of coupling. If made directly through metal electrodes, the capacitor potential is the most significant variable. If made via a time changing magnetic field, design for maximum rate of change of current is the aim. Finally the circuit chosen will influence in some degree the choice of switching, although low impedance and inductance are the usual requisites, and closure delay is the chief criterion.

Evaluated as a series network of capacitance, inductance and resistance, commercial capacitors display measured low frequency properties given in Table I. Considerable improvements have been made over the past ten years in capacitor design and are continuing.

TABLE I

Capacitor	Voltage+	Capacitance+	Inductance	Resistance
GE 14F9*	5KV	5×10^{-6} f	$.36 \times 10^{-6}$ h	.035Ω
West. 11176638*	6KV	1×10^{-6}	$.36 \times 10^{-6}$	.18
GE 14F63*	15KV	1×10^{-6}	$.32 \times 10^{-6}$	.12
GE 14F59*	25KV	1×10^{-6}	$.57 \times 10^{-6}$	.16
GE 26F681*	7.5KV	1×10^{-6}	$.35 \times 10^{-6}$	.26
GE 25-807-2-7*	3KV	12×10^{-6}	2.5×10^{-6}	.08
GE 14F3*	5KV	15×10^{-6}	1.4×10^{-6} h	.08
TOBE XN249B	8KV	40×10^{-6}	0.10×10^{-6} h	.035
Sprague P51111	4KV	100×10^{-6}	0.0375×10^{-6} h	.01
CD NRG204	20KV	15×10^{-6}	0.06×10^{-6} h	

* Manufactured before 1950.
\+ Nominal.

Design improvement is well shown by the fact that TOBE XN249B has been superceded by CD NRG303, for which the inductance has been reduced to 0.02×10^{-6} h.

Numbers such as given in Table I are not unique because internal structure of the capacitor is not the simple series circuit envisioned. The result is that the three constants are all frequency sensitive. Two capacitors were studied with this in mind. Data on them are given in Fig. 1.

The results showed that R/L is approximately constant, both decreasing as frequency increases, to a minimum at about 10^5 cps. Capacitance behaves similarly, dropping to about 75% of its DC value at this frequency. These findings suggested that the conductance patns to the various portions of the foil of the capacitor increased in impedance as the frequency increased, and reduced the effective capacitance.

Successful capacity measurements were made at low frequencies by resonation against an inductance which had in turn been measured against a standard mica capacitor. As the required amount of inductance decreased, so that the inductance of the capacitor became appreciable, a different method had to be used. Oscillograms of the capacitor transients when discharged successively through two inductively identical resistors were sufficient for this determination. Using only slightly different resistances would not shift the period a measurable amount, but could be observed in the damping decrement. This left two equations in two unknowns after the relationship between R and L had been determined from the decrement.

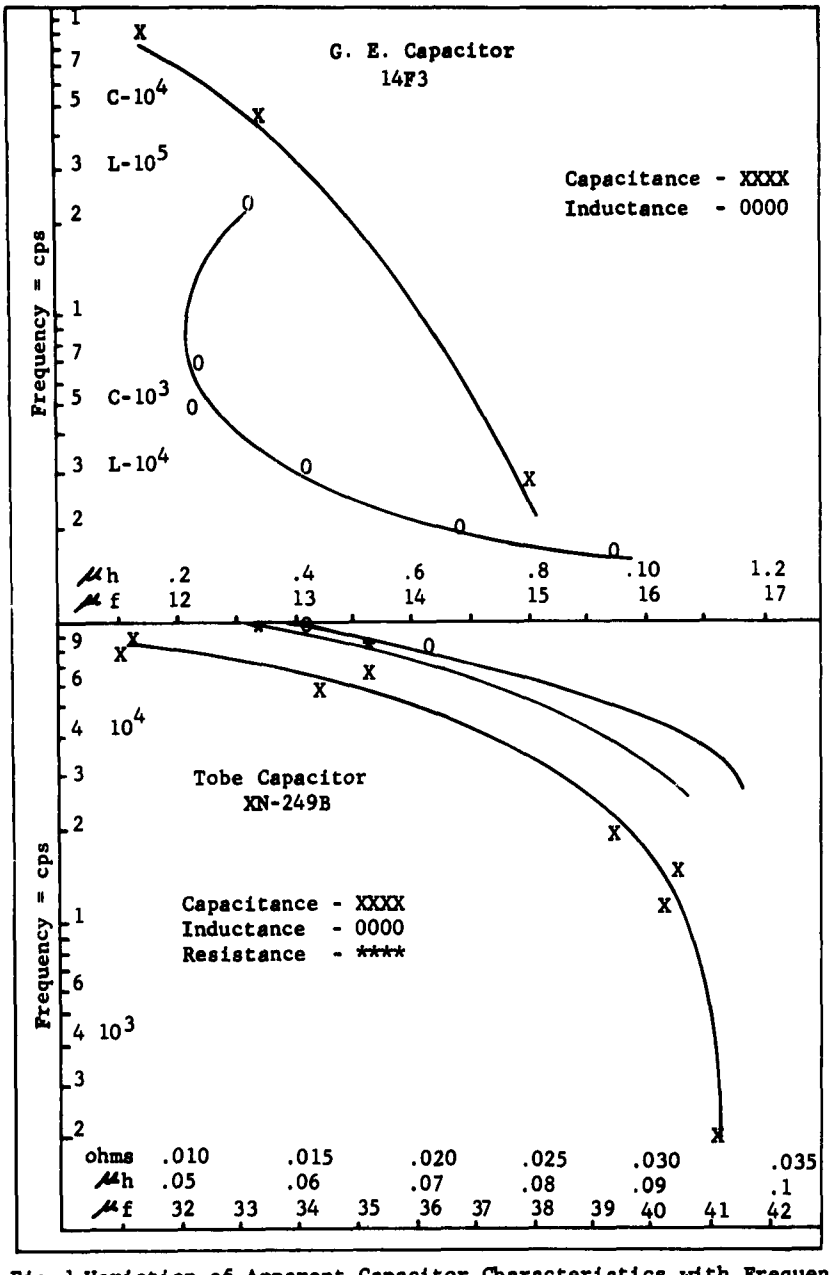

Fig. 1. Variation of Apparent Capacitor Characteristics with Frequency

One assumption which was shown to be valid was that the standard mica capacitor, used to measure added inductances, contained resistance and inductance which were constant with frequency.

The abrupt discharge of many of the capacitors we have employed was accompanied by an intense transient oscillation decaying to zero from the full capacitor potential in about 30 cycles, at a frequency of 30 to 100 megacycles depending on the particular capacitor. This oscillation was unaffected by external circuit constants, and we believe that it was a long line oscillation of the capacitor foils. It was particularly objectionable as a source of triggering signals for pulse synchronized auxillary equipment. It was possible to suppress it by introducing a filter at the output of the capacitor, consisting of the critical damping resistor (when used) divided into two portions, with two 0.1 μfd bypass capacitors.

The damped discharge of a single capacitor can be modified in various ways to produce desired effects. Thus, the capacitor can be replaced by a pulse forming network, or the capacitor can be abruptly shunted at any selected point in the oscillation to alter the normal damped behavior. Basically the damped discharge produces a current I which varies as

$$I = \frac{V_o}{\omega L} e^{-\frac{R}{2L}t} \sin \omega t \; ; \qquad \omega = \sqrt{\frac{1}{LC} - \frac{R^2}{4L^2}} \; ;$$

where V_o is initial capacitor voltage and L and R are lumped equivalent series constants. The fact that R includes a non-linear resistive element (the discharge tube) will be considered later. At present we shall assume that the tube resistance is swamped by circuit resistance as is usual in the critically damped case.

The maximum value of I occurs at $\omega t = \tan^{-1} \frac{2\omega L}{R}$ and is

$$I_{max} = \sqrt{\frac{C V_o^2}{L}} \; e^{-\frac{R}{2\omega L} \tan^{-1} \frac{2\omega L}{R}} .$$

The maximum power delivered to a linearly resistive load r occurs at the same instant and is

$$P_{max} = \frac{r C V_o^2}{L} \; e^{-\frac{R}{\omega L} \tan^{-1} \frac{2\omega L}{R}} .$$

The potential difference across a linearly resistive load would of course vary in proportion to the current. It is apparent in this approximation that a minimization of inductance and maximization of stored energy ($C V_o^2/2$) is the direct route toward optimization of currents, power, and electric fields in the discharge tube.

When the discharge tube is considered as a nonlinear element in

the circuit, these conclusions may require some modification. It is found, for example, that since the tube offers an infinite resistance prior to breakdown, the potential difference across it is a maximum at the outset, and may have a second minimum value when the current is at its peak. Analysis of discharge data to be presented in Chapter III shows that most gases display a resistance trend which can be rather well approximated by the expression

$$R = R_o\, e^{-\beta t} + R_m + \frac{V_c}{I}\ .$$

Then for such an element, in a circuit which also includes series linear elements R, L and C, the charge on the capacitor varies as

$$L\,Q'' + (R + R_m + R_o\, e^{-\beta t})\,Q' + Q/C + V_c = 0.$$

Substitution of $\xi = (R_o/\beta L)\, e^{-\beta t}$ and $y = \xi^{-n}\,(Q + C\,V_c)$ leads to the confluent hypergeometric equation

$$\xi\, y'' - \left[1 \pm \sqrt{\frac{(R+R_m)^2}{\beta^2 L^2} - \frac{4}{\beta^2 LC}} - \xi\right] y' - \left[\frac{R+R_m}{2\beta L} \mp \sqrt{\frac{(R+R_m)^2}{4\beta^2 L^2} - \frac{4}{\beta^2 LC}}\right] y = 0.$$

when $n = (R+R_m)/2\beta L \pm \sqrt{(R+R_m)^2/\beta^2 L^2 - 4/\beta^2 LC}$. In critically damped circuits, the radical in these expressions is zero, and the equation for y is greatly simplified. Its solution, in the notation of Erdelyi (13) is

$$y = C_1\, \Phi(a,\ 1; \xi) + C_2\, \Psi(a,\ 1; \xi)$$

where $a = (R+R_m)/2\beta L$.

When $t = 0$, $\xi = R_o/\beta L\ (=s)$; and $y = s^{-n}\,(Q_o + C\,V_c)$, together with $I = dQ/dt = 0$.

This leads to

$$C_1 = \frac{(Q_o + C\,V_c)\, s^{-a}\, a\, \Psi(a+1,\ 1;\ s)}{a\, \Phi(a,\ 1;\ s)\, \Psi(a+1,\ 1;\ s) - \Psi(a,\ 1;\ s)\, \Phi(a+1,\ 1;\ s)}$$

and

$$C_2 = \frac{-(Q_o + C\,V_c)\, s^{-a}\, \Phi(a+1,\ 1;\ s)}{a\, \Phi(a,\ 1;\ s)\, \Psi(a+1,\ 1;\ s) - \Psi(a,\ 1;\ s)\, \Phi(a+1,\ 1;\ s)}.$$

Finally the solution for the current is

$$I = -\frac{R+R_m}{2L}\, \xi^a \left[C_1\, \Phi(a+1,\ 1;\ \xi) + a\, C_2\, \Psi(a+1,\ 1;\ \xi)\right].$$

Tables of the functions $\Phi(a, 1; \xi)$ and $\Psi(a, 1; \xi)$ have been computed for the range a: 0.01 (0.01) 2.00 and x: 0.01 (0.01) 1.00. (14)

The foregoing analysis was based on the absence of pinching in the discharge. This condition is not always fulfilled, especially at low pressures and high currents. When pinching occurs, the inductance of the discharge column varies rapidly in time, rising to rather large values. This has the effect of superimposing a voltage modulation upon the normal discharge. The recurrence rate of this modulation (it has no frequency in the proper sense of the word) is determined by radial mechanical motions of the plasma column which are governed by equations nearly identical with those for the linear expansion of the plasma, except that the initial driving pressure is magnetic. This will be discussed in a later chapter.

The effect of the pinch upon the circuit is primarily through the change of inductance. If the pinch compression were uniform and adiabatic, and the conductivity were that of a fully ionized gas, then the decrease in area would be matched by an increase in the conductivity which exactly would balance it. Neither is exactly true, of course, but the result indicates that we need not regard the resistance as strongly variable.

Suppose then that the inductance varies as $L + \ell(t)$ where max $\ell(t) \ll L$. In an arbitrary RLC circuit the equation will be

$$\frac{d^2}{dt^2}(L + \ell(t))\, I + R\frac{dI}{dt} + \frac{I}{C} = 0.$$

Let us presume that $I = Ff$, where f is a small rapidly varying modulation on the major circuit behavior F. For concreteness we will assume that F can be approximated as $\sin \omega_0 t$, and is the solution with $\ell(t) = 0$, while f varies as $\sin \omega t$, where $\omega \gg \omega_0$. Then the single differential equation reduces to the set

$$LF'' + RF' + F/C = 0$$

and

$$(L + \ell)\, f'' + (R + 2\ell')\, f' + \ell'' f = 0.$$

The solution of this is, for $R \ll 2\ell'$

$$f = \frac{L}{L + \ell}$$

which states that to a first approximation the inductance is to be treated as a constant insolving the original equation. If now the voltage oscillation across the tube owing to the pinch is computed it becomes

$$V_{total} = V_{pinchless} - RI\frac{\ell}{L}.$$

Since $\mathcal{L}$ is approximately $(\mu_0 h/2\pi) \ln (r_o/r)$, where h is the length of the column and r_o is its initial radius, one can estimate the degree of pinching in our devices from the voltage oscillations.

The pinch produces scarcely noticeable changes in the current, but striking changes in the potential difference across the discharge column. Since it will be seen later that the field in the column is the governing factor in the electron-driven shock waves, multiple shocks are observed to occur when pinching takes place, as in Fig. 2 in hydrogen, and only a single shock is observed when a strong axial magnetic field is present to prevent pinching.

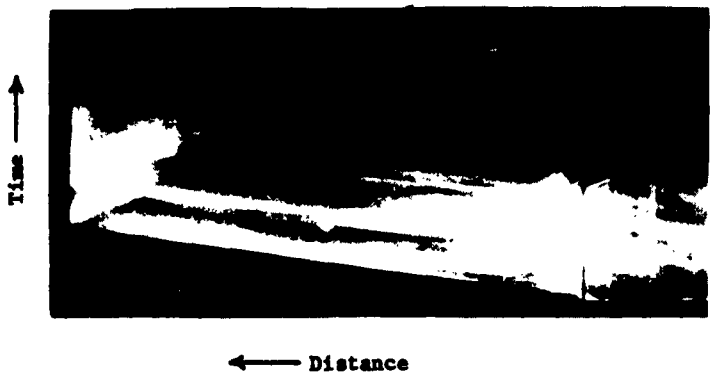

Fig. 2

Connections and switching are two important considerations if ultimate performance is desired from any given apparatus. Parallel plate lines consisting of wide strip conductors sandwiching thin dielectrics of mylar or polyethylene (400-700 volts/mil thickness) are very useful in minimizing inductance, as also are coaxial lines in which outer and inner conductor are both large, again with a thin separating dielectric. Inductance formulas neglecting skin effects for these situations are:

Parallel plates ($\mathcal{L}$ long, t thick, s spaced, w wide in meters).

$$L = 4 \times 10^{-7} \mathcal{L} (s + 2/3\ t) \text{ henries.}$$

Coaxial tubes r_1, r_2, r_3, r_4 (indices from inside to outside) in meters.

$$L = 10^{-7} \mathcal{L} \left[\frac{r_2^2 - 3r_1^2}{4(r_2^2 - r_1^2)} + \frac{r_4^2 - 3r_3^2}{4(r_4^2 - r_3^2)} + \frac{r_1^4}{(r_2^2 - r_1^2)^2} \ln \frac{r_2}{r_1} + \ln \frac{r_3}{r_2} + \frac{r_4^2}{(r_4^2 - r_3^2)^2} \ln \frac{r_4}{r_3} \right]$$

When $r_1 = 0$, the sum of the first and third terms is $\frac{1}{2}$.

Use of these low inductance-high capacitance types of connection occasionally proves disadvantageous when peculiar combinations are attempted. For example, when a gas-insulated mechanical switch is closed in a parallel-plate line leading to a discharge tube, the uncharged line serves as a short circuit so that the switch breaks down prematurely, before closure, at the gap width where the Paschen minimum is reached. In the absence of the line, the high impedance situation in the discharge tube prior to its breakdown permits the switch to be closed before its dielectric disrupts.

Switching may be accomplished in a variety of ways. Ignitrons, thyratrons, vacuum switches, pressurized switches, oil switches, spark gaps, and in some special situations no switch at all, have been used successfully.

At the outset, when the Rayleigh phenomenon was wholly unintelligible, mechanical switches were the switch of choice with the University of Oklahoma group to ensure that the phenomena observed were not the result of superposition of discharge effects. If the main switch required synchronization with some other event, such as a rotating mirror's position, low inertia vacuum switches such as the 1S22 with tungsten or molybdenum contacts were used. Quick closure was achieved by discharging a capacitor through a solenoid with low mass armature. To obtain long life, it was necessary to evacuate these switches continuously. Currents in excess of 10,000 amperes could then be handled by these switches for 1000 repetitions. If synchronization was not needed, relays were used having palladium silver contacts, immersed in hydrogen at atmospheric pressure. Again moving mass was minimized and capacitor-activated solenoids were used so that the velocity of closure would be large. Then if the discharge tube was itself carefully deionized and leakage currents paralleling it were minimized, there was no breakdown of the gas between the switch contacts during closure because the distribution of the electrostatic potential difference gave a less-than-breakdown value across the switch. Whenever the research problem necessitates leakage paths around or through the discharge tube, vacuum switches are the only feasible mechanical kind. It was found that in practice contacts frequently reopen immediately after closure. This was caused by the stationary electrode moving away under impact compression, rather than by bouncing of the moving electrode. Gas insulated switches from which reopening was eliminated (by facing the contacts, by minimizing the mass of the moving electrode, and by increasing the holding force acting on the armature) closed without arcing up to capacitor potentials of around 3000 volts, but still appeared to break down again above this potential. Since the maximum discharge current increases linearly with the capacitor potential, it was presumed that at this critical point the fall in potential across the contact impedance exceeded the breakdown potential of the gas, and hence precipitated a gas discharge around the point of contact. A hydrogen atmosphere around the switch had the additional benefit of preventing oxidation during this period of arcing.

An ideal mechanical switch would be capable of standing off potentials of the order of 10^5 volts, would be extremely quick in closing (10 - 100 μsec), would close and remain closed during the discharge, and would have low inductance and contacts capable of carrying 10^5 amperes. Such a switch was designed and built, but has not been used extensively because of recent improvements in ignitrons for capacitor discharge usage. The design is given in Fig. 3. In addition to coaxial arrangements, graphite against tantalum contacts are the principal innovation. The graphite contact must be set into a shrunk-fit cup to give it strength against magnetic forces at the large current densities it encounters.

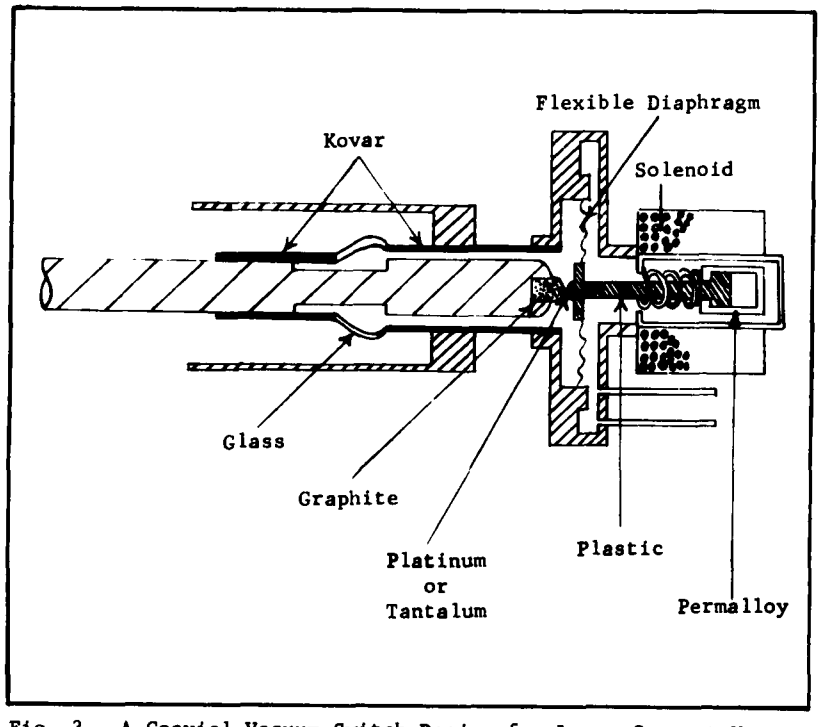

Fig. 3. A Coaxial Vacuum Switch Design for Large Current Usage

Ignitrons have become increasingly available with small dimensions, adequate voltage standoff, and adequate current maxima, so that when breakdown delay and jitter in synchronization of the order of 5 $\pm$ 0.2 microseconds is tolerable their reliability and convenience makes them invaluable as switches. Turner (15) has measured the characteristics of one ignitron (GL7171) in capacitor discharge

service and found the inductance to be 0.035 μh and the resistance to be less than 0.01 ohm at 80,000 amperes.

Thyratrons, in general, have peak current limitations which make them of marginal value as switches in this service. The recent discovery that large fields rather than large currents produce maximum flow speeds suggests a possible new range of usefulness of these devices at extremely low pressures. Occasionally the inherently low breakdown delay and jitter, which can be made as small as 10^{-8} seconds, offer a sufficiently great advantage to justify the sacrifice of thyratrons at overcurrents of as much as 100 times maximum ratings. A thyratron has been devised (16) in which the discharge begins in a high impedance low current thermionic cathode circuit, and shifts to a low impedance high current cold cathode circuit, but is not yet commercially available. The inductance of a 1907 thyratron with coaxial shield was 0.15 μh.

Triggered air or gas filled gaps are widely used as quickly and easily constructed switches with large current capacity (17). There are objections to them which their general simplicity and inexpensiveness tend to overcome completely for many applications. They are noisy, and their energy loss curve peaks toward low energies of operation. With a general trend toward high voltages and currents, however, their range of usefulness coincides rather well with the range of interest.

Shock tubes can be operated without switches under certain conditions. If precision control of the breakdown voltage is not required, and a functional relation between the pressure electrode-spacing product and the breakdown voltage can be tolerated, the shock tube can be operated as a breakdown oscillator, firing at a frequency governed chiefly by the charging time constant of the capacitor. This mode of operation has proved useful in some spectroscopic problems where accumulation of radiant energy from many repetitions was the only way to solve the problem of low intensities of interesting radiation. In one case as many as 20,000 shock waves were needed to provide sufficient radiation, and no switch would have withstood this many cycles.

A switchless shock tube design which has been considered but not built by the author's group would incorporate the principle of the high voltage cold cathode thyratron into the shock tube itself. By placing a perforated plate electrode as a grid structure in front of the end electrode as anode, the shock tube might be triggered directly as in Fig. 4, especially at the low pressures which are of much present day interest.

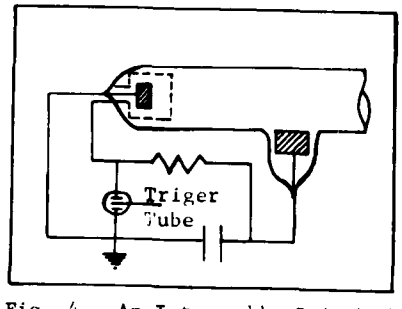

Fig. 4. An Internally Switched Electric Shock Tube Driver.

Choice of electrode materials in the construction of shock tubes depends

on how clean the driver gas must be maintained. In general, low volatility seems to be the most significant characteristic; although for equal volatility, large heat conduction is the second desirable attribute. Platinum has proved to be very effective, followed closely by arc-cast molybdenum; nickel is adequate for many pruposes, and copper is of some value. Sintered tungsten was unsuitable, and arc-cast tungsten has not been tried.

For the glow-to-arc transition to occur, on which the electron shock tube's operation depends, it is necessary that the cathode be neither insulated by too thick a layer of oxides, nor cleaned by discharge action to a point that the field emission is inhibited (18). Using zinc-alloyed aluminum the former case was achieved in practice, while using ultra-purity aluminum, the latter situation came about.

Tube walls are a severe problem in maintenance of gas purity whether the shock tube is operated with electrodes, or as an induced discharge without them. Vycor and fused quartz are the most suitable common transparent materials, although sapphire has been used (19) and is definitely the superior material. If transparency is not required, sintered alundum is available and shows little or no release of volatile material into the discharge. The chief area of volatilization both of wall and electrodes seems to be at the junctions of the walls with the electrodes. Careful shaping of the surfaces at these points can minimize the difficulty. Introduction of a diffusion-arresting magnetic field along the axis of the shock tube also helps.

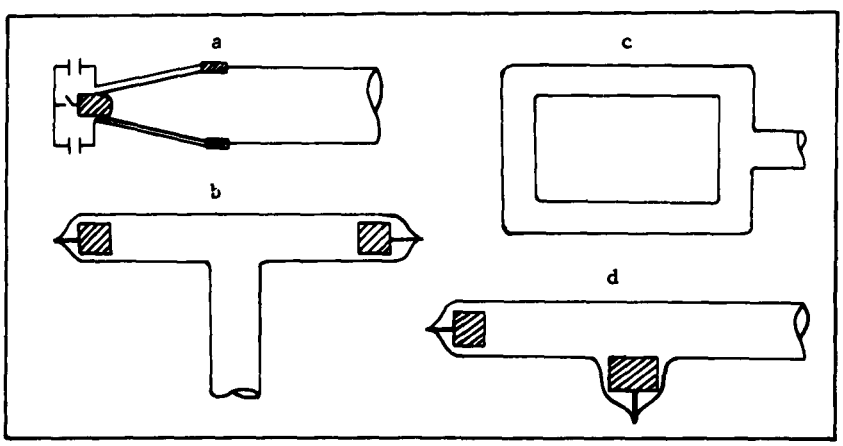

Fig. 5. Various Shock Tube Styles. (a) Conical Form (b) "T"-tube Form (c) Rayleigh Form (d) Linear Shock Tube Form.

The shape of the discharge tube has only a minor influence on the maximum velocity of the shock flow but a major influence on the behavior of the afterflow of expanding gases from the driver. Three principal tube styles have been used, the "T" tube, the linear shock tube and the conical linear shock tube, Fig. 5. The "T" was an early paraphrase (20) of the original Rayleigh apparatus, where the main discharge was at right angles to the expansion chamber. Because it is not as well adapted to investigations which might be correlated with theory as is the linear shock tube, in which the main discharge is along a portion of the same column that the expansion chamber occupies, the University of Oklahoma group abandoned it in 1952.

The linear shock tube can be constructed in either of two ways. In one case a cylindrical block of metal with a concave face conforming to the inside radius of the shock tube is set into a side arm at the point where the diaphragm would be placed in a conventional shock tube. In the other, a hollow ring electrode is used at this point. In either case, the end of the driver chamber is terminated with a plane-faced cylinder of metal. The former technique has the advantage that it is easy to make in an all-glass-and-metal design. The latter offers greater symmetry for mathematical analysis. Experience has shown that it is best to make the end electrode the cathode, since otherwise the cathode spot locates itself at random over the surface of the side or ring electrode and introduces an uncontrolled variation in discharge chamber length.

The third style of tube is the conical driver designed by Josephson (21). This has the advantage of producing a maximum of shock speed for a given capacitor, Fig. 6, but the disadvantage of not being amenable to linear tube theory. Providing magnetic insulation and a certain amount of magnetic driving force by wrapping the return lead around the driver cone enhances the drive still further.

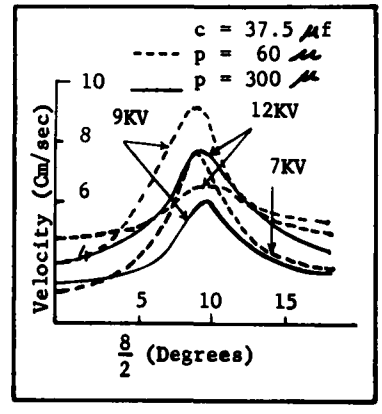

Fig. 6. Effect of Cone Angle on Shock Speed (After Josephson)

Kolb (22) has modified the "T" tube to produce powerful drives by returning the current on a strap lying directly behind the discharge arm, and opposite to the expansion tube. The resulting drive is initially at least two-fold as fast as thermal drive alone. Because of the rapid decrease of the generally cancelling fields of the main discharge current and the current in the strap, the strap current can only be looked upon as the cause of the initiation of the drive. Its field forces the discharge to loop into the side arm, whereupon its driving effect upon the front of the current diminishes rapidly, being replaced by a drive produced by the efforts of the "hairpin" current

to straighten itself. Despite its failure to participate in the drive after initiation, the strap return current does serve a continuing function in preventing the "hairpin" from short circuiting back into the discharge tube. If the problem is idealized as in Fig. 7 the magnetic force from the two primary portions of the current is

$$F = \frac{\mu_o I^2 g}{2\pi}\left[\frac{\ell}{(a+r)\left[\ell^2+(a+r)^2\right]^{\frac{1}{2}}} + \frac{g}{r(g^2+r^2)^{\frac{1}{2}}} - \frac{\ell}{r(\ell^2+r^2)^{\frac{1}{2}}}\right].$$

Under the rather probable operating condition that $a = 2g$, this force even reverses direction when r is only slightly greater than g. In terms of the dimensionless variables $\rho = r/\ell$, $\delta = g/\ell$, the geometrical expression in the bracket is plotted in Fig. 8.

Any continuing magnetic drive comes from the fields of the sides of the hairpin acting on the cross tube current, and to a certain degree from the curvature of the cross tube current itself. Both of these vary as 1/g, and the first effect can be written as $F = (\mu_o I^2)/2\pi$, whence the magnetic pressure driving the shock will be steady, and approximately $p \propto (2\mu_o I^2)/\pi^2 g^2$.

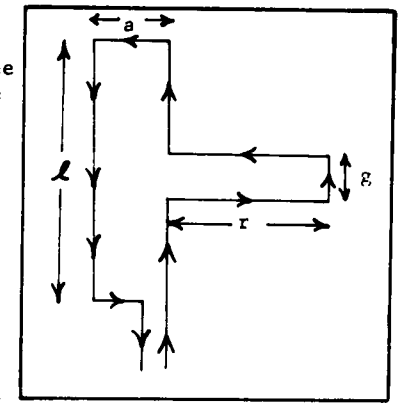

Fig. 7. Current Path in Strapped T-tube Drive

It seems a matter of some doubt whether in fact the magnetic mechanism does not instead act chiefly to bring the hot electrons of the main discharge current into the side arm where their electron pressure supplies a drive which is thus not insulated and weakened by expansion as in the linear shock tube. The latter process would predict a shock velocity which depended on $\sqrt{kT_e/M}$, and is in accord with the experimental results reported by Kolb (22), e.g., the decrease of velocity with distance x follows approximately an $x^{-\frac{1}{2}}$ law, and would be expected since $T_e \propto E \propto V/x$; the flow energy is strictly proportional to the capacitor voltage V; and finally the shock velocity varies inversely as the pressure at high pressures, but is constant at low pressures as is to be expected when the electron temperature is determined by the tube diameter for Kundsen gas conditions. Tube voltage has not been reported, so that it is not possible to make an absolute comparison of velocities with the electron pressure theory, but if the full capacitor voltage had appeared across the discharge, the predicted value at one particular point of comparison would have been 7×10^6 cm/sec, while the observed value there was 3.5×10^6 cm/sec. This implies that about a quarter of the capacitor voltage actually appeared across the discharge, a factor which is about that usually observed.

It seems certain however that magnetic drive is indeed present in the various auxilliary arrangements employed by Kolb for augmenting the magnetic fields.

In the "T" tube, operated thermally, it might be remarked in passing that at constant spacing, the location of the electrodes relative to the side arm where the fronts are observed was found to have little effect on the fronts as long as the side arm lay between the electrodes. The velocity was slightly less when the side arm was very near to either electrode.

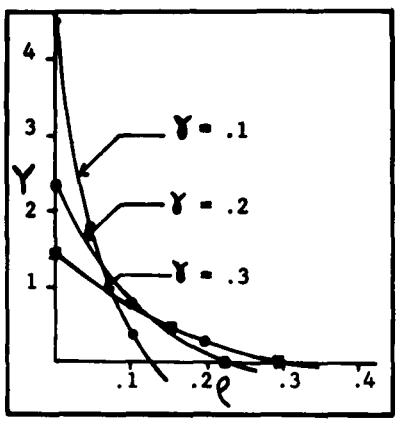

Fig. 8. Static Current Portion of Back Strap Drive

2-3 Other Techniques for Plasma Flow Production. For completeness, some of the less directly related plasmamotive engines will be described here also. Bloxom (23), adapting the principle of the explosion fuse, has developed a linear form shock tube in which the discharge chamber is made with a horn fiber walls. The heated gas evolved from the walls by the arc forms a high pressure driver predominantly composed of hydrogen, which drives a powerful shock ahead of it into whatever gas is chosen for the expansion chamber.

Bostick (24) has produced a plasma drive by striking an arc between conducting rods on opposite sides of the inside of a long cylindrical tube. The magnetic force of the currents in the conductors upon the arc moves the arc plasma rapidly down the tube, again generating a shock wave in advance of it. The device is sometimes called a rail driver, and should be governed by essentially the same principles as the magnetic component of the drive in the back-strapped T-tube.

Petschek and Kemp (25), and Patrick (26) have described experiments in which the rail driver principle, but with return currents in the gas as in the back-strapped T-tube, is made cylindrically symmetrical by use of an annular configuration. The discharge begins as a radial current in the annulus between concentric electrode cylinders but is driven outward by interaction between these radial currents and the azimuthal field which is present in the region between the electrodes, into a continuation annular region with non-conducting walls. As the drive progresses, two concentric axial sheet current arcs form to connect the electrodes with the propagating radial arc. A variety of refinements with auxilliary magnetic fields has been tried, and high velocities of propagation have been achieved.

Meyer (27) has described a traveling magnetic field drive in which a slug of plasma is introduced into a solenoid just ahead of

was used after shaping, delaying and gating to trigger the discharge. Both electronic and optical techniques were necessary to assure that the trigger pulse would always be created at the same phase in the rotation cycle of the mirror.

We will follow such a pulse from its formation to its termination. Light from an infrared source which was placed off the optical axis of the mirror system reflected from the mirror and back onto a photo tube to produce a voltage pulse. Built together with the photo tube on the pulse forming chasis were a pulse shaper, a variable time delay, and a cathode follower through which the pulse traveled. The delayed pulse then traveled by coaxial cable to the gating chassis where it was re-shaped and gated. The voltage on the discharge condenser controlled the gate. This was done optically with the associated circuitry on the gating chassis. Next, the pulse traveled by coaxial cable to the power supply chassis where the pulse was greatly increased in voltage and power; then, by coaxial cable to the switch for the discharge which was variously a mechanical one, or an ignitron, or a hydrogen thyratron. Each element in the chain will be given special attention.

Since the phase relation of any sixty cycle pick-up and the generated pulse was continuously varying, little pick-up could be allowed. Negative voltage with a.c. ground was supplied so that the emissive surface of the 925 phototube could be used as a partial shield for its collector to eliminate stray signals. In addition to this, a brass shield encased the tube. One stage of amplification changed the negative pulse (point A, Fig. 9) to the positive one (B in Fig 9) needed to fire a 2D21 miniature argon filled thyratron. The pulse generated by the thyratron had 140 V peak and about 1/2 μsec. width (C in Fig. 9). Voltage was reduced by tapping down on the 2D21 cathode resistors before the pulse was fed to the one shot multivibrator. The multivibrator was of standard design using a 0.1% linearity helipot to vary the time. Direct coupling to the cathode follower minimized components required, prevented loading, and also supplied the positive grid voltage needed to allow a large negative square wave (D in Fig. 9) to pass. Again at the cathode of the cathode follower the pulse height needed to be reduced. The pulse was fed into a 30 ft. coaxial cable which would have completely deformed the square wave if resistors only were used. By trial and error a capacitor was selected to place across the resistor, between the cathode and coaxial cable, which corrected the shape of the trailing edge of the square wave (E in Fig. 9). This edge was the portion to be used since it had the delay property desired.

The wave was changed from an almost square wave to a positive pulse (F in Fig. 9), at the trailing edge of the square wave, by use of a germanium diode and capacitor arrangement. It was then applied to a gating tube utilized as a grounded grid amplifier, since the next circuit could only use a positive signal.

Also on this chassis, were an infrared light source and circuits for capacitor voltage control gating. This light reflected from the

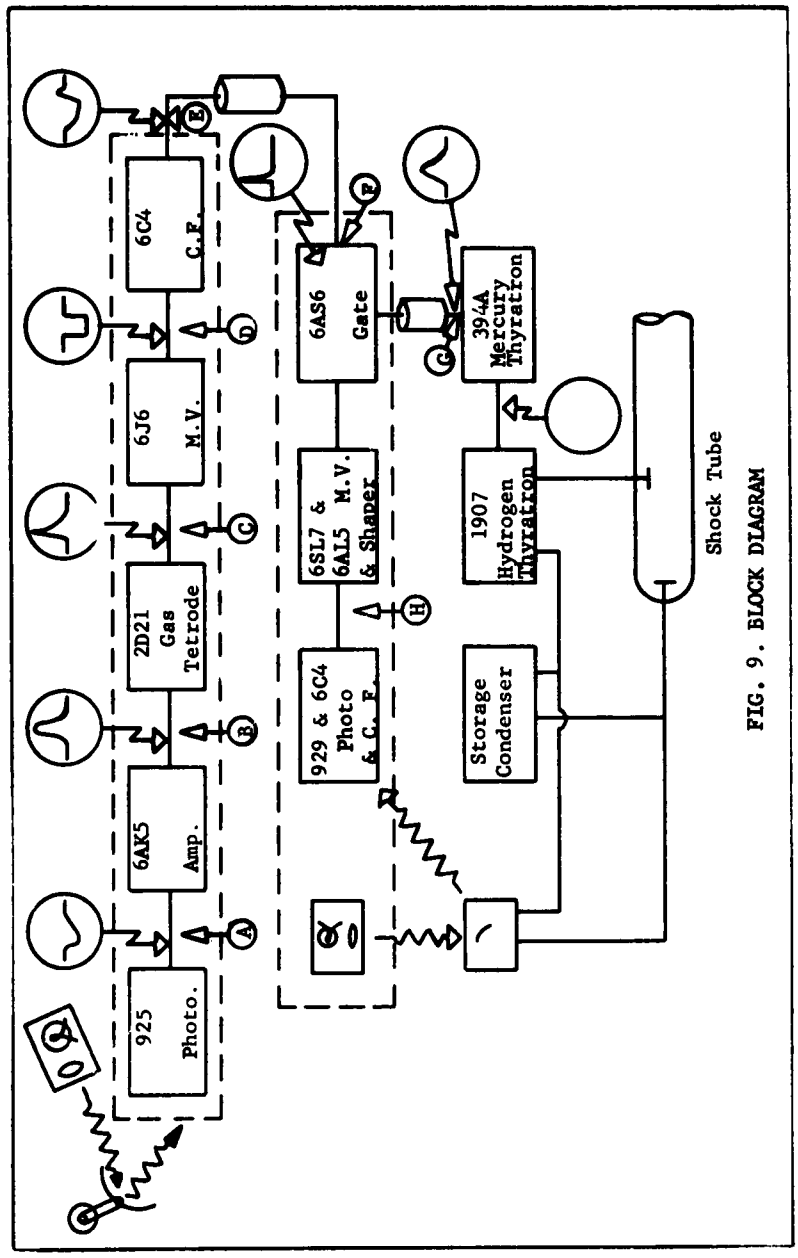

FIG. 9. BLOCK DIAGRAM

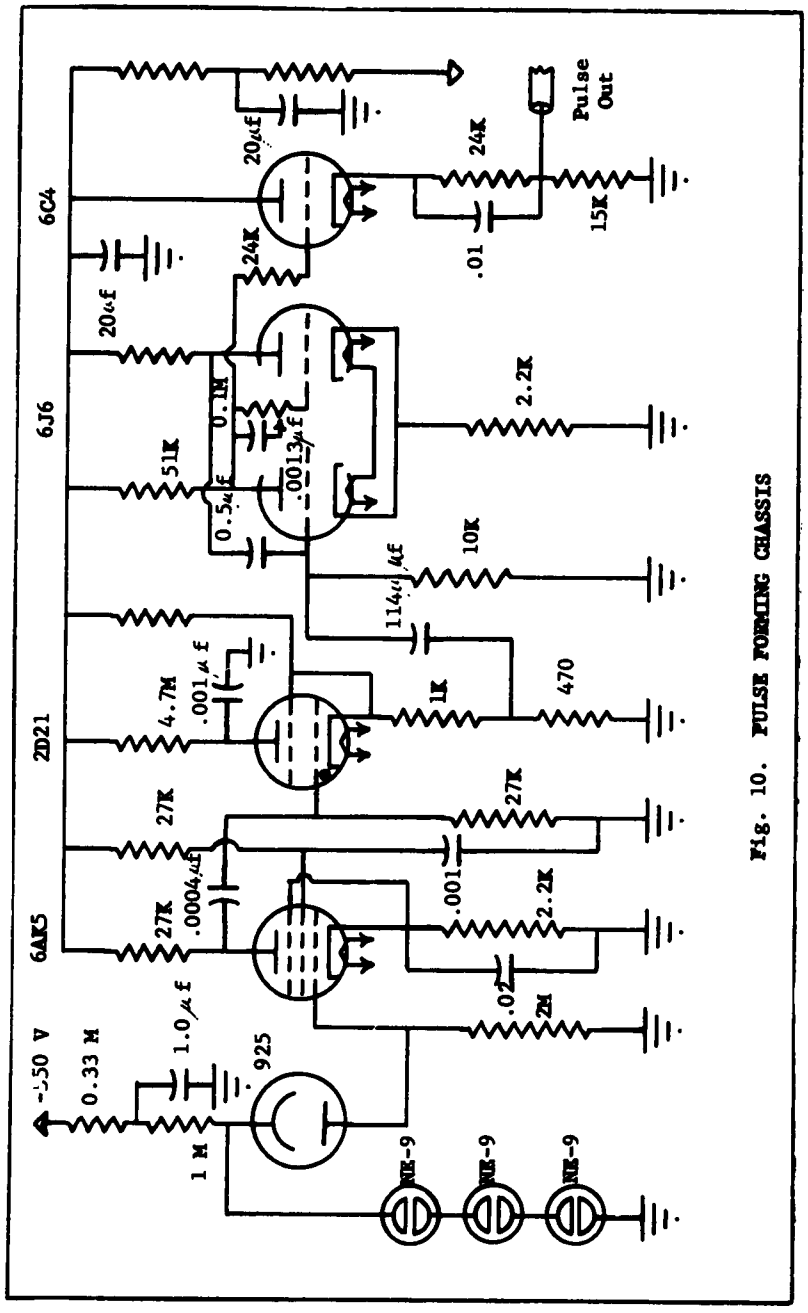

Fig. 10. PULSE FORMING CHASSIS

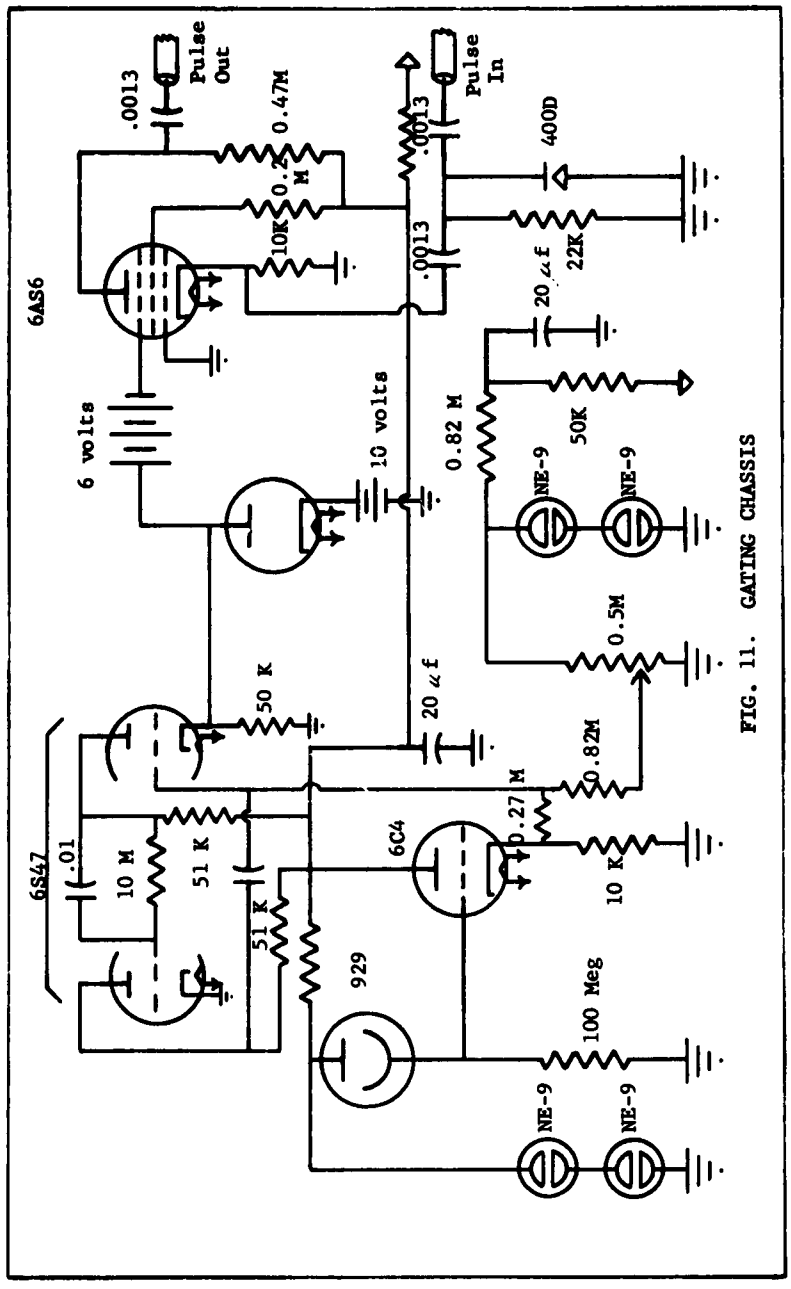

FIG. 11. GATING CHASSIS

mirror of a sensitive stiff-suspension galvanometer which was pre-set to reflect the light into the phototube, 929, at a given voltage. In order to increase precision, the galvanometer was placed 5 meters away and tension was changed on the suspension that the movement was free rotating on only a small region of voltage. Such a large optical arm required the sensitivity of the phototube to be very high. This was achieved by making its load resistance 100 megohms and at the same time adjusting the potential across it to 115 volts instead of 90 volts, the normal maximum for a gas phototube. The phototube was of the gas filled type which glows at about 120 volts losing all sensitivity. Under these conditions about 30 volts variation was available at the cathode of the phototube's cathode follower. This voltage fed one arm of a bridge, and at the other arm of the bridge, was a variable negative potential. In the center to the bridge (H in Fig. 9) the voltage fluctuated sufficiently to allow a multivibrator, in cutoff when no light struck the phototube, to be free running when the weak reflected light was on the tube. A positive pulse was taken from one cathode of the generator and was rendered square by the shunting action of a diode battery arrangement. Using direct coupling was necessary since the pulse was about 1/9 second duration which would make RC coupling out of reason.

Details of the circuits for the pulse forming and gating chassis are given in Figs. 10 and 11.

Three DC voltages were generated on the power chassis (Fig. 12). A 394A mercury thyratron was also included which could be operated with the load either in its plate or cathode circuit. When used, tube-switch loads were placed in its cathode circuit. Mechanical relay solenoids on the other hand were placed in its plate circuit. If the tube was to have its filaments heated with AC, a center tap was needed to the load and to ground. Using a hundred ohm load resistor, with 700 V on the thyratron's anode, the cathode rose to 700 V in less than 0.01 μsecond (G in Fig. 9). It was found by experimenting that this pulse was not changed in size or shape when the load was taken from the center tap of the standard filament transformer. Synchronization with these circuits could be achieved to $\pm$ 0.2 μsec under ideal conditions, and not worse than $\pm$ 2 μsec under the worst.

The velocity u of a wave can be determined for a mirror camera from the angle ϕ between a stationary reference trace and the moving traces on the photographed image, and applying the relation

$$u = \frac{2\omega p}{\cot \phi}$$

where ω is the angular speed of the mirror and p is the object distance. It is important to note that increased ease of measurement of ϕ is obtained by increasing p, not the writing arm (i.e. image distance) q.

If the actual thickness of the flow pattern under study is greater than the slit width w used in front of the shock tube,

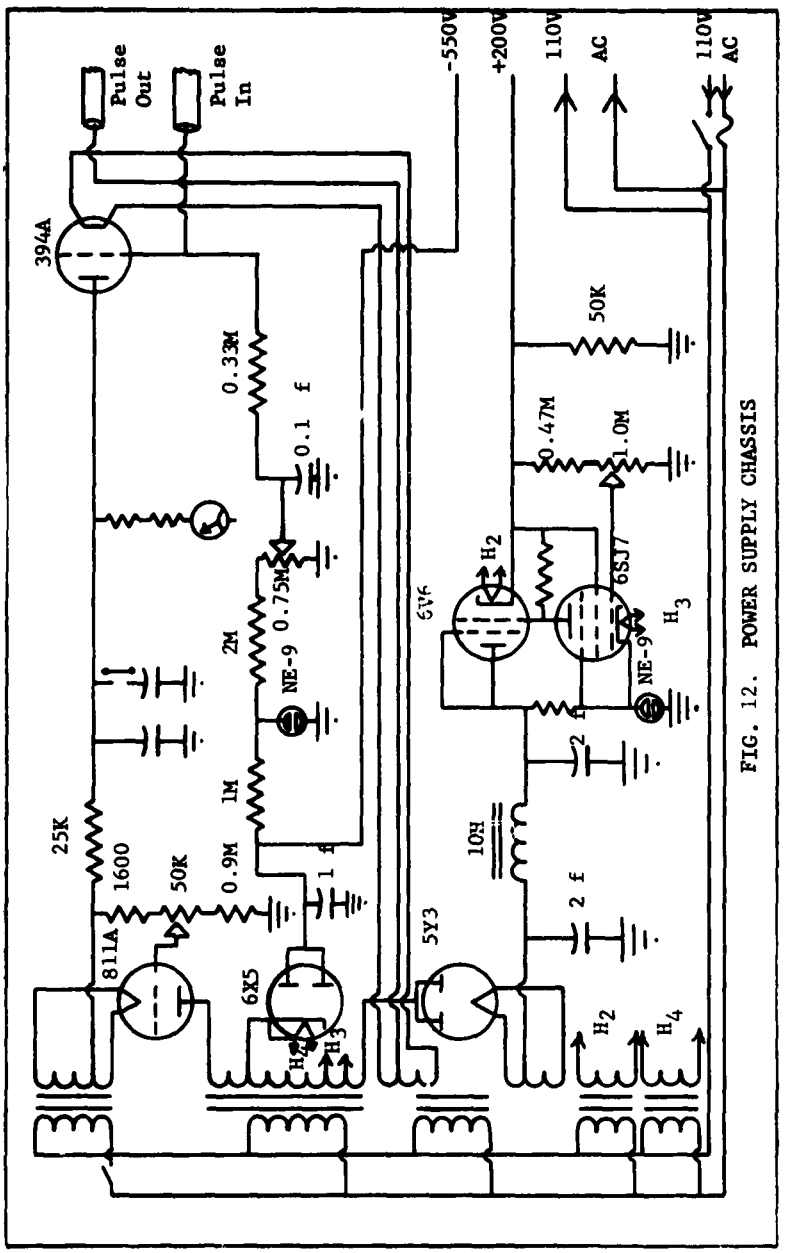

FIG. 12. POWER SUPPLY CHASSIS

the photographic speed of the mirror camera is proportional to

$$\frac{d^2 w}{q^2 p \omega}$$

where d is the lens or mirror diameter. Thus one gains high velocity detection at the expense of photographic speed when one increases p.

Drum cameras are frequently convenient for wave studies at moderate speed. A cylindrical cup of light high tensile strength material such as aluminum is spun at high speed, and the shock tube is imaged by a fast lens on a photographic film held flat against the inside of the cup wall by the rotation. Usually the light is brought along the axis of rotation of the cup from the open side and reflected 90° by a plane mirror against the cup wall. Use of a hydrogen or helium atmosphere around the cup will reduce the temperature rise due to friction.

Breaking strength of the cup material limits the linear speed v which can be achieved practically to a rather small value, relatively speaking. If S is the breaking strength and ρ the material density,

$$v < \sqrt{\frac{S}{\rho}} .$$

For aluminum the maximum value is 3.3×10^4 cm/sec; for copper 3.3×10^4 cm/sec; for magnesium 4.2×10^4, for molybdenum 5.2×10^4; for steel 5.6×10^4. Dimensions of the equipment are a factor only in convenience of optical arrangements. The drum camera equation is

$$u = \frac{p\, v}{q \cot \phi}$$

Space Technology Laboratories (28) have developed a very fast wave speed camera using an image converter tube. Used in studies on the super fast pinch this camera was able to record waves with speeds as great as 5×10^7 cm/sec with a fairly large angle of detection.

The second most important tool has been the spectrograph. Much information has been obtained from the analysis of the radiation processes in the tube. Ideally the radiation should be resolved with respect to wavelength, to time, and to position of occurrence. It is difficult to realize this condition. Each wave speed picture occupies a considerable plane area, and to provide wavelength resolution can only be accomplished by forming different simultaneous photographs in different sites. This is possible for only a limited number of wavelengths owing to limitations on total film area. Usually one must settle for resolution with respect to two of the three variables. Then the information is interesting to the extent that the missing variable is unimportant, or can be sampled itself in some limited degree.

Space and frequency resolution for integrated time can be obtained by imaging the shock tube along the slit of a spectrograph. If the luminosity is entirely concentrated in a thin wave front of presumed homogeneity, the time integration need not be harmful. Space and frequency resolution for selected times can be had by use of a Kerr cell shutter. It is difficult to obtain Kerr cell materials which transmit an ideal band of wavelengths. Most materials cut off the ultraviolet seriously. A second method is to image the wave speed camera on the slit of the spectrograph with the space axis of the camera parallel to the slit. The rotating concave mirror camera is especially useful here because it is achromatic. Close synchronization is needed which usually requires use of a large hydrogen thyratron such as the 1907 as switch. Both methods suffer from the low light intensities available after both time and frequency resolution. If the reliability of the synchronization is great enough, multiple shocks can be superimposed, but this assumes that they are wholly reproducible from shot to shot. Likewise, if more than one time interval is to be studied, different shots are required. Fortunately, the electric shock tube can produce a relatively reproducible flow and can be interated fairly quickly. In one experiment as many as 20,000 shots were superimposed, the whole operation lasting 24 hours (Fig. 13).

Time and frequency resolution at a fixed point in the flow can be gained by imaging a wave speed camera on the spectrograph slit with the time axis parallel with the slit. Another way, having the advantage that it eliminates the need for plate calibration and gives intensities directly, is to attach a photocell or photomultiplier, with oscillograph recording, to a monochromator. However, to obtain an overall picture of the kinematic behavior of the entire spectrum requires analysis of a very large number of oscilloscope traces at different wavelengths and positions in the flow.

Time and space resolution at single frequencies is perhaps best attained by use of interference filters with an ordinary wave speed camera. If some prior inkling of the frequencies of interest has been gained by taking lumped or partially resolved spectra, this may be the most successful technique.

Complete resolution can be approximated in two ways. First the shock tube may be imaged on the slit of a spectrograph, and the image plane may be formed on the surface of a drum camera (29). If the wave speed is within the camera's range and the spectral lines of the gas are widely enough spaced that the duration of the luminosity does not result in overlapping monochromatic patterns, excellent information can be obtained. Proposed, but never as yet built, is a combined spectrograph and mirror camera, in which a fore-slit, collimator lens, and prism or grating are introduced into the optical path of a rotating concave mirror. The second method referred to above cannot actually be said to give spectral resolution, yet provides useful information of the same general type with considerable ease. This is the use of color film, instead of black and white film, with any ordinary wave speed camera. If the spectrum of the

wave is generally known, and is not too complex, the method is valuable. It can be used, for example, to discriminate the entrance epoch of impurities into a hydrogen plasma.

Accurate photographic plate calibration with a luminosity of the brevity of that from electric shock waves poses a problem of some difficulty. Care should be taken to make the calibration in the same wavelength of light as is under study. One solution is to compare a series of spectra taken with superimposed successive discharges of the tube on the assumption that reciprocity law failure is small for brief discharges, and that any intermittency effect is eliminated by the internal comparison of the data. This assumption is countenanced in some degree by Mees (30) and by information supplied by photographic manufacturers. It was further borne out in practice by the agreement between data taken at different levels of intensity.

Another and more reliable technique of plate calibration is the neutral step filter. It is only necessary to be sure that the irradiation of each step is the same as that of the others. This is sometimes difficult to fulfill, however.

Absolute standards of source intensity are also needed for some problems. MacPherson (31) has shown that the positive crater of the carbon arc is a reliable standard with an intense gray body emission, owing to control of its temperature by the boiling point of the liquid carbon in the crater.

From the data for liquid carbon in the International Critical Tables, the pressure correction for atmospheric variation is

$$dT = 0.31\ dp$$

where dp is in mm Hg deviation from 760 mm.

MacPherson reports that a 5/16" spectroscopic quality carbon electrode at ten amperes has an average (over crater area) monochromatic power emission per unit area per steradian per cm wavelength given by

$$J_\lambda = \epsilon_\lambda C_1 \lambda^{-5}\ e^{-C_2/\lambda T}$$

where $\epsilon_\lambda = 0.780$, $C_1 = 1.177 \times 10^{-12}$, $C_2 = 1.432$, and $T = 3840^\circ$ at standard atmospheric pressure (on the presumption that MacPherson made the correction to standard pressure - the correction is not serious anyway, perhaps 10° for normal fluctuations over the United States).

Computing J_λ for a series of wavelengths gives Table II. The arc, seen through a standard hole of radius s of smaller dimensions than the arc spot produces a monochromatic flux $\Phi_{o\lambda}$ of

$$\Phi_{o\lambda} = \frac{\pi s^2 A J_\lambda}{d^2} \text{ watts/cm}$$

into the slit (of area A) of the spectrograph. This is usually used to generate a photoelectric response voltage. The linear relation

$$V_{o\lambda} = k_{\lambda} \phi_{o\lambda}$$

can then be used to obtain the constant k_{λ} for the photocell.

TABLE II

λ	J_{λ} watts/steradian/cm^2/cm$_{\lambda}$
6000 A°	2.88×10^6
5500	2.00×10^6
5000	1.66×10^6
4500	1.20×10^6
4000	7.70×10^5
3500	4.00×10^5
3000	1.43×10^5
2500	1.87×10^4

Making a plot of $V_{o\lambda}(\lambda)$, and using care not to alter the adjustments of the spectrograph when shifting to the unknown source, and arranging both standard and unknown sources at distances such that the collimator lens of the spectrograph is incompletely filled by the pencil of light from the source, a relative intensity comparison can be made.

The unknown radiating tube, if it contains an optically thin radiating gas may be discussed in terms of quantity $\mathcal{J}_{\lambda}$, the power radiated per cm^3 volume per steradian per cm wavelength. Then the monochromatic radiant flux received at the spectrograph at a distance from a tube of radius r will be:

$$\phi_{\lambda} = \frac{\pi r^2 \ell A}{p^2} \mathcal{J}_{\lambda}$$

where ℓ is the length of tube viewed.

Thus, if the V_{λ} is the response of the photosystem to the unknown signal, then

$$\mathcal{J}_{\lambda} = \frac{p^2 s^2}{\ell r^2 d^2} \frac{J_{\lambda}}{V_{o\lambda}} V_{\lambda} .$$

Interferometric, shadowgraph, and schlieren techniques have always played an important role in flow and shock studies, and interferometers are beginning to come into use in the electric shock tube (32). Alpher has had great success in determining electron concentrations in ordinary shock tube by interferometry.

Much of the same information as microwaves can give is available here also, on the short wavelength side of the plasma frequency.

Microwaves have occasionally been suggested as a diagnostic tool to observe electron concentrations. Owing to the brevity of the flow process, the large electron concentrations present (which will reflect rather than transmit ordinary microwaves), and the unfavorable relative size of normal apparatus to the usual microwave wavelengths which favors pronounced diffraction effects, little use has been made of them so far. A current effort is under way to use the reflection of microwaves against an oncoming shock wave with the shock tube as wave guide to study wave speeds by doppler effect, and perhaps also electron distributions in the front (35).

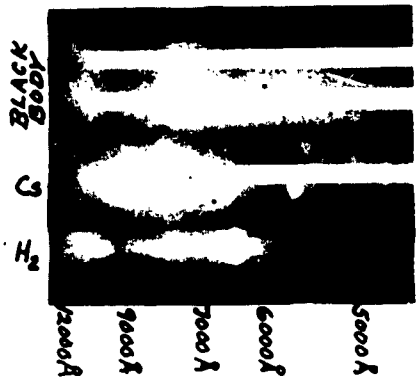

Fig. 13

Fig. 14

Measurement of discharge currents and tube potentials requires careful design of shunts and dividers to produce reliable results. Selby (36) has provided a general analysis of these problems. One design of current probe which has proved successful is shown in Fig. 14. A cylinder of graphite is hollowed out and introduced between two rods of copper of the same outside diameter as the graphite. Mating flat conical faces are cut on the juxtaposed ends. The inner copper rod is attached to one plate of a parallel plate line. The outer rod is attached to the other plate of the line, the continuation of which forms a coaxial shield around the assembly of rods. A screw, insulated from the outer plate and the graphite passes down the hole into a threaded seat in the inner plate rod, thus furnishing both an electrical pickoff and a mechanical force to draw the rod together. The screw attaches to the center conductor of a standard coaxial fitting, and the outer conductor of the same fitting joins the copper rod which is attached to the outer plate. The inner copper rod and graphite are insulated from the outer shield by mylar of sufficient thickness to withstand the voltages

generated across the graphite. Finally, the ends of the graphite rod are plated with copper and soldered to the copper rods before the retaining pressure screw is drawn up. To a first order the inductance of the element is zero. Graphite has been satisfactory, but there is no reason that it could not be replaced with a metallic element of nichrome for very high currents if the frequencies are not too large. Properly constructed, the device can be an absolute standard, calculated from the resistivity of the element.

A handy method of measuring current which must be calibrated has been described by Turner. It consists of 15 turns of #22 wire wound on the polyethylene core of an RG/9U cable. The cable is terminated and the signal, proportional to (dI)/dt, is put into an R-C integrator with a time constant of 200 μsec. The probe coil can be inserted into any convenient current loop in the circuit under study. One calibrates by use of the period, decrement and capacitor voltage of a short circuited discharge. The sensitivity of this particular probe was found to be 3.2×10^3 amperes per volt of integrated signal.

Voltage dividers must be freed from the effect of unknown distributed capacitances. The design may incorporate a large capacitor in series with the divider to take advantage of the transient nature of the discharge, or it may involve direct connection. In the latter case the power dissipation must be adequate to meet a possible failure of the discharge tube to fire. Two typical probes will be described. One of the first style is shown in Fig. 15. In this design a low impedance divider can be used.

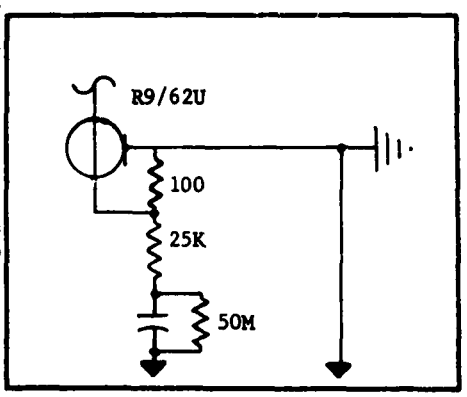

Fig. 15. Low Impedance Voltage Divider

A divider of the second style utilized twenty 200K one watt resistors in series. The resistors, arranged in a zig-zag path, were mounted in a three inch diameter hollow lucite cylinder, 4 inches long, with external connectors at opposite ends. Nineteen resistors were paralleled with a variable trimmer capacitor. The twentieth was paralleled by a fixed capacitor across a coaxial lead which conducted the signal to the recording oscilloscope. Castor oil was used to fill the whole probe. Power dissipation at the rated value was 40 watts; but was only attained when over 10 KV was applied. The castor oil bath provided a heat transfer medium and was also the dielectric for the trimmer capacitor. Its dielectric constant, which is over 4 and its reasonably high dielectric strength allowed two 1/2 inch diameter plates to act as the trimmer capacitor. Castor oil was chosen since Pyranol attacks lucite and most other oil

dielectric media have a lower dielectric constant.

During the design studies on this divider, it was found that if a grounded shield was placed around all resistors, and no capacitor was present across the measuring position, the transient characteristics were very unsatisfactory. Removing the grounded shield made an improvement and, even then, the position of the unit in respect to any ground conductor affected a change in the transient response. These were due to the distributed capacitance along the resistor chain. By adding the large capacitor across the metering position, one could then use a larger trimming capacitor. This did not eliminate the distributed capacitance, but did make its effect negligible, thus correcting the probe sensitivity to positioning. Tests conducted using a probe constructed this way gave transient responses of similar quality to that of the standard oscilloscope probes. Square waves from a high frequency square wave generator and pulses produced by a capacitor discharge through a resistor switched by a 2D21 thyratron were used for test signals.

Still a third style of convenient but non-absolute voltage measurement has been used. It has the advantage of being free from a need for mutual grounds between the oscilloscope and apparatus. It consisted of an ideal transformer with a step down ratio of 20:1 connected directly across a high impedance oscilloscope. A compact primary of 500 turns was wound on a large ferrite ring and insulated by mylar and epoxy resin potting from a compact secondary of 25 turns closely laid over the primary. The secondary voltage of such a transformer, if the coefficient of coupling is very near unity, will follow the primary voltage in detail.

Detection and measurement of the conductivity of expanding gases has been carried out a number of ways. Depending on whether the condition $\operatorname{div} \vec{i} = 0$ is fulfilled by complete orbits in the plasma, or must include an external circuit passing through cold electrodes in contact with the plasma, one measures either the electronic conductivity or the ionic conductivity. This will be discussed in Chapter X.

The first type of measurement is in general non-absolute and requires calibration against materials of known conductivity such as Hg, C, Al, and Cu. It may be realized in several ways. In one method (37) a resonant circuit comprising the tank circuit of a tuned-grid tuned-plate self-biasing push-pull oscillator was used as the conductivity detector. The circuit was allowed to oscillate at a level too low to produce light. In this condition moderate or weak shocks (non-ionizing shocks) produced no change in the grid-bias; however, the device was still very sensitive to small changes in the conductivity of the gas in the expansion chamber, providing the conductivity was not too large. When the conductivity became very large, losses in the gas reduced the sensitivity to zero by preventing the circuit from oscillating.

Another technique (37) for estimating conductivity made use of

a tuned radio frequency transformer wound coaxially on a half centimeter length of the expansion chamber. The primary of this transformer was connected to a 3 megacycle signal generator which furnished about 20 millivolts. When the gas was not conductive, the secondary furnished a 30 millivolt signal to an oscilloscope. The oscilloscope was triggered by the discharge in the heating chamber and usually used with a sweep speed close to 30 microseconds per centimeter. Only the modulation envelope of the 3 megacycle signal appeared in photographs of the oscilloscope trace. The second device was not nearly as sensitive as the first; hence it was not so easily saturated by large changes in the conductivity. For this last reason the second method could be used with greater success than the first behind the contact surface. A typical envelope is shown in Fig. 16.

Lin, et.al. (38), have used two adjacent coils coaxial with the shock tube with a steady magnetic field originating from one of them. The flow of the plasma displaces the magnetic field lines hydromagnetically so that a change of flux occurs in the second coil. This can be calibrated by firing metallic and metalloid slugs, designed in shape and size to imitate the plasma front, through the coil configuration before it is placed around the shock tube. Others (39) have checked the method and confirm its effectiveness.

Fig. 16. Conductivity Envelope

The second type of measurement is exemplified by the work of Clotfelter (40), and Sakuntala et. al. (41). The results of this method will be discussed in Chapter X. Two metallic probes are placed opposite each other in the flow, and insulated carefully up to the face of the probe. It is important that whatever insulation is used makes an inside connection to the probes, and does not touch near the face of the probe (Fig. 17). Otherwise the anomalous conductivity which is observed with many presumed insulators when bathed in plasma will give an uncertainty of area, and may even short circuit the two probes via the walls of the shock tube.

Fowler and Sakuntala have shown (42) that when highly ionized gases are in contact with normally nonconducting surfaces, especially glasses, superficial conductivity is observed over the nonconductor, and its magnitude seems to be a function of the ion (presumably electron) concentration in the plasma. At a plasma concentration of 10^{16} to 10^{17} ions/cc, superficial conductances of the order of 1 mho or less have been estimated.

The effect was observed in the course of probe measurements of

the type being described here. A flowing hydrogen plasma was passed down a tube through a transverse magnetic field, and probes were introduced into the plasma through holes in the glass walls. Normally the plasma resistances observed are of the order of 1000 ohms, but when the probes are allowed to touch the glass walls on both sides, the indicated resistance between the probes (while normally infinite in the absence of the plasma) is less than an ohm during the flow of the plasma past the probes.

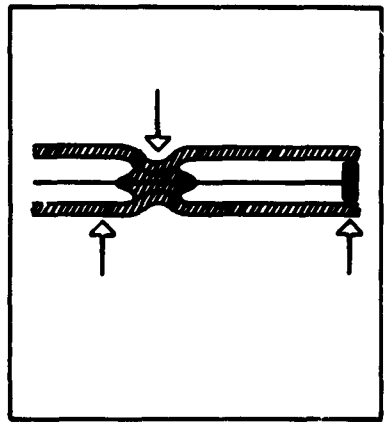

Probe Design

Fig. 17

It is believed that this effect is related to previously known probe effects in which sealing of probes directly into the ends of glass rods always results in apparent probe areas far greater than the area of metal exposed. This effect has been generally assigned to "working of the glass", but now appears to be a result of the superficial glass conductivity when a plasma containing electrons impinges upon the assembly.

Pyrex glass was the most striking material worked with, but similar though reduced effects were observed with Vycor. The effect was absent when plastics such as polystyrene were used as walls.

An external EMF can be applied to the probes, or a magnetic field can be placed mutually at right angles to the flow and the probe axes to give an internally generated induction EMF. In either case current into a known external resistor is measured, and in the latter case, by observing open circuit EMF's, flow velocities can be deduced as well.

It is necessary to take considerable precautions with the probe measuring circuit to ensure that there are no induction loops which couple with the main discharge currents. The last electrode of the shock tube should be at ground potential, the current return on the shock tube should be coaxial, and the external resistor in the probe circuit should be formed of two equal resistors, grounded at their midpoint, and physically perpendicular to the discharge column.

For weak signals, two low impedance cathode followers using parallel plate 417A triodes and made an integral termination of individual coaxial cables, were connected with their grid leads directly against the probe outputs from the shock tube. By rotating these triodes so that their electron flow was along the lines

of the magnetic field, their characteristics were unaffected by even very strong fields. A picture and circuit of the cathode follower unit is given in Fig. 18.

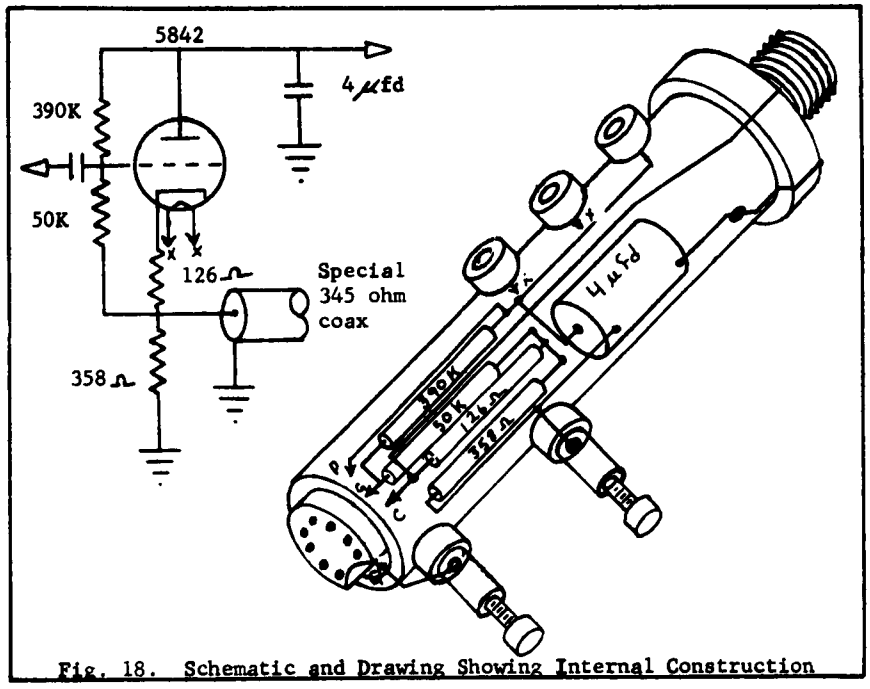

Fig. 18. Schematic and Drawing Showing Internal Construction

Measurement of pressures in the shock tube is usually made by inference from the shock velocities. Direct quantitative checks upon pressure are quite difficult in these high speed regimes because of the rapid mechanical response needed from the measuring system. Also, the mechanical systems needed are usually too bulky for use in the relatively small electric shock tubes. Whether or not mechanical detectors can be made to give useful quantitative information about the passage of moving shocks, they can serve a purpose for the study of pressure in the stagnant gas behind a reflected shock. Here the detector can be made the reflecting piston, so that it interferes with the flow pattern negligibly, and the relatively long duration of the plasma pressure gives adequate time for response. Atkinson (43) employed a steel-diaphragmed magnetic microphone as a shock detector in this configuration, but did not make exact quantitative measurements. Assuming his detector to have been linear, with a natural response frequency ω , the pressure could have been evaluated by taking the initial second derivative of the response signal S according to the expression

$$p = \frac{(S'')_o}{A\omega}$$

Estimates made showed that pressures of the order of atmospheres were indeed present in the reflected shocks as anticipated.

Piezoelectric crystals can be used in place of the diaphragmed microphone. Shielding of the crystal from electrostatic effects of the plasma can be done by grounding the face nearest the plasma, or by removing the crystal to an arbitrary distance at the end of a pressure bar according to the technique of Jones (45), who has applied these bars to the detection of plasma flow axially out of a transverse pinch.

One of the virtues of the electric shock tube is that it can, with suitable care, be made to deal with relatively pure gases. Experimenters in gaseous electronics have over the years developed techniques for enhancing the purity of their gases to a high degree (46). In all probability the purity needs of the electric shock tube are considerably less than the known art permits. Secondary reactions which play an important role in steady electrical discharges do not have time to take place here. Cross sections σ for such processes are characteristically $\sim 10^{-16}$ cm^2, agitation velocities v are $\sim 10^5$ cm/sec, total particle densities n are $\sim 10^{16}$ cm^{-3}, and one finds that since the time constant for entry of a foreign elatation species of concentration fraction f at the expense of a basic species is $1/T = (f\ n)\sigma v$, f need only be less than 10% to assure no more than a single generation of growth in 100 μsec. Standard methods of purification and handling are thus wholly adequate. Argon, helium, krypton, neon and zenon can be purchased spectroscopically pure. Hydrogen can be purified by passage through heated palladium thimbles. Oxygen is easily obtained from heated potassium permanganate, and nitrogen from gently heated sodium azide.

Two useful devices for gas handling and measurement have been devised locally in the course of this research. A hollow dosing stopcock which incorporates a bypass directly is shown in Fig. 19. Used in series with a cutoff stopcock on the gas reservoir, it makes it unnecessary to move the cutoff stopcock more than a few times in the life of the reservoir (during regreasing of the system), and reduces the total number of stopcocks needed by one. A double range Macleod gauge was designed for this work. By using two measuring capillaries of different size stacked with the smaller on top, and making two fiducial marks, one at the top of the small capillary, and one at or near the top of the large capillary, it was possible to have a dual range absolute gauge in which the ranges overlapped enough for precision measurement on all scales. A correction on the large capillary scale was needed for the unused volume above the lower fiducial mark. The gauge shown in Fig. 20 measured pressures from 10^{-5} to 20 mm Hg, and had the added advantage that it was often possible to detect the presence of condensible vapors by comparing the readings on the two scales.

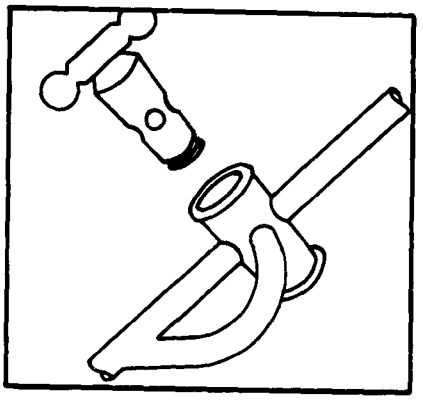

Dosing Stopcock with Bypass

Fig. 19

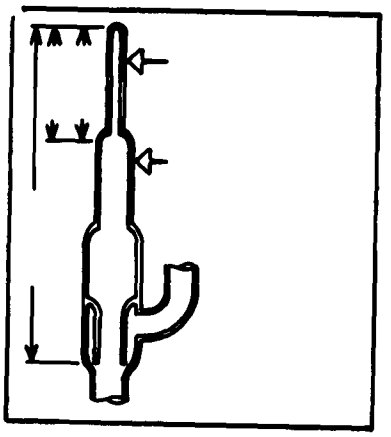

Double Range Macleod Gauge

Fig. 20

Investigation of shadow patterns around airfoils in mechanically driven shock tubes has been done by Geiger, Mautz, Hollyer, and Laporte (44). By application of this technique to electrically driven shocks, valuable information might be obtained. The basic experimental difference is the gas flow is luminous and will mask the shadows with the intense radiation which accompanies the electric discharge.

The shadow-graphing light source, to be acceptable, in this case needs a half intensity width of less than a microsecond. Also, if the light of the luminous gas can not be overridden, and must be filtered out, the spectra of the two radiations should not be identical.

The light source consisted of a confined air spark, similar to Geiger et. al. Fig. 20 (a). Their original design used a tickler electrode placed between the cathode and anode. When a high voltage pulse was sent to the tickler, a discharge was initiated between it and the cathode which triggered a spark discharge between the anode and the cathode. A small hole drilled through a glass plate confined the discharge along its entire path. Luminosity was high and its half intensity was 0.2 μ seconds.

The first source tried for generating the tickler pulse was an ignition coil; but its inherently slow voltage rise made the shortest time of initiation of discharge much too large. The second generator was a capacitor discharge utilizing a thyratron (5C22) for the switch. For some reason, there was serious time jitter in the main discharge initiation. This jitter could easily have been present, and would have been tolerable, in the conventional shock tube.

Using the second pulse generator, almost no time delay was observed between the small light pulse produced by the tickler electrode discharge, and the trigger pulse to the thyratron. From this consideration, a two electrode system was developed (Fig. 20 b).

Two 0.1 μfd capacitors were charged in parallel to 6 KV and then were switched by a 5C22 thyratron to a series configuration. When the electrode spacing of the spark unit was adjusted so that a spark could be initiated at a voltage only slightly over 6 KV, overvolting it with 6 KV caused an immediate spark. The light intensity was reduced to 80% of that of the 3 electrode system and the half intensity width was increased to 0.4 μ seconds.

Metal, (tungsten and aluminum), was eroded from the two electrodes and entrained in the tongue of flame which projected from the spark cavity. After a number of flashes, the discharge path became altered by deposited metal and the confining hole would have to be cleaned with carborundum. To protect the lens system, a clear glass shield was erected.

An accurate synchronizing system was needed. A phantastron was employed as the heart of this electronic delay. The stability of the phantastron warranted installation of a ten turn helipot for setting the delay.

The phantastron proved to be inherently sensitive to trigger pulse width and to negative pulses on the input grid. A circuit capable of negative pulse clipping and having a relatively short time constant for positive pulses was therefore introduced in its input circuit. Thus, all trigger pulses were reduced to a similar shape.

The output of the phantastron was a negative pulse of varying width with the delayed information appearing as its rise. A variable-time-constant differentiating circuit converted the pulse to a positive delayed pulse which controlled a grounded grid amplifier. The amplified positive pulse then triggered a 2D21 (gas tube) discharging a 0.25 μfd capacitor through a 1500 Ω resistor. From the resulting sharply rising voltage, the 5C22 in the spark light trigger circuit was ignited.

The phantastron proved insensitive to line voltage variation if both plate and filament voltages were simultaneously unregulated. Therefore, a very small inexpensive power supply was used which supplied 28 ma at 300 volts.

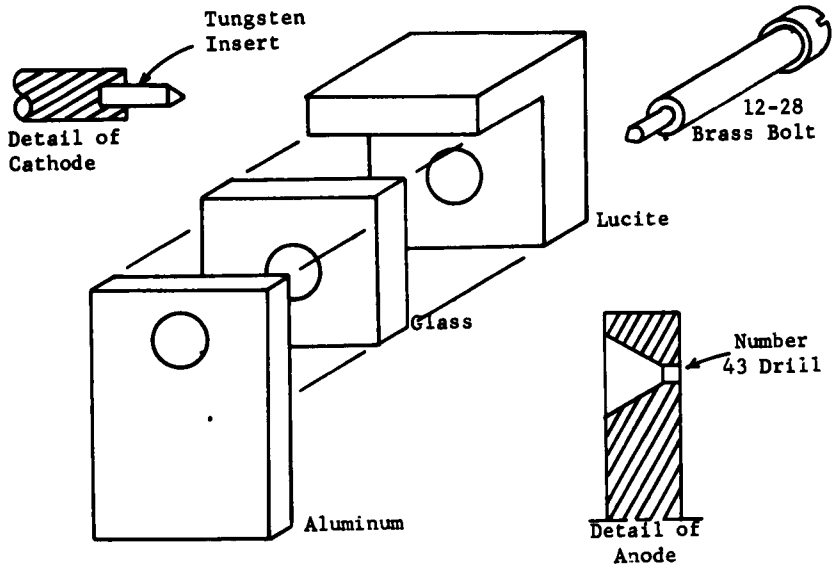

SPARK LIGHT SOURCE

Fig. 20 (a)

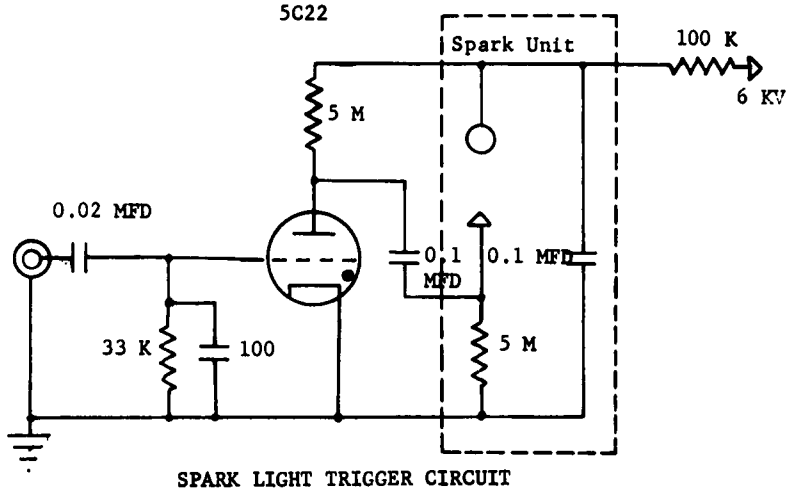

SPARK LIGHT TRIGGER CIRCUIT

Fig. 20 (b)

CHAPTER III

ELECTRICAL BEHAVIOR OF GASES IN THE DRIVER DISCHARGE

3-1 Empirical Relations. Gases for use in the electric shock tube are selected on a variety of bases, of which having a spectrum with a limited number of strong lines is one important consideration. Atomic mass is another, but in general molecular structure seems to be unimportant since nearly complete dissociation is achieved, in most regimes of operation. The electrical characteristics of seven gases, hydrogen, helium, oxygen, nitrogen, neon, argon, xenon have been studied in some detail. Potential differences and currents were measured oscillographically with carefully designed probes. Discharge inductance corrections were estimated and found to be negligible in this range of data, although they are of increasing importance at the higher current rise times found in more powerful apparatus.

The experiments were conducted with an open shock tube which allowed the heated gas to expand, and so the conductivity during the latter phases of the discharge might have been affected by the disturbed region around the electrode. However, measured rates of expansion, coupled with ideal gas theory, showed that the region of the discharge which was affected by the expansion during the entire discharge was never more than 10% of the interelectrode separation, and on the average over the range of data taken was of the order of 2%. Furthermore, carefully superimposed traces of both current and voltage show no electrical difference between open, expanding discharges and closed discharges over the entire pressure range in helium, where expansion velocities are the largest of any of the noble gases.

The resistance data for all seven gases were representable by an empirical formula discovered by Lee (47) and previously referred to, i.e.,

$$R = R_o e^{-\alpha t} + R_m + \frac{V_c}{I} \quad .$$

Further empirical analysis of the great mass of accumulated data shows that certain approximate dependences on operational parameters can be detected in these coefficients.

The exponent α was a constant for all conditions at $(5.4 \pm 1.0) \times 10^5$ sec^{-1}. The constant R_o was described by the equation $k_o \rho^{2/3}/V$, and the constant R_m was described by the equation $k_m \rho^{1/5}/V$, where ρ

is initial gas density in mm Hg and V is initial capacitor potential. The coefficients k_o and k_m varied with the nature of the gas and are given in Table III. The potential V_c is also given in Table III.

TABLE III

	Hydrogen***	Helium	Neon	Argon	Xenon	Oxygen***	Nitrogen***
k_o	450	150	70**	220	220	450	510
k_m	110	90	90	200*	175*	180	170
V_c		18±5	19±2	17±6	14±5		

*A somewhat better fit is obtained with $12\mathscr{p}^{1/5}/V^{2/3}$.
**Below 4 mm Hg. R_o is essentially pressure independent at 250/V ohms.
***Determined from much less data than the noble gas constants.

3-2 Theory of the Driver Discharge. The breakdown of the discharge chamber results in substantial ionization in a time interval very short compared with either the discharge of the capacitor or the expansion of the driver plasma. At the outset, during the transition upward from glow discharge levels of ionization the equation of chief interest in the ionization process is

$$\frac{\partial n_e}{\partial t} = \overline{\sigma_i v_e}\, n_e N,$$

where n_e is electron concentration, v_e is electron velocity, σ_i is ionization cross section, N is neutral molecule concentration, and the average is over the electron distribution. Generally Maxwell-Boltzman statistics are adequate. From this the time constant for attainment of the ionized state is

$$1/\tau = \overline{\sigma_i v_e} N.$$

The quantity $(\tau \mathscr{p})^{-1}$ is given in Fig. 21 (a,b,c,d) for various gases as a function of T_e. The meaning of $\mathscr{p}$ is often misunderstood. It is spoken of as "the pressure in mm Hg" but in fact one always means "the particle density in units of the density that would be present at 1 mm Hg and 0°C", i.e., in units of 3.54×10^{16} particles/cc. A script $\mathscr{p}$ will be used when this quantity is denoted, while a roman p will be used for true pressure.

The curves in Fig. 21 (a,b,c,d) are computed from a curve fit to the data of Smith (48) and others. Smiths data for helium fits with excellent precision (maximum error 5%) to the curve

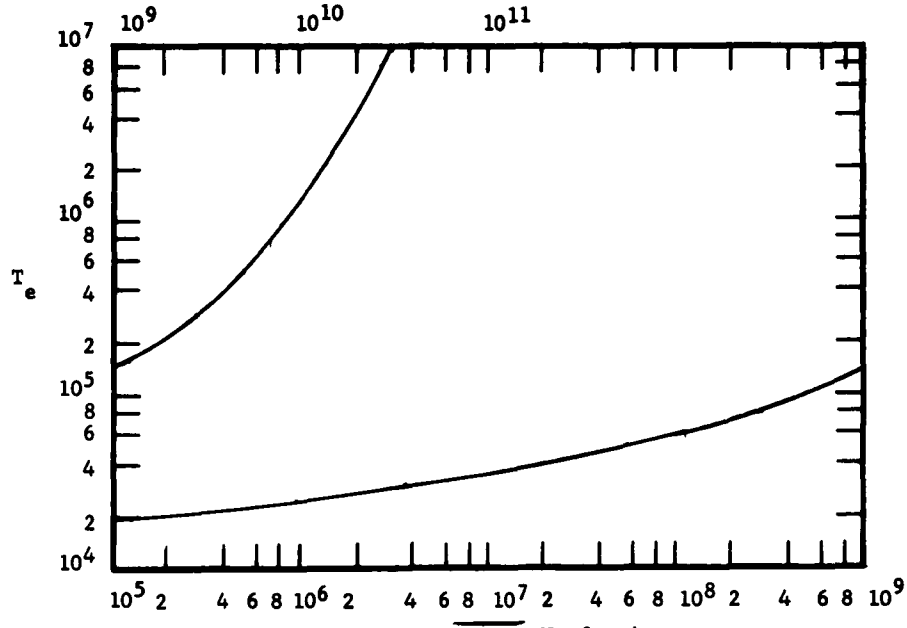

Fig. 21a $\overline{\sigma_i v_e}$ No for Argon

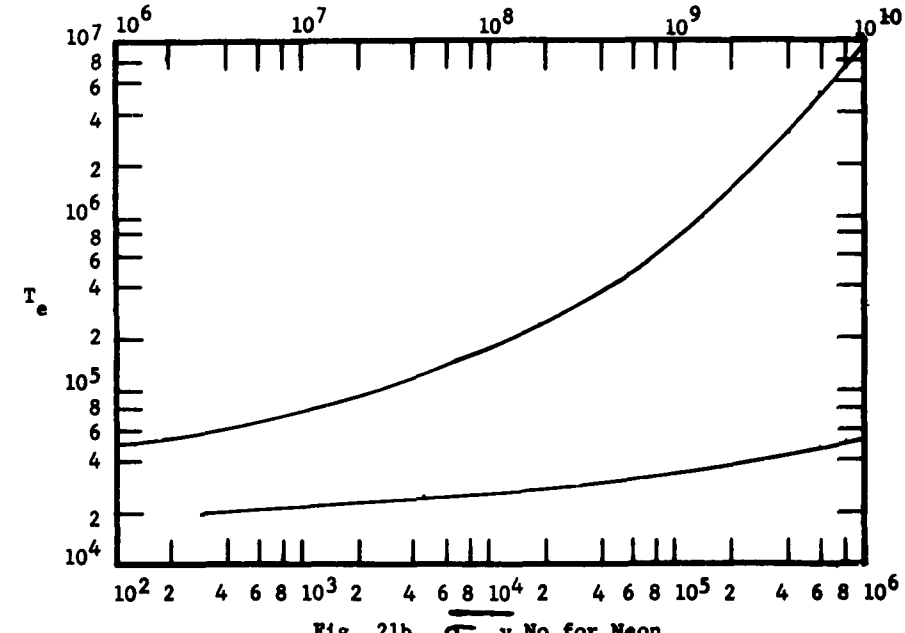

Fig. 21b $\overline{\sigma_i v_e}$ No for Neon

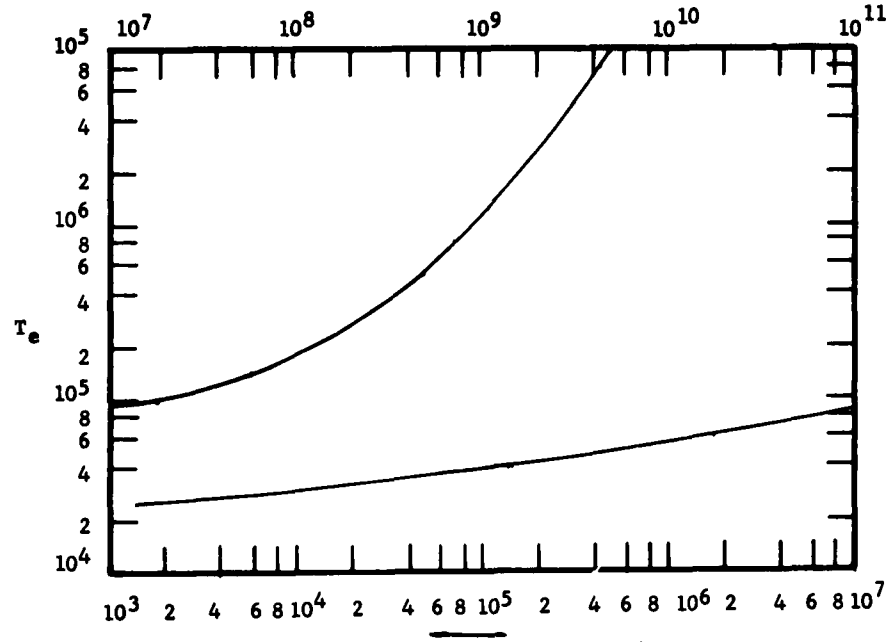

Fig. 21c $\overline{\sigma_i v_e}$ No for Helium

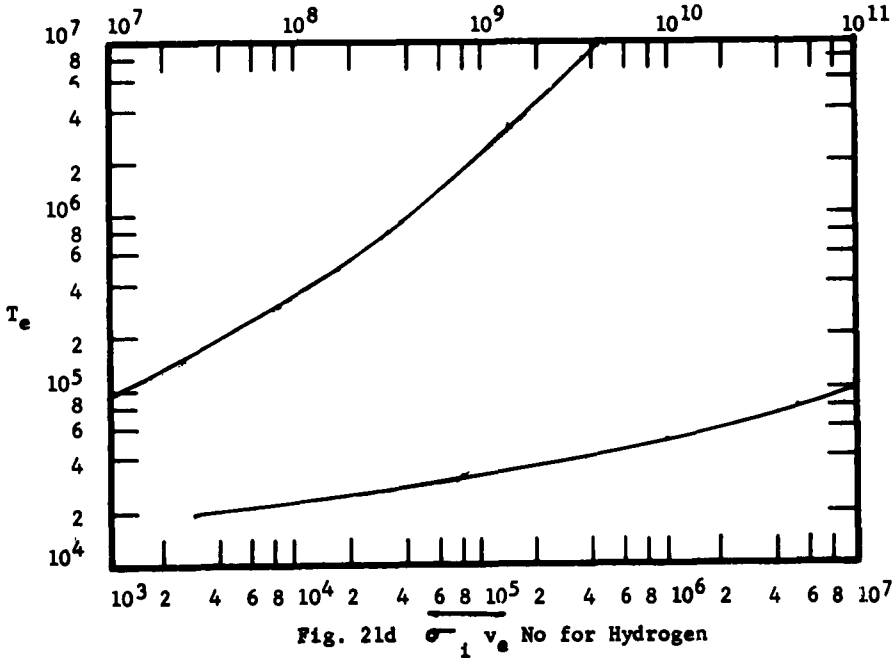

Fig. 21d $\overline{\sigma_i v_e}$ No for Hydrogen

$$\sigma_i = \sigma_o \frac{v_i^2}{v^2} \left(1 - \frac{v^2}{v_i^2}\right)^{\alpha}$$

where $\sigma_o = 4.6 \times 10^{-17}$ and $\alpha = 1.10$. Here v_i is the velocity of an electron with 24.5 ev energy. Other gases do not fit quite as well to this curve, especially at electron energies above 500 ev, but are certainly usable for many purposes. The corresponding parameters are given in Table IV.

TABLE IV

Ionization Curve-Fit Parameters

	σ_o	α
Helium	4.6×10^{-17}	1.10
Neon	5.4×10^{-17}	1.25
Argon	4.6×10^{-16}	1.00
Hydrogen (atomic)	6.8×10^{-18}	1.50

The time constant τ for one e-folding does not tell the whole story. Because the rise of ionization is from some low value of order $n_o = 10^1$ ions/cc to a value of order $n_f = 10^{16}$ ions/cc, the actual time elapsed toward full ionization is extended $\ln (n_f)/n_o$ times, a factor which is not much different from 30, considering practical ranges of the values of n_f and n_o. It is important to notice, however, that merely one or at most two e-foldings can bring the ionization from the relatively low 10% levels to the high 90% levels, so that attainment of full ionization may seem to come about with a long induction or delay period when nothing much is happening, followed by a very rapid rise period of the order of τ.

As the ionization process nears its end, the slower internal processes of diffusion, saturation and recombination together with the external circuit limitations on the current available take over to modify this result, and it is these processes which govern the ultimate level of the ionization in the column. The balance equation for electron concentration then becomes

$$\frac{\partial n_e}{\partial t} = \overline{\sigma_i v_e} n_e (N - n_e) - \alpha n_e^2 + D \nabla^2 n_e.$$

Here α is the recombination coefficient and D is the ambipolar diffusion coefficient.

Diffusive effects can generally be neglected in the early stages of the breakdown where things happen too quickly for diffusion to act. Ionization proceeds more or less uniformly across

the section of the discharge, with small gradients and smaller curvatures to the concentration curves, except near the walls. Here we can apply the linearized theory (49) of the positive column to make an estimate of the importance of diffusion.

The solution of the radial field equation of the column is rapidly varying only near the wall, even when n_e varies at its most (as $J_o(r)$). Hence we assume that near the wall, in terms of a coordinate x measured inward from the wall, $n_e = a + bx$. Then the equation becomes

$$\frac{d^2 E}{dx^2} - \frac{4\pi e^2 D_e}{k T_e D_+} (a + bx) E = + \frac{4\pi e D_e}{D_+} b.$$

This equation has as its exact solutions Bessel functions of 1/3 order, but is adequately approximated for our purposes by neglecting bx in a + bx to give

$$E = \frac{k T_e b}{e a} e^{-\theta x} - 1, \text{ with } \theta = \frac{4\pi e^2 D_e a}{k T_e D_+}.$$

The constants a and b we determine as follows: $n_+(0) = 0$, so

$$\left(\frac{\partial E}{\partial x}\right)_0 = - 4\pi e a = -\sqrt{\frac{4\pi k T_e D_e}{D_+ a}}.$$

But a is very nearly equal to n_e, the value of concentration in the column center, because the equation $n_e = a + bx$ only applies for a short distance, after which n_e is constant. Then

$$b = \sqrt{\frac{4\pi e^2 D_+}{k T_e D_e}} n_e^{3/2}.$$

Diffusive loss from a unit length of volume is therefore

$$2\pi R \sqrt{\frac{4\pi e^2 D_+ D_e}{k T_e}} n_e^{3/2}.$$

This must be compared with the other losses for an assessment of significance. Electronic recombination and saturation both have the same concentration dependence, i.e., the combined loss per unit length of tube is

$$(\alpha + \overline{\sigma_i v_e})\, n_e^2\, \pi R^2.$$

Let us first compare (as far as possible) recombination and saturation using helium as an example. A composite curve of the data of Townsend (50), von Engel (51), and Bickerton (52) has been used to convert the abscissas from electron temperature to E/p. Radiative recombination coefficients have been estimated from Cillie's formula (53) for hydrogen-like atoms. Comparison has also been made with Smit statistics. From Fig. 22 it is concluded that for $E/p > 10$ saturation will always be dominant over radiative recombination.

Comparison with dissociative recombination represents a greater problem because the energy dependence of this process is not certain, because also the necessary helium molecules will not be stable under the intense electron bombardment in the discharge, and because of depletion of neutrals which could form molecules in this highly ionized gas. It probably is not much more effective than radiative recombination in these surroundings, and so the rough rule $E/p > 10$ still applies. Atkinson (37) found evidence of dissociative recombination at high pressures (100 mm Hg) in the shock tube which will be discussed in Chapter VI.

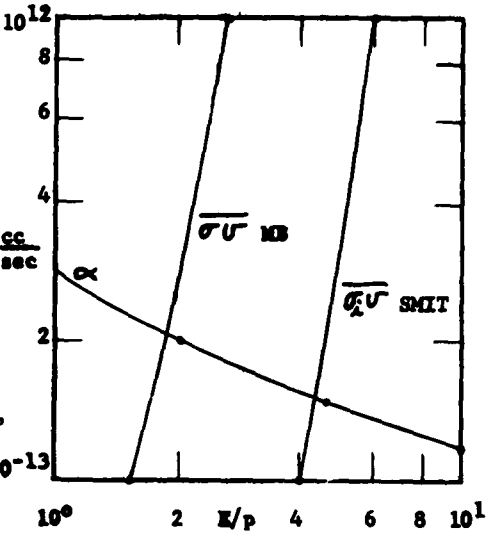

Fig. 22

Because of the saturation term $\overline{\sigma_i v_e}\, n_e^2$ is at most equal to the production term $\overline{\sigma_i v_e}\, n_e N$, we must use the latter for comparison in establishing the importance of the diffusion term. Then the ratio of the production term to the diffusion loss is

$$4\epsilon(\gamma p)(p D_+)\left(\frac{\pi N_0}{k T_+ \epsilon}\right)^{\frac{1}{2}}\left(\frac{\alpha}{p^{3/2} R}\right)^{\frac{1}{2}}$$

where ϵ is $(D_+ T_-)/D_- T_+$, a slowly varying function of electron temperature (given for helium in Fig. 23), and α is the fraction of ionization. The entire coefficient of the variable term ($\alpha^{1/2}/p^{3/2} R$) is plotted as a function of E/p in Fig. 24, by the same technique of estimation of E/p as in Fig. 22. In general $p \gtrsim 1$ mm Hg and $R \lesssim 1$ cm, while the variable factor α is of order 0.5 for most of the interesting cases. It follows from

Curve I of Fig. 24 that the diffusion term often exceeds even the production term for ion concentrations beyond very early ones prevailing in the tube. Other curves plotted on Fig. 24 give further insight. Curve II gives the value of α at which production is exceeded by diffusion in the nominal case $p^{3/2} R = 1$. Curve III gives the time at which this occurs in abscissal units of seconds times initial pressure in mm Hg. Curve IV gives the time required for a plasma shock generated by the given E/p to move the nominal distance of 1 cm. Clearly the calculations embodied in these curves can be extended to a particular situation. Points lying on the right hand sides of curves II and III are production limited, and on the left sides are diffusion limited.

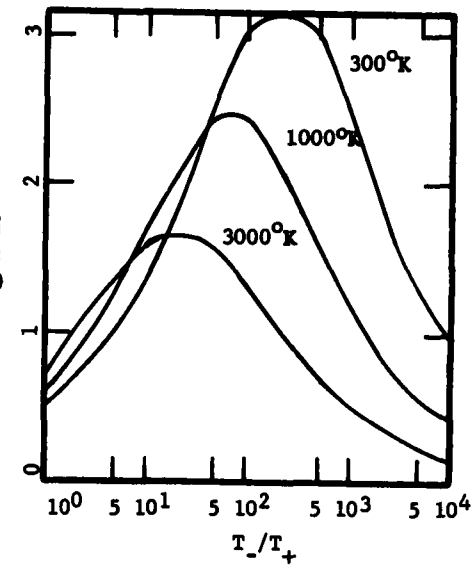

Fig. 23

Since the ultimate performance of the driver discharge has proven to be diffusion limited, the equations that must be solved to describe ion concentration in it are

$$\frac{\partial n_e}{\partial t} = \overline{\sigma_i v_e} N n_e + D_e \left(\nabla^2 n_e + \frac{e}{k T_e} \nabla \cdot E n_e \right)$$

$$\frac{\partial n_+}{\partial t} = \overline{\sigma_i v_e} N n_e + D_+ \left(\nabla^2 n_+ - \frac{e}{k T_+} \nabla \cdot E n_+ \right).$$

One must also write two equations for energy balance, the more important of which is the electron equation. Here the time rate of change of internal energy is equated to the electrical power gain, minus the rate potential energy is going into ionization and the rate that electron kinetic energy is being transferred to the volume by diffusion of particles. A term might also be included for heat conduction, but it will be assumed with reason that space derivatives of the electron temperature are negligible. Then

$$3/2\ k \frac{\partial n_e T_e}{\partial t} = i_e \cdot E - e V_i \overline{\sigma_i v_e} N n_e - \frac{m^2}{M} \overline{\sigma_m v_e^3} N n_e$$

$$+ 3/2\ k T_e D_e \left(\nabla^2 n_e + \frac{e}{k T_e} \nabla \cdot E n_e \right).$$

Here V_i is the ionization energy and σ_m is the elastic cross section.

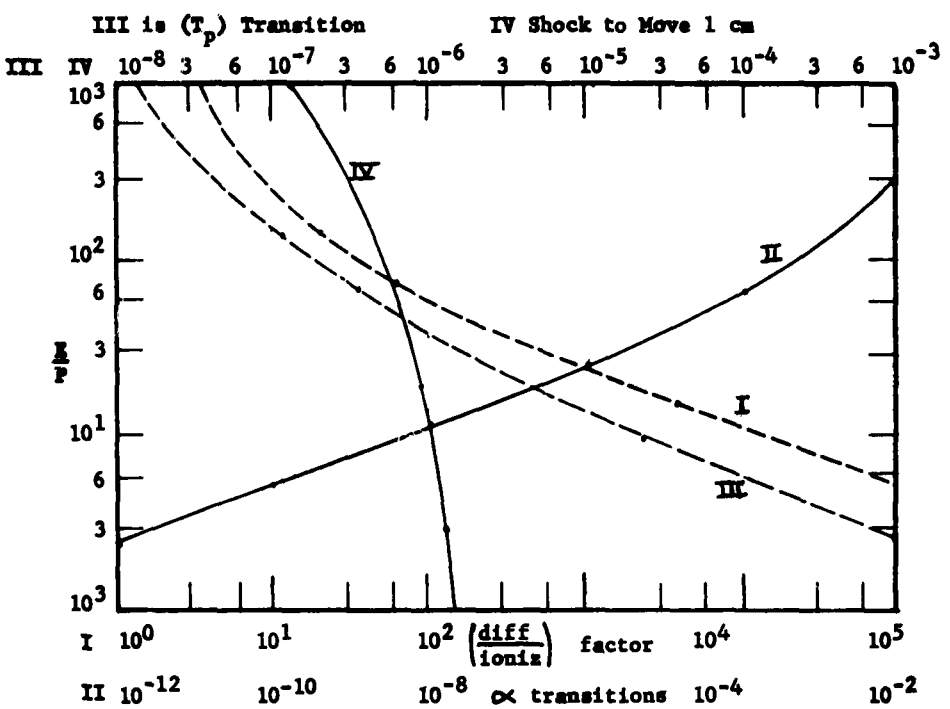

Fig. 24

The energy equation for the heavy particles reduces to

$$3/2\ k \frac{\partial T_+}{\partial t} = \frac{m^2}{M} \overline{\sigma_m v_e^3}\ n_e.$$

Further consideration of the equation for electron energy under the conditions of these experiments shows that $(\partial T_e)/\partial t$ is small compared with the energy fluxes in the other terms; that i_e is essentially the total current, and that E is the axial field. Then combining the energy equation with the diffusion equation and setting $n_+ = n_e = n$ yields

$$i E_z = (e V_i + 3/2\ k T_e) \overline{\sigma_i v_e}\ N n + \frac{m^2}{M} \overline{\sigma_m v_e^3}\ N n.$$

Linearizing the ion balance equations one derives the Schottky equation and radial field equation under the local neutrality and

ambipolarity conditions.

$$\frac{\partial n}{\partial t} = D \nabla^2 n + \overline{\sigma_i v_e} \, n N \qquad \left(D = \frac{T_e}{T_+} D_+ \right)$$

$$\frac{i}{e} - \frac{1}{4\pi e} \frac{\partial E}{\partial t} = D_e \nabla n - \frac{D_+}{4\pi e} \nabla (\nabla \cdot E) + \frac{D_e e}{k T_e} n E .$$

Finally the application of Kirchhoff's 2nd law to the entire circuit gives

$$L \frac{dI}{dt} + RI - Q/C + \ell E_z = 0,$$

it being assumed that there is a uniform field in the column. Here Q is the charge on the capacitor and ℓ is the length of the discharge chamber.

The empirical data apply to a time well after breakdown. In this regime the Schottky equation separates into a space equation

$$\frac{1}{r} \frac{\partial}{\partial r} r \frac{\partial R}{\partial r} + \lambda^2 R = 0$$

of which the solution is $J_o(\lambda R)$, and a time equation

$$\frac{dn}{dt} = (\overline{\sigma_i v_e} N - \lambda^2 D) \, n.$$

The radial field equation has two vector components

$$\frac{i}{e} - \frac{1}{4\pi e} \frac{\partial E_z}{\partial t} = \frac{e D_e}{k T_e} n E_z$$

and

$$- \frac{1}{4\pi e} \frac{\partial E_r}{\partial t} = D_e \frac{\partial n}{\partial r} - \frac{D_+}{4\pi e} \frac{\partial}{\partial r} \frac{1}{r} \frac{\partial r E_r}{\partial r} + \frac{D_e n e E_r}{k T_e} .$$

All processes are quasi-static, and the time derivatives of E will be set equal to zero.

The effective equations of the low pressure pulsed discharge are recapitulated below:

$$i = \frac{D_e e^2 E_z}{k T_e} n$$

$$i E_z = (e V_i + 3/2\ k T_e) \overline{\sigma_i v_e}\ n N + \frac{m^2}{M} \overline{\sigma_m v_e^3}\ N n$$

$$L \frac{di}{dt} + R i - \frac{q}{C} + \frac{\ell}{A} E_z = 0$$

$$i = - \frac{dq}{dt} \left(= - \frac{1}{A} \frac{dQ}{dt} \right)$$

$$\frac{dn}{dt} = (\overline{\sigma_i v_e} N - \lambda^2 D) n$$

The new symbol A is the area of the discharge chamber. The first two equations can be rewritten as

$$E_z^2 = \frac{k T_e}{e^2 D_e} \left[(e V_i + 3/2\ k T_e) \overline{\sigma_i v_e} N + \frac{m^2}{M} \overline{\sigma_m v_e^3} N \right]$$

and

$$i^2 = \frac{e^2 D_e}{k T_e} \left[\frac{(e V_i + 3/2\ k T_e)}{e} \overline{\sigma_i v_e} N + \frac{\frac{m^2}{M} \overline{\sigma_m v_e^3} N}{e} \right] n^2$$

E_z is given as a function of T_e for helium in Fig. 32-A.
The properties of these equations are determined chiefly by the dramatic variation of the ion production function $\overline{\sigma_i v_e} N$ in time. Small variations of electron temperature can produce large changes in this quantity. We therefore introduce the function $\overline{\sigma_i v_e} N$ as a new variable α, rewriting the equations as

$$E_z^2 = \left[(e V_i + 3/2\ k T_e) \alpha + \frac{m^2}{M} \overline{\sigma_m v_e^3} N \right] \frac{k T_e}{e^2 D_e}$$

$$i^2 = \frac{e^2 D_e}{k T_e} \left[(e V_i + 3/2\ k T_e) \alpha + \frac{m^2}{M} \overline{\sigma_m v_e^3} N \right] n^2$$

$$\frac{dn}{dt} = (\alpha - \lambda^2 D) n.$$

Differentiating the second equation logarithmically with respect to the time, and replacing (dn)/dt by the ion balance relation,

$$\frac{2}{i}\frac{di}{dt} = \frac{(e V_i + 3/2\ k T_e)\frac{d\alpha}{dt}}{(e V_i + 3/2\ k T_e)\alpha + \frac{m^2}{M}\overline{\sigma_m v_e^3}\, N} + \frac{2}{n}\frac{dn}{dt}$$

$$= \frac{(e V_i + 3/2\ k T_e)}{(e V_i + 3/2\ k T_e)\alpha + \frac{m^2}{M}\overline{\sigma_m v_e^3}\, N}\frac{d\alpha}{dt} + 2(\alpha - \lambda^2 D)$$

This has the formal integral

$$\frac{(e V_i + 3/2\ k T_e)}{(e V_i + 3/2\ k T_e)\alpha + \frac{m^2}{M}\overline{\sigma_m v_e^3}\, N} = i^{-2} \exp^{-2}\left(\frac{\lambda^2 D + \frac{m^2}{M}\overline{\sigma_m v_e^3}\, N}{e V_i + 3/2\ k T_e}\right) t$$

$$\int 2i^2 \exp^2\left(\frac{\lambda^2 D + \frac{2m^2}{M}\overline{\sigma_m v_e^3}\, N}{e V_i + 3/2\ k T_e}\right) t\, dt$$

By use of the differential equation for the circuit the integration can be completed in closed form if the contribution of the discharge tube to the circuit (i.e., $d E_z/dt$) is negligible. This is certainly not true at the outset of discharge, but becomes progressively more valid in the critically damped case for which the empirical data are available. Failure to include this term probably accounts for our lack of success in obtaining the empirical results known for small times t. One obtains now

$$\frac{(e V_i + 3/2\ k T_e)\lambda^2 D + \frac{m^2}{M}\overline{\sigma_m v_e^3}\, N}{(e V_i + 3/2\ k T_e)\alpha + \frac{m^2}{M}\overline{\sigma_m v_e^3}\, N} =$$

$$\left[\frac{\left(1 - \frac{3R}{aL} + \frac{2R^2}{a^2L^2} + \frac{2}{a^2LC}\right) + \left(\frac{i'}{i}\right)\left(-\frac{2}{a} + \frac{4R}{a^2L}\right) + \frac{2}{a^2}\left(\frac{i'}{i}\right)^2}{\left(1 - \frac{3}{a}\frac{R}{L} + \frac{2R^2}{a^2L^2} + \frac{4}{a^2LC} - \frac{4R}{a^3L^2C}\right)}\right] + C_1\, i^{-2}\, e^{-at}$$

where $\underline{a}$ is the time coefficient in the exponent from the previous equation.

If this solution is returned into the original equation for $\underline{i}$, it will be a solution if

$$C\left(1 - \frac{R}{aL} \quad \frac{2\alpha}{a}\right) = 0. \qquad \left[\alpha = \sqrt{\frac{R^2}{4L^2} - \frac{1}{LC}}\right].$$

To choose the parenthesis equal to zero results in an expression for the time dependence which does not behave properly at $t \to \infty$. Therefore we choose $C \equiv 0$. Then the final form of the solution is

$$\frac{(e\,V_i + 3/2\,k\,T_e)\,\lambda^2\,D + \frac{m^2}{M}\,\overline{\sigma_m\,v_e^3}\,N}{(e\,V_i + 3/2\,k\,T_e)\,\alpha + \frac{m^2}{M}\,\overline{\sigma_m\,v_e^3}\,N} =$$

$$= \left[\frac{e^{2\alpha t}\Big/\left(1 - \frac{R}{aL} + \frac{2\alpha}{a}\right) - \frac{2}{(1 - R/aL)} + e^{-2\alpha t}\Big/\left(1 - \frac{R}{aL} - \frac{2\alpha}{a}\right)}{(e^{\alpha t} - e^{-\alpha t})^2}\right]$$

$$= \left[\frac{e^{2\alpha t}\Big/\left(1 - \frac{R}{aL} + \frac{2\alpha}{a}\right) - \frac{2}{(1 - R/aL)} + e^{-2\alpha t}\Big/\left(1 - \frac{R}{aL} \quad \frac{2\alpha}{a}\right)}{4\,L^2\alpha^2\,e^{R/L\,t}\,I^2\,V_o^2}\right]$$

It follows now that the tube resistance $\frac{V}{I} = \frac{\alpha E_z}{I}$ is given by the expression

$$\frac{V}{I} = \frac{\frac{2\alpha L\alpha}{V_o}\sqrt{\left(\frac{k\,T_e}{e^2\,D_e}\right)\left[(e\,V_i + 3/2\,k\,T_e)\,\lambda^2\,D + \frac{m^2}{M}\,\overline{\sigma_m\,v_e^3}\,N\right]}}{\sqrt{e^{(2\alpha - R/L)t}\Big/\left(1 - \frac{R}{aL} + \frac{2\alpha}{a}\right) - \frac{2e^{-R/L\,t}}{(1 - R/aL)} + e^{-(2\alpha + R/L)t}\Big/\left(1 - \frac{R}{aL} - \frac{2\alpha}{a}\right)}}$$

This function possesses the general properties found empirically, although it indicates that for many purposes a form of analysis of the data superior to the one used could now be devised. Of particular interest are the inverse dependence on V_o, and the behavior as inverse I for large t. The behavior from i_{max} toward small t seems to be present in the equations, but has not been successfully obtained explicitly as yet.

The solution of the equations at and around t = 0 is not adequately described by these results. Here the basic equations are the power equation as before, but including the term in $(d\ T_e)/dt$. The field in the tube will be assumed to be fixed at $E_o = V_o/\ell$, while the current will be rising as $I = V_o\ t/L$. Eliminating the production term from the power equation by use of the ion balance equation, the former can be written

$$\frac{d}{dt}\, n(3/2\ k\ T_e + e\ V_i) = \frac{V_o^2}{Lv}\, t - \frac{m^2}{M}\, \overline{\sigma_m\, v_e^3}\, N\, n - \lambda^2\, D\, n\, e\, V_i$$

where v is the volume of the discharge vessel. Then

$$n = \frac{k\ T_e}{e^2\ D_e}\, \frac{i}{E_z} = \frac{k\ T_e\ t\ell}{e^2\ D_e\ AL}$$

Hence

$$\frac{d}{dt}\, (3/2\ k\ T_e + e\ V_i)\, \frac{t\ k\ T_e\ \ell}{e^2\ D_e\ AL} = \frac{V_o^2\ t}{Lv} - \left[\frac{m^2}{M}\, \overline{\sigma_m\, v_e^3}\, N + eV_i\, \lambda^2 D\right] \frac{kT_e t\ \ell}{e^2 D_e AL}$$

This equation shows that T_e stabilizes at a value given by

$$\left(\frac{m^2}{M}\, \overline{\sigma_m\, v_e^3}\, N + eV_i \lambda^2 D\right) \frac{kT_e\ \ell}{e^2 D_e\ LA} - \frac{V_o^2}{Lv} - \frac{(3/2\ k\ T_e + e\ V_i) k\ T_e \ell}{t\ e^2\ D_e\ LA} = 0.$$

The time beyond which the stabilization takes place determines the character of the early wave motions from the electric shock tube. Let t_c be the critical time at which the third term equals the first. Then

$$t_c = \frac{3/2\ k\ T_e + e\ V_i}{\left(\frac{m^2}{M}\, \overline{\sigma_m\, v_e^3}\, N + e\ V_i\, \lambda^2 D\right)}$$

and the temperature which will be attained beyond this time is given by

$$\frac{E_o}{p} = \left(\frac{kT_e}{e}\right) \left[\frac{\frac{m^2}{M}\, \overline{\sigma_m\, v_e^3} + \frac{e\ V_i\ \lambda^2\ D}{p^2\ N_o^2}}{p\ D_e\ k\ T_e}\right]^{\frac{1}{2}}$$

We hypothesize that if t_c is less than the time required for electrons at the temperature T_e to escape to the tube wall, either by free escape ($t = r/\overline{v_e}$) or diffusion ($t = 1/\lambda^2 D$) breakdown will occur as a flash discharge and shock waves can be generated electrically. Fig. 25 shows the result of this analysis in helium. There is a critical field for each pressure, and below a limiting pressure-times-radius no discharge at all is possible. Theory and experiment agree in setting this limiting pressure at around 0.2 mm Hg x cm in helium in tubes of 1.5 cm diameter. It is noteworthy that this critical field curve resembles the Paschen curve, but is in no way the same phenomenon.

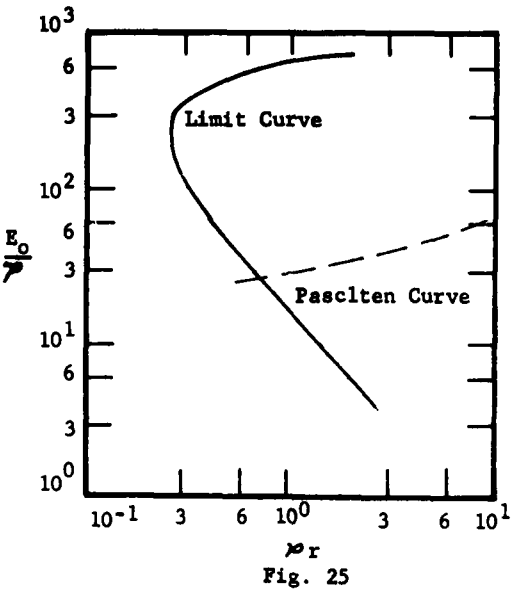

Fig. 25

3-3 Energy Input Efficiencies. Although the empirical resistance function is sufficient for calculation of energy input to a given driver gas, Flansburg (54) has computed the energy input in various cases, and it is often worth while to have these curves readily available. They are given in Fig. 26 to 30 as the total energy delivered to the driver from a 15 μfd capacitor. In Fig. 31 the fraction of energy delivered as a function of time is also given. The driver was 15 cm long and 1.5 cm in diameter.

3-4 Maxwell-Boltzman Averages of Gas Properties. Numerous measurements are available of the cross sections for various molecular processes as a function of particle velocity, (55). In general these must be averaged over the electron distribution to be of maximum usefulness for the kinds of computations envisioned above.

Goldman (56) has programmed computer averages of elastic collision frequency and elastic power loss by Maxwell-Boltzmann electrons, and these curves are given in Appendix I.

3-5 Non-linear Situations. A final note on the possibility of solutions when the discharge approaches saturation ionization follows. We consider the equation for ion concentration. Although non-linear, we assume that the effect of its non-linearity is essentially upon the time rather than the space dependence. Thus

$$D\left(\frac{\partial^2 n}{\partial r^2} + \frac{1}{r}\frac{\partial n}{\partial r}\right) + \overline{\sigma_i v_e}\, n\,(N-n) = \frac{\partial n}{\partial t}\,.$$

Dividing (1) by n^2 one obtains

$$-\frac{D}{r}\left(\frac{\partial}{\partial r} r \frac{\partial 1/n}{\partial r}\right) + \frac{2D}{n^3}\left(\frac{\partial 1/n}{\partial r}\right)^2 + \overline{\sigma_i v_e}\left(\frac{N}{n} - 1\right) = -\frac{\partial 1/n}{\partial t} .$$

It is possible to neglect the non-linear term, as will be justified later.

We separate with

$$\frac{1}{n} = RT + \frac{1}{N}$$

whence

$$\frac{1}{r}\frac{\partial}{\partial r} r \frac{\partial R}{\partial r} = +\lambda^2 R \text{ and } \frac{\partial T}{\partial t} = (\lambda^2 D - \overline{\sigma_i v_e} N) T$$

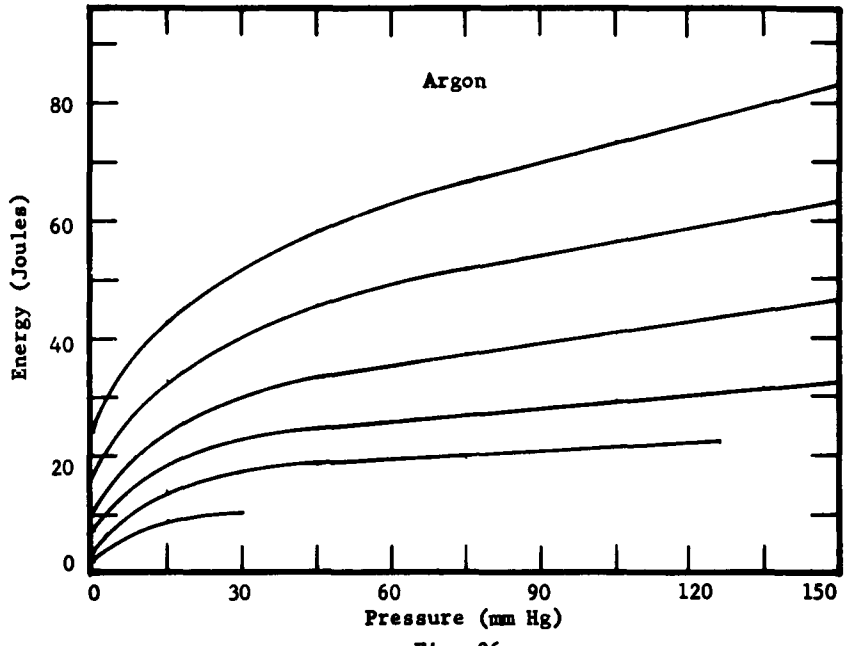

Fig. 26

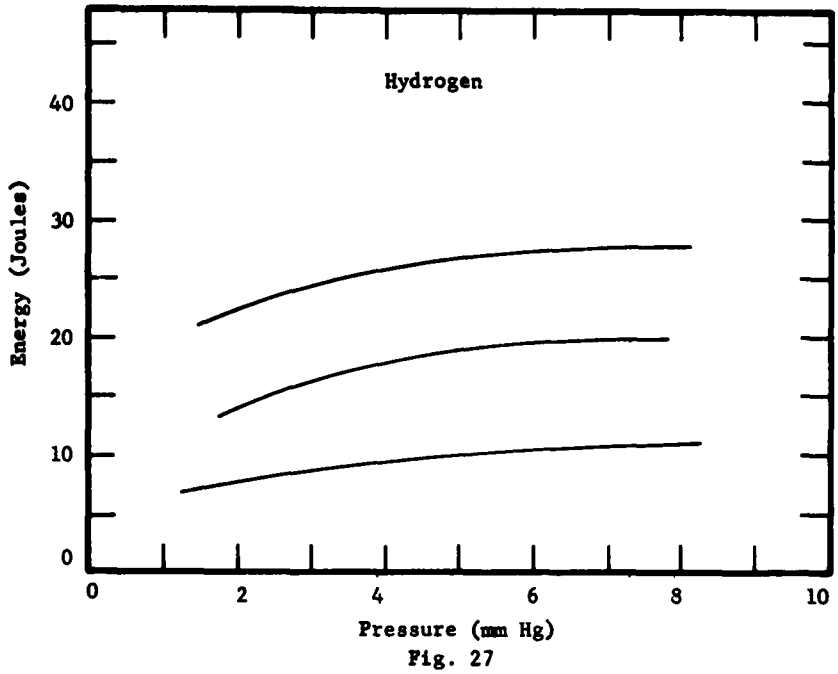
Hydrogen
Energy (Joules)
0
10
20
30
40
0
2
4
6
8
10
Pressure (mm Hg)

Fig. 27

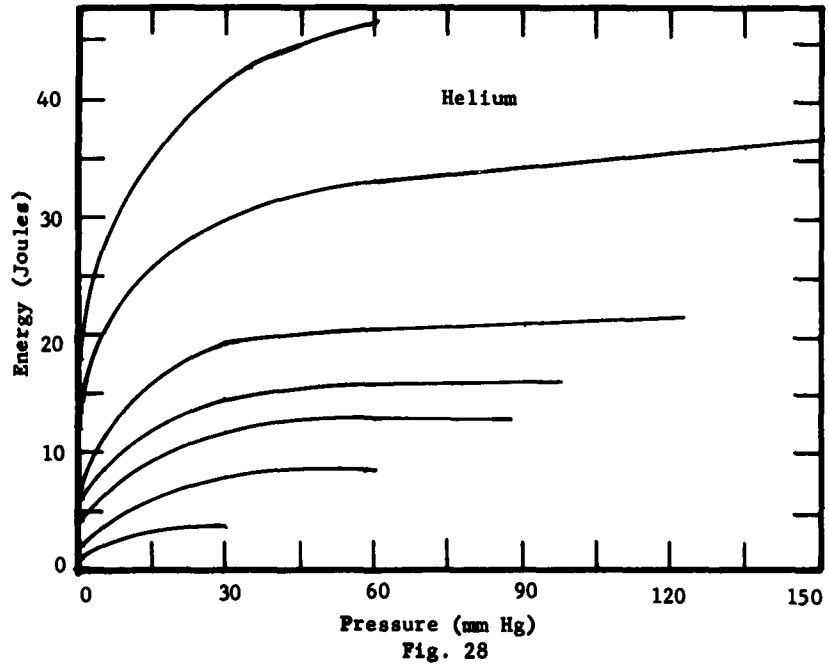
Helium
Energy (Joules)
0
10
20
30
40
0
30
60
90
120
150
Pressure (mm Hg)

Fig. 28

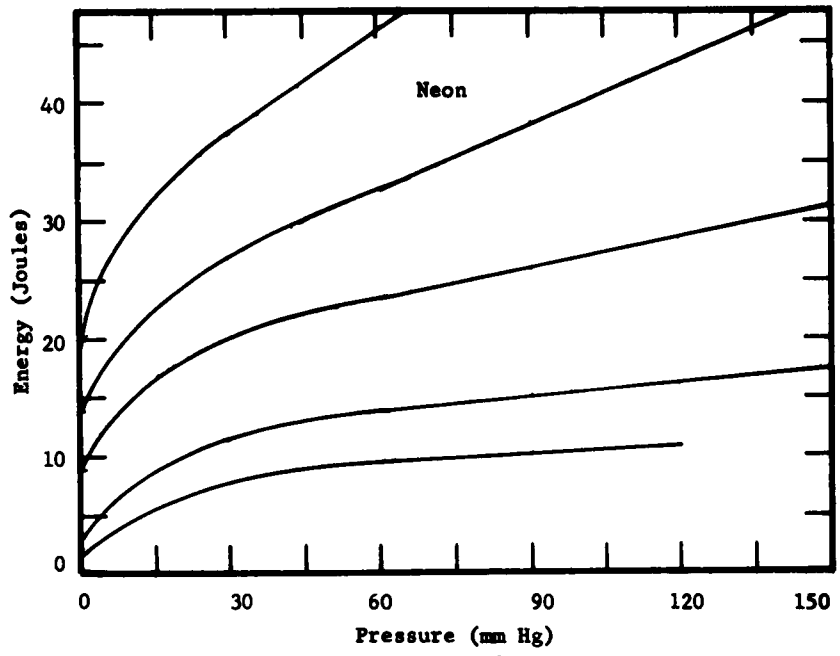
Neon
Energy (Joules)
0
10
20
30
40
0
30
60
90
120
150
Pressure (mm Hg)

Fig. 29

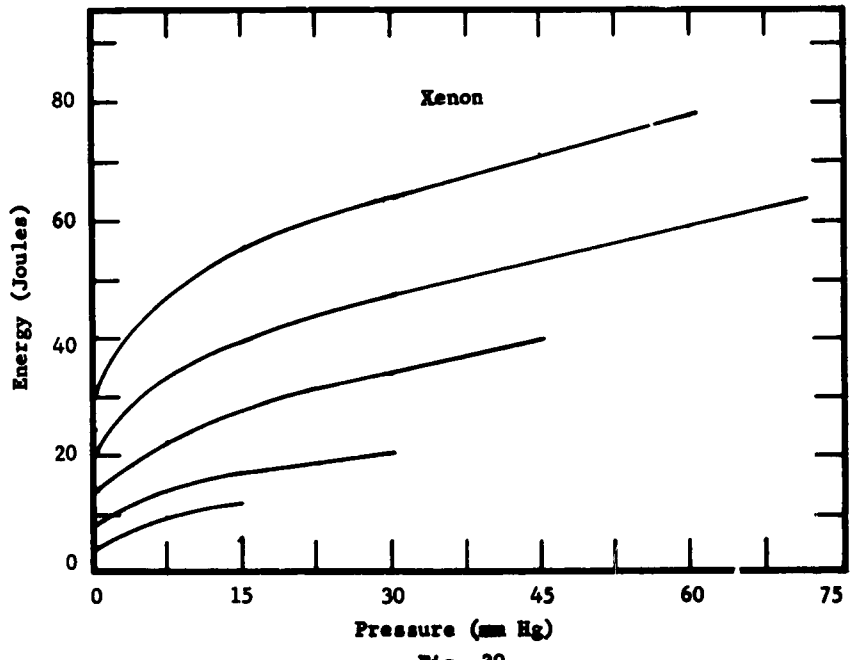
Xenon
Energy (Joules)
0
20
40
60
80
0
15
30
45
60
75
Pressure (mm Hg)

Fig. 30

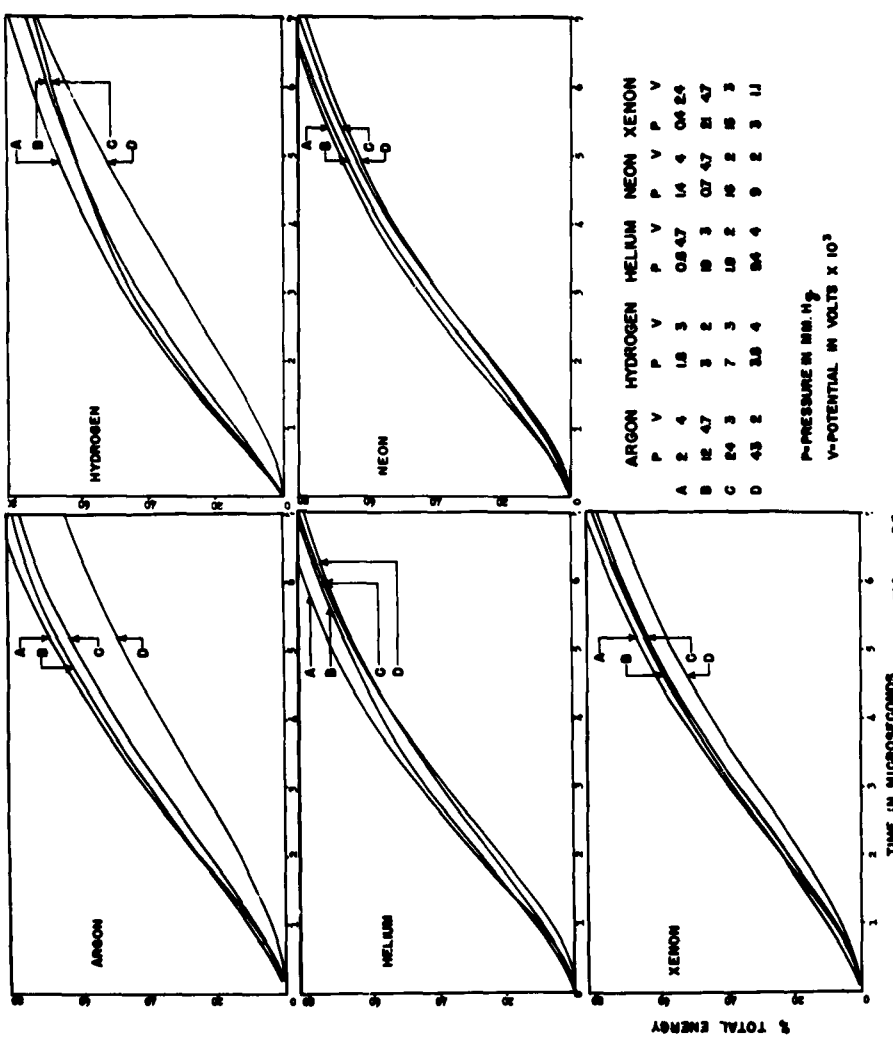

Fig. 31 Power Inputs

and

$$\left(\frac{1}{n_o} - \frac{1}{N}\right) e^{\int(\lambda^2 D - \overline{\sigma_i v_e} N)dt} \quad J_o (i \lambda r)$$

is the solution. Here n_o = central concentration of electrons at time t = 0. Subsequent work in Chapter V will show that n_o is probably uniquely determined by the breakdown process in the tube.

As an initial condition we certainly have the same concentration gradient at the wall as existed before saturation set in. Hence, using

$$\frac{dn}{dr} = - n^2 \frac{dn}{dr}^{-1},$$

and evaluating (dn)/dr at the wall and comparing it with the usual Schottky solution we have the condition:

$$\frac{\lambda a i J_1 (\lambda a i)}{J_o^2 (\lambda a i)} = \sqrt{\nu_o/D_o}\, a \quad J_1 (\sqrt{\nu_o/D_o}\, a).$$

Here ν has been introduced in place of the expression $\overline{\sigma_i v_e} N$. Expressed as a trancendental equation

$$\frac{x i J_1 (x i)}{J_o^2 (x i)} = y J_1 (y)$$

The argument y is plotted as f(x) in Fig. 32. For low density situations, it is evident that

$$\lambda^2 = \frac{(\overline{\sigma_i v_e})_o N}{D_o}$$

is the solution. For high densities, it is probable that the diffusion equation must be modified to include constriction efforts.

We can now estimate the validity of the approximation. It demands that

$$2r \frac{d \ell n\, n}{dr} < 1$$

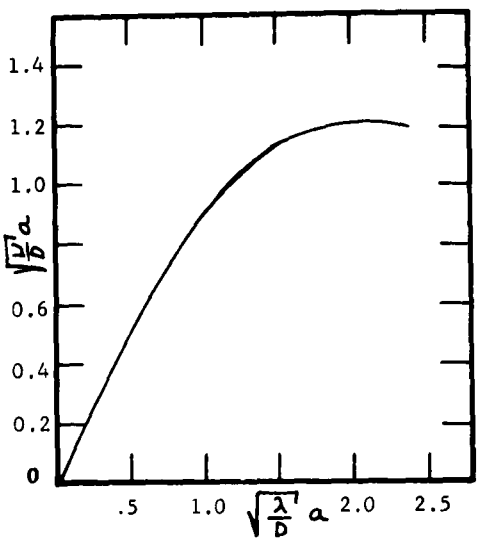

Fig. 32

This takes its maximum value at r = a, when t = 0 or t = . Thus the error is less than

$$\frac{2i\sqrt{\nu/D}\,a \quad J_1(i\sqrt{\nu/D}\,a)}{J_o(i\sqrt{\nu/D}\,a)}$$

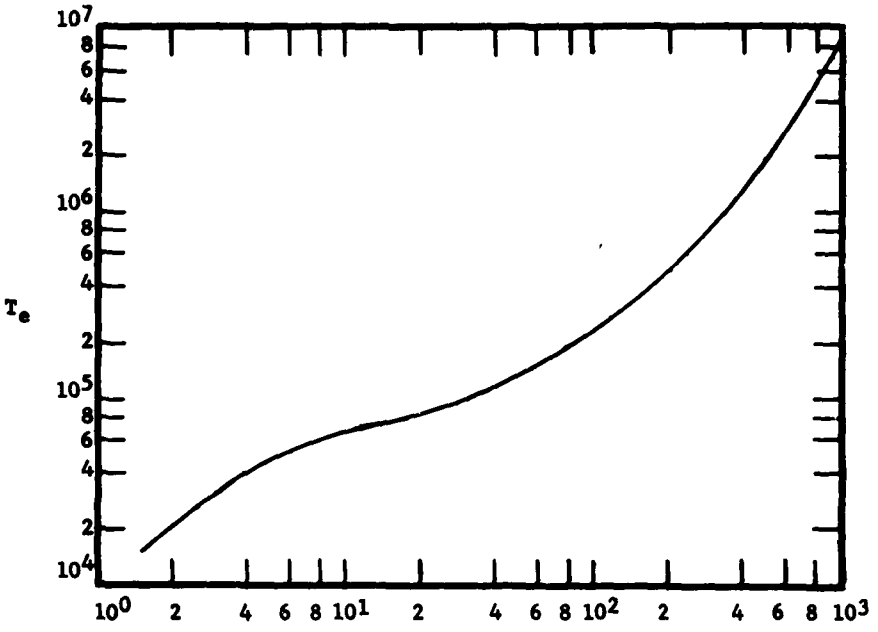

Fig. 32-A E_z/p

Over the allowed range, this gives

$\sqrt{\nu/D}\,a$	error
0.0	0.0
.2	.04
.4	.158
.6	.34
.8	.59
1.0	.89
1.2	1.22

The values found for the error suggest that the approximation is very good over all the domain for most situations, and over most of the domain for all situations.

CHAPTER IV

ELECTRON DRIVEN PLASMA SHOCK WAVES

4-1 Experimental Results - General Considerations. After the application of a high potential to the discharge chamber containing low pressure gas ($\lesssim$1 mm Hg) three classes of outward moving luminous waves have been observed. (1) A promptly originating precursor wave moving at speeds in the 10^8 cm/sec range. This will be discussed further in Chapter V in connection with breakdown waves, to which it seems to bear a close relation. (2) A promptly originating shock wave moving at speeds in the 10^6 cm/sec range. (3) A delayed shock wave moving at these same speeds, which eventually overtakes Wave Two.

When the initial pressure in the discharge chamber exceeded 1 mm Hg, luminous shock waves were not usually observed at the relatively low energies employed in this work. Under these circumstances, the leading edge of the luminosity was generally the contact surface flow, and was composed of hot gas from the driver cooling radiatively and otherwise. Such flows are proceeded by nonluminous shocks which can also be detected.

The basic picture of a thermalized plasma driving a shock wave into cold gas which is excited and ionized by massive particle collisions is not broad enough to account for the wealth of phenomena observed. If it does apply to anything, it is to Wave Three and to the luminous contact surfaces at high pressure. Nevertheless, the descriptive aspect of shock wave theory has a certain validity for discussing the observations, and an idealized representation of this description is shown schematically in Fig. 33.

Early hypotheses of the nature of these propagating luminosities were legion and many experiments were performed to identify with certainty the various aspects of electric shock tube flow to establish the basic correctness of this explanation of the Rayleigh phenomenon. That flow motion of the gas proper was present was shown by Kleider (57), who detected Doppler shifts between the light from fronts arranged to advance towards spectrograph and the light from fronts arranged to recede from the spectrograph (Table V). Similar evidence was found by Coleman (58) and Seay (59), who used a thin (1000 Å) collodion diaphragm to separate the driver gas from the shocked gas initially, and were able to detect the spectrum of the driver gas progressively throughout the expansion chamber. The shocked gas spectrum was never definitely observed, presumably because of the effect of the collodion diaphragm. It was observed weakly in reflected shocks, however. Lee (60) and Clotfelter (61)

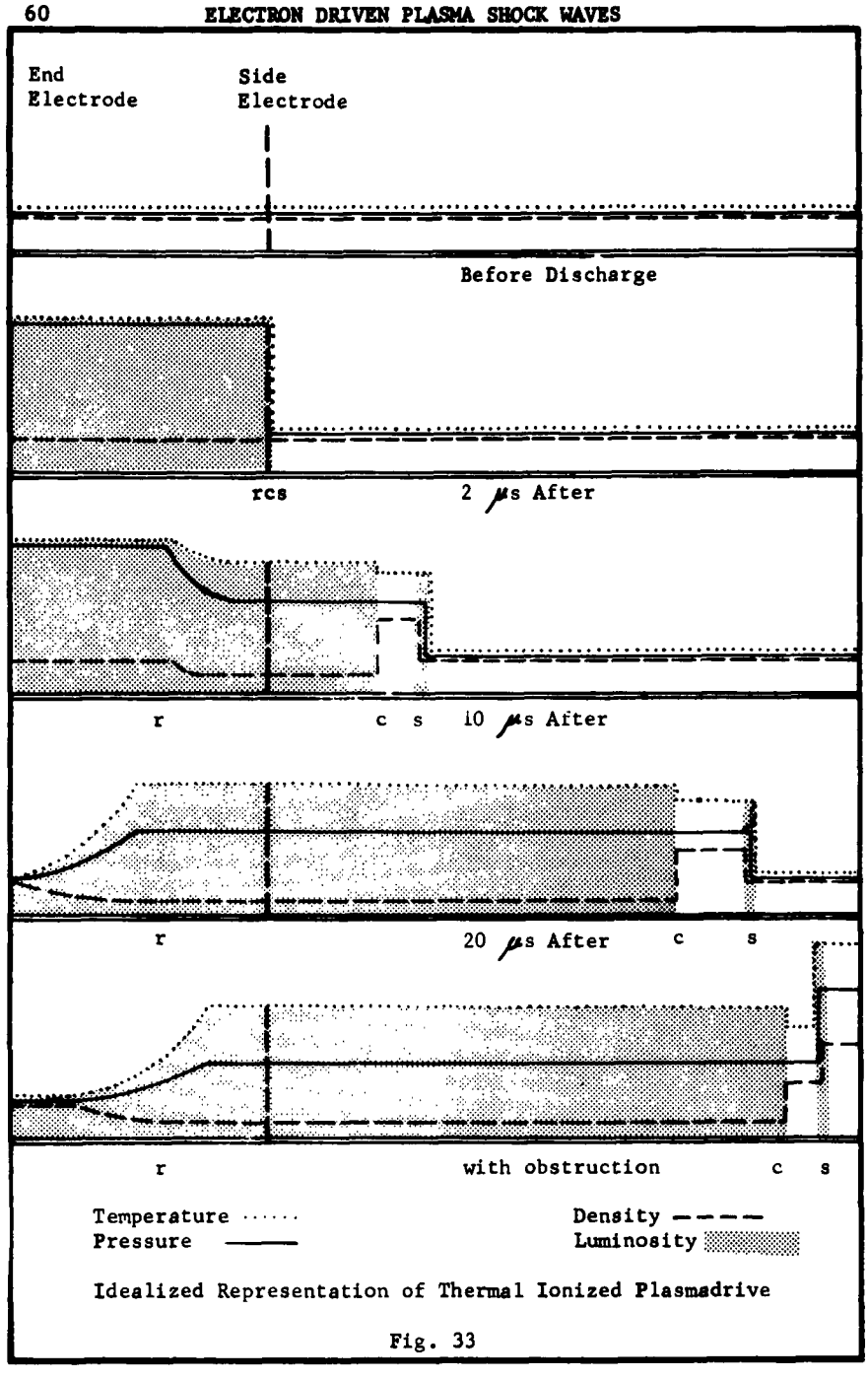

Idealized Representation of Thermal Ionized Plasmadrive

Fig. 33

carried out measurements of electromagnetic induction as the shock and flow moved through a transverse magnetic field, and Clotfelter observed that the flow velocities calculated agreed well with wave speeds of the luminous flow (Table VI). This latter experiment will be described in detail in Chapter X with the inclusion of additional phenomena.

TABLE V

Doppler Effect Measurements of Velocity

Velocity (Doppler)	Velocity (Mirror)
28.0 Km/sec	18.0 Km/sec
39.0	20.0

TABLE VI

Induction Measurements of Velocity

Velocity (Induction)	Velocity (Mirror)
8.2 Km/sec	8.1 Km/sec
7.1	7.8
6.2	6.8
7.4	6.5
7.8	6.2

4-2 Experimental Studies on the Delayed Wave. In the rush of early work no distinction was made between the prompt shock wave (Wave Two) and the delayed shock wave (Wave Three). The result is that the early analyses are somewhat blurred with reference to the phenomenon under measurement. An effort has now been made to classify these results under one head or the other, but this cannot be completely accomplished without a major reworking of the old results. In general, since the delayed wave either overtakes the prompt wave, or else the latter weakens to extinction before the former passes it, it was customary in the early analyses to take a graphical average of the two in the former case, or ignore the prompt wave in the latter case, so that most of the work done may be said to have dealt with the delayed wave only. Thus, Atkinson (62) investigated the extent to which the Rankine-Hugoniot theory could be applied to the delayed shock waves and their following contact surfaces. He mapped the flight of the shock with an acoustical detector (Chapter II) and compared this with the motion of the contact surface as seen in its own light. Atkinson concluded at the end of his work:

> "Under a wide range of experimental conditions the qualitative appearance of the mirrorgrams corresponded quite well with the flow patterns produced by a diaphragm

shock tube. More specifically, it was possible to classify the observed fronts into two categories: C-type (C = contact surface) luminous fronts which reflect before reaching a piston placed in the expansion chamber, and S-type (S = shock) luminous fronts which reach the piston before reflecting. For certain initial pressures and capacitor potentials the mirrorgrams showed only a brilliant C-type front that might be interpreted as the contact surface; whereas for other conditions the C-type front was preceded by a fainter S-type front travelling with a greater velocity. This S-type front might be interpreted as a luminous shock front.

A shock detector placed in the expansion chamber permitted the determination of the average shock velocity U over an approximate 10 cm interval. The world lines of the shock front and the S-type front coincided. From the shock velocities U an average gas flow velocity u* was computed. During the early stages of the expansion the velocity u* was usually found to be slightly less than the luminous C-type front velocity u. During the later phases of the expansion, u* was usually slightly greater than u. This agreement furnished quantitative evidence that the C-type luminous front had been correctly identified as a contact surface.

As the initial pressure is reduced, the S-type front becomes more and more conspicuous. At pressures less than one mm of Hg it is sometimes impossible to detect a C-type front at all. Ionization by the shock was proposed as an explanation for this low pressure behavior.

In the upper range of initial pressures studied, the luminosity about a centimeter behind the contact surface was observed to decrease almost discontinuously to a very low value. The simple perfect gas theory of shock tube operation would explain a gradual reduction of light output behind the contact surface, but it fails to explain the discontinuity which suggests a light-quenching wave moving through the tube with a velocity slightly greater than the contact surface velocity. Shock waves of rarefaction are known to be possible in condensable gases. Theoretical considerations showed that conditions favoring the conversion of rarefaction waves into rarefaction shocks also exist in an ionized gas obeying Saha's equation. Presumably the rarefaction wave reflected from the end of the compression chamber could steepen into a shock of rarefaction and thus account for the abrupt decrease of brilliance behind the contact surface."

Tables are given in Appendix II showing the agreement found by Atkinson between the measured flow speed of the luminous contact surface and the calculated flow speed of this surface to be expected

from the measured shock speeds.

The suggestion by Atkinson that rarefaction waves in plasmas might in some cases steepen into shocks coincided with other rather meagre but intriguing observations about the rarefaction waves. Waves presumed to be rarefaction waves because their speed magnitudes were appropriate, but marked by sharp luminosity discontinuities had been observed early in the investigation receding down the driver chamber. Later Seay (63),in tubes contaminated with collodion fragments, observed bright spots in the driver chamber which underwent abrupt accelerations at instants proportional to their distance away from the open end of the chamber, Fig. 34. As will be suggested in the next section, there is some reason to believe theoretically that this is an appropriate behavior for plasma rarefactions. Insufficient work has been done, however, on either theory or experiment, to establish this fact unequivocally.

Fig. 34. Evidence for Rarefaction Waves

The strong attenuation of the flow in the early electric shock tubes has been a matter of concern, dissatisfaction, and uncertainty. Such strong attenuation promised to limit the usefulness of the device as an aerodynamic tool. In general the attenuation is still not wholly understood and insufficient experimental and theoretical effort has been given to it. Five major suggestions can be advanced as possibilities for this attenuation:

(1) <u>The shortness of the driver chamber, making the flow more of a blast wave than a shock tube flow</u>. Harris (64) has developed the theory of such a wave and finds that flow velocity would be expected to decrease as the inverse square root of the flight distance. Against this explanation is the known fact that the shock should move three times the length of the driver chamber before the rarefaction wave reaches the <u>end</u> of the chamber. Blast wave theory would not be expected to apply before this time, while the attenuation sets in before this. In favor of it is the energy dependence found by Flansburg i.e. $U \propto W^{1/3}$.

(2) <u>The smallness of the shock tubes used, causing turbulent boundary layers to eat up the flow as it advances</u>. Although this is an impressive possibility, there is some contrary experimental evidence of a disorganized kind to suggest that attenuation is not very closely related to tube diameter. There is supporting experimental evidence by Flansburg (65) which will be discussed directly

below, going to show that an inlet length may exist with consequent implications of turbulence.

(3) Diffusion and/or radiation cooling of the flow. The attenuation seems to set in rather abruptly, as an exponential process like this one might be expected to produce. On the other hand, the attenuation often seems to be more a rather abrupt deceleration to a new fixed velocity than an exponential slowing down.

(4) Equilibration cooling. The non-equilibrium, two component flow theory of the plasma which we now accept (see Section 4-2) suggests an exponential equilibration of the temperatures of the components which might result in two plateaus of flow velocity. How this could come about is not clear at present because the total pressure of the plasma remains constant even though the partial pressures of its components change.

(5) Thermal Coupling between the flow and the driver gas. Paxton (66) observed that there is a strong indication that the flow speed of the plasma is instantaneously proportional to the power input into the driver. If it be assumed that the basic shock description is inadequate, and that there is strong heat conduction coupling throughout the expansing driver, he found that this observed relationship could follow at once.

We conclude that several of these processes may be active at the same time, but that there is a strong indication that a revision of the theory of the drive could be made to include heat conduction from the driver. In Chapter IX, data obtained from our final version of the electric shock tube seems to substantiate this viewpoint.

Flansburg investigated the relationship between delayed shock maximum flow velocities and final total energy per unit mass of gas delivered to the driver discharge. Shock tube theory would expect this to vary as $U \propto (W/m)^{\frac{1}{2}}$. Blast wave theory finds $U \propto (W/m)^{1/3}$. Flansburg's calculations show that the latter dependence is indeed closely fulfilled (Fig. 35), but as mentioned previously, there is every reason to suppose that simple shock tube theory still applies at the time the measurements of flow speed are taken. Since the arguments followed in the blast wave theory are largely dimensional ones, several alternatives are still possible. If, for example there were turbulence in the flow and hence an inlet length of the dimensions of the tube diameter, then the maximum flow velocity might be related to the energy which had been delivered to the gas by the time that the flow reached this point, and hence the total energy would be scaled with a factor $1/U$, giving a $U \propto (W/m)^{1/3}$ dependence. Again, Fig. 31 shows that the fraction of final energy in the gas at any instant is roughly proportional to the time. If the measurements which were called maximum velocities (and these points require a great deal of rationalization to select from rather muddy photographs) were usually at about the same distance down the tube, the energy in the tube at the instant of measurement would again be scaled by a factor of $1/U$.

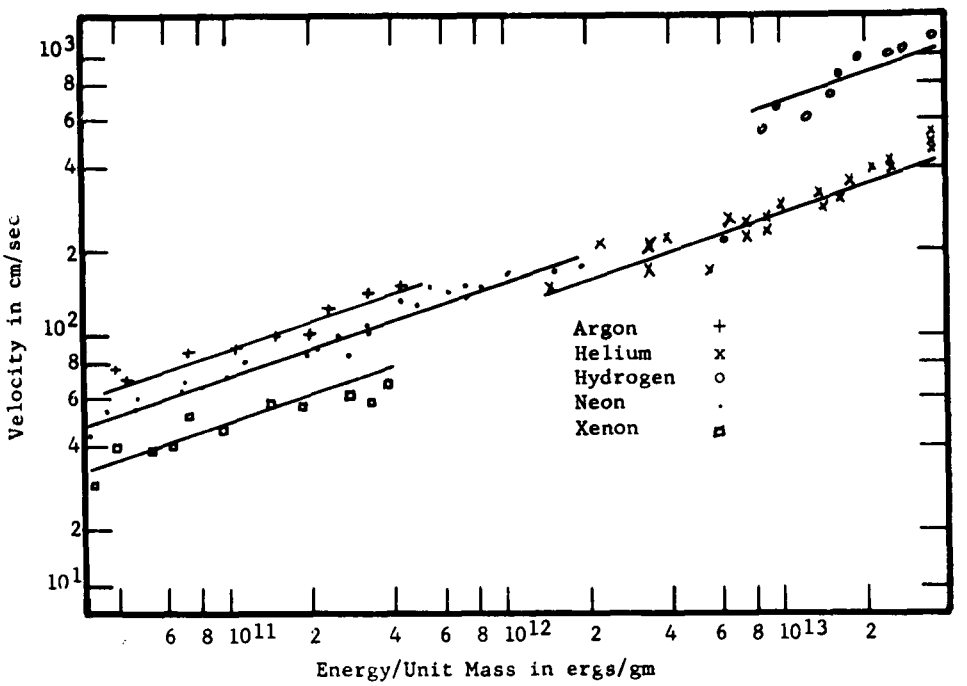

Fig. 35

Hints of turbulent behavior were seen in Kerr cell pictures of the flow, Fig. 36, and calculation of the Reynolds numbers present showed them to be on the turbulent borderline at least. Therefore additional work was begun on tubes of variable diameter to see if the inlet length phenomenon could indeed be detected.

Since the older measurements on which the work of Atkinson, Lee, and Flansburg was based has a somewhat indeterminate electrical geometry, every effort was made by Hughes (67), using extra potential leads (separate from the discharge current leads and running back from the surface of the electrodes) to obtain exact potential differences across the gas for use in accurate energy calculations. The precautions taken proved unnecessary, in that the results continued to agree well with the older work. Hughes found, however, that the prompt shock waves became an exceedingly prominent feature of the flow as the tube diameter was decreased, and it was evident that it would no longer be possible to ignore the early structural complexities of the fronts. Working still with the delayed fronts, Hughes found that small diameter tubes began to present significant resistance to the circuit resulting in a prolonged current cycle. Plotting flow velocity against simple total energy input per unit mass gave a severe stagger to the curves of different diameter tubes. Restricting the energy input to that portion which was in the discharge prior to the flow

Fig. 36 Repeated Kerr-Cell Pictures of Plasma Shock in Argon

initiation (a matter of some subjective decision) greatly improved the consistency of the data and once again could be interpreted as giving the $U \propto (W/m)^{1/3}$ relation observed by Flansburg, but could be imagined to correlate nearly as well with $(W/m)^{1/2}$. The data for argon are presented in Fig. 37, and although they seem to support the blast wave theory, the discovery of the prompt wave has so greatly altered our thinking that the entire problem of the delayed wave needs restudy. No real evidence was found for viscous or turbulent behavior.

Paxton, in the course of his study of the prompt waves, added certain information to our knowledge of the delayed wave. For tubes of diameters below 4 mm the delayed shock front gradually loses velocity and finally disappears in very small tubes, while at the same time current is prolonged greatly by the increasing resistance, and the wall heating by the discharge becomes excessive as shown by erosion, crazing, etc. It is apparent that an indeterminate situation has been reached in which there is never a time when the gas is hot enough to drive a thermal shock.

Further evidence of the thermal character of the second front is found in the spectra of the flows. The luminosity of the prompt front is found to consist of gas excitation only. The delayed front shows spectra of wall impurities at the lower pressures and smaller tube diameters, indicating that during this phase the gas is indeed very hot. Other indications that the delayed front is driven by the massive particles is found in the fact that its velocity is sensitive to the polarity of the discharge while the velocity of the prompt front is not. When the polarity is such that the mobility motion of the positive ions coincides with the direction of flow motion, the velocity is noticeably higher than conversely. This "electric wind" would theoretically have amounted

to about 2 x 10^2 m/sec in argon, a definitely detectable magnitude which was of the order of that observed.

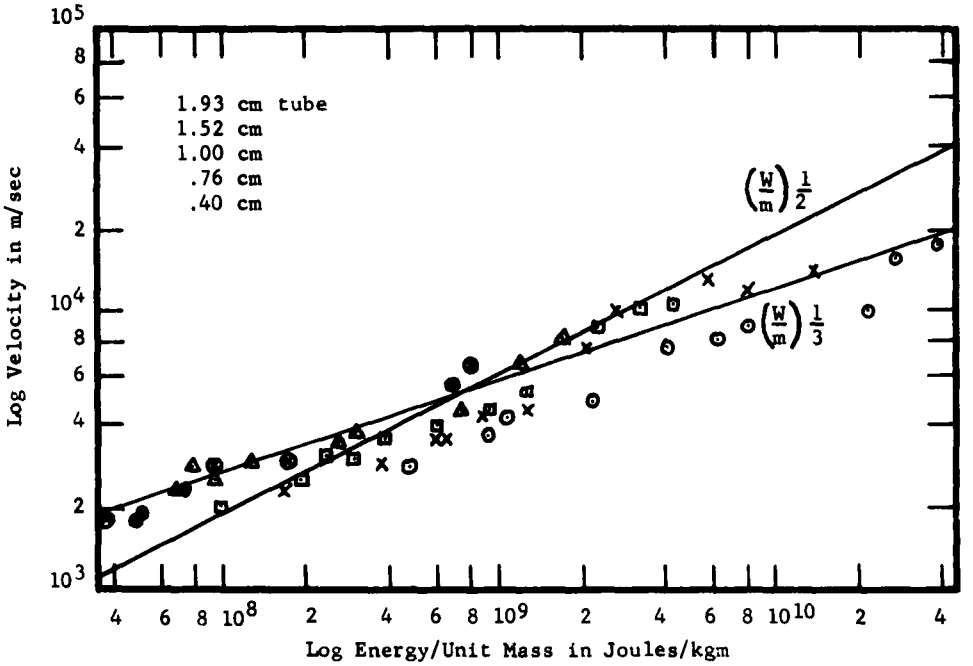

Fig. 37

4-3 Experimental Studies on the Prompt Shock Waves. Hughes's observation of the prompt shock waves was at first associated with the pinching which takes place in the driver, and his efforts to correlate the velocities with the tube current were at first deemed fairly successful (Fig. 38).* Subsequent thought showed that the time required even for magnetic effects was too long to account for the promptness of appearance of these waves, and that the nature of the heating process in a discharge was such that only the electron gas possessed sufficient internal energy at these early instants to account for the flow observed. Paxton (66) therefore undertook to correlate the prompt velocities with electron pressure rather than gas pressure, using the socalled reduced field (E/$\not p$) as a measure of electron temperature. This attack was instantly successful and Paxton extended the work of Hughes to even smaller tube diameters, to other gases and to a wide range

*The phenomenon is incorrectly attributed to this process in a symposium publication (68).

of energy storage capacitors in an effort to find situations which varied drastically in energy and current inputs without substantial changes in E/φ.

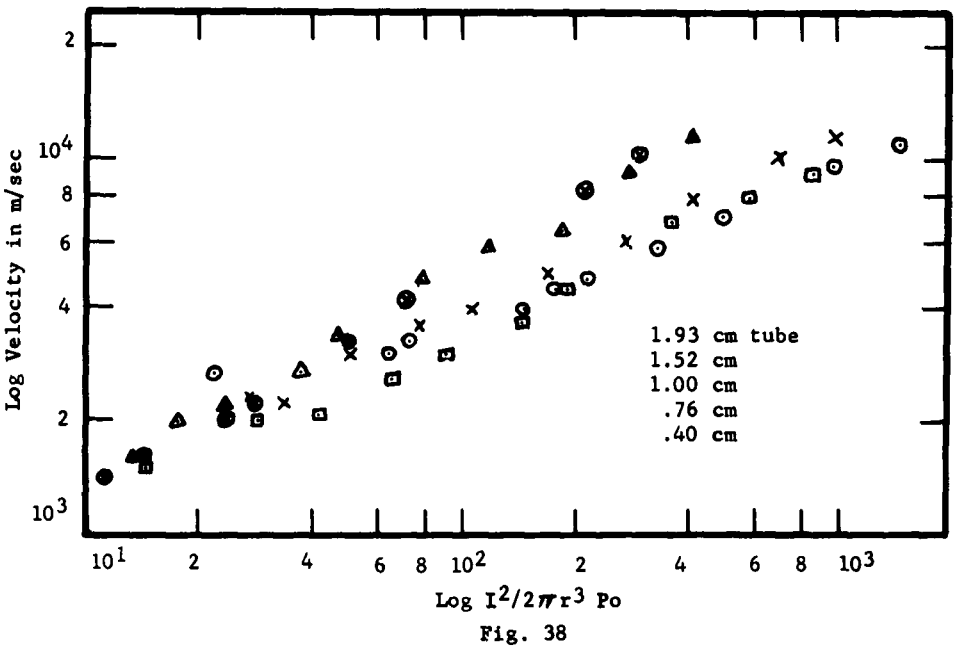

Fig. 38

It was possible to doubt that the onset of luminosity in the discharge chamber which coincided with the initial advance of the prompt front (which coincidence in turn caused us to label it as "prompt") was in fact a true measure of the length of time that the electric field had been applied. If the field had actually been present for a long dark time, the gas might have been hotter than supposed. Therefore it was necessary to establish that the rise of tube luminosity was not delayed in any significant amount behind the instant of applying voltage to the tube. Two methods were used. A photocell was directed at the tube and its output viewed on an oscilloscope whose sweep was sensitively triggered by the rise rate of the current. The delay of the rise of luminosity was found to be less than that in the photocell circuit ($\sim 2\mu$sec.), but the whole system was subject to interpretation difficulties, so that a second technique was adopted. A Kerr cell, again triggered by the rise rate of the current was used to image a spot of light on the rotating mirror records as a fiducial mark. The time delay observed by this means for the onset of luminosity after

current onset was found to be certainly less than 1 μsec. It is, of course, hardly reasonable that an electrically hot discharge could be dark anyway.

The shock character of the prompt front was investigated by placing a plane obstacle in the path of the flow and observing its reflection. The front went all the way to the obstacle, and showed a reflection which would be classed as shock reflection. An apparent shock-shock interaction then occurred upon collision of the delayed front with the reflection of the prompt front. In general the prompt front did not seem to be as well defined as a true shock front, however.

Plotting prompt front flow velocity against E/p presumes that some theory exists for converting E/p into electron temperature. Successes of this correlation are therefore a joint test of both this theory and the electron pressure theory of the wave, and disagreements may equally well be a failure of the first theory as of the second. The expression chosen in the first attempts at correlation was a minor modification of the Compton theory (69)

$$k T_e = \frac{1}{3} \frac{(e E/p)}{\bar{P}_c \left[1 + 2.405/\bar{P}_c a\right]} \sqrt{\frac{M}{3m}}$$

which was derived on a basis of simple collision theory (Section 4-4). Using this expression, with E measured as nearly as possible at the time of initiation of the wave (a somewhat subjective judgement in some cases owing to pinch fluctuations in the apparent value of E), and making use of the empirical observation that ionic mass must be involved in the acceleration because of the vast disparity of velocities in different gases, a plot was made of U_s as a function of kT_e/M, where M is ionic mass. To this graph were subsequently added high energy points taken by Turner (70) in a magnetically insulated shock tube, by Hales and Josephson (71) in a conical shock tube, and by Heflinger and Leonard (72) in a superfast pinch experiment, to give Fig. 39. Two additional extremely energetic points can be obtained from the expansion of the Crab nebula, depending on how seriously one takes the discussion of this problem which is presented in Section 4-6.

4-4 Electron and Gas Temperature Changes. Several questions arise in the matter of heating the electrons and the massive particles of an ionized gas. Many of them have arisen and received some consideration already in Chapter III. (1) How fast does an electron gas change its average energy in a changing field? (2) How fast can the heavy ions be heated directly from the field? (3) How fast can heavy particles be heated by electron collision? (4) How fast will an electron gas equilibrate with the heavy particles in the absence of a field? (5) In each case above, what final values will be attained?

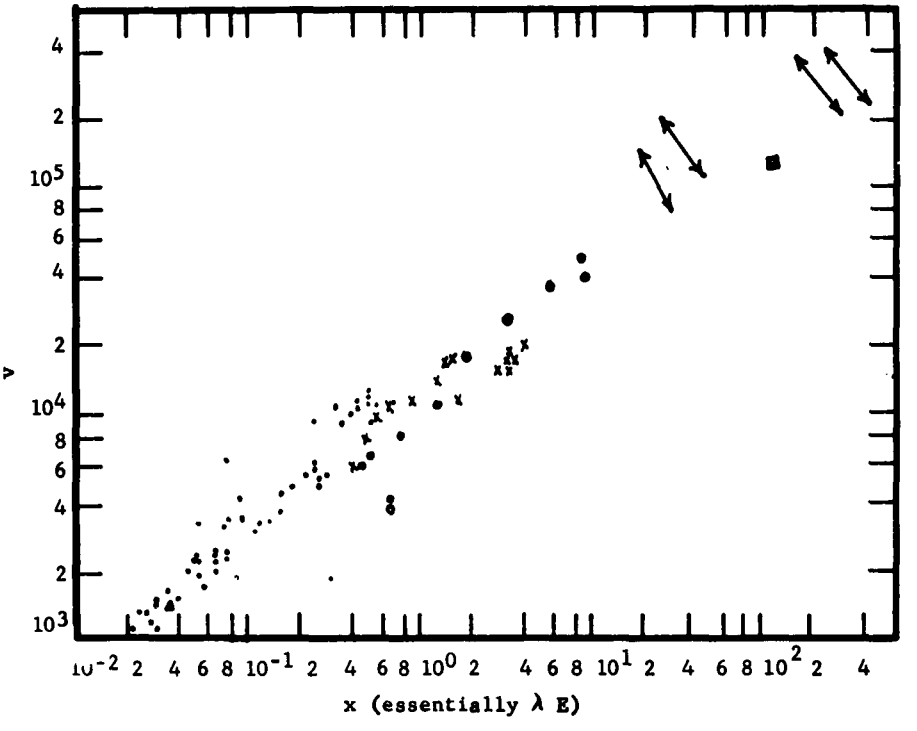

Fig. 39

Calculations of this type have been made by Spitzer (73) for a fully ionized gas, but hydrogen is almost the only gas which can be ionized fully in the laboratory, and even this is rarely achieved. Nevertheless, the ionic component of a partially ionized gas plays an important role. In a mixture of ions and neutral particles, with an ionization fraction α, the effective cross section for collision can be written

$$\sigma_m = (1 - \alpha)\,\sigma_0 + \alpha\sigma_+$$

where σ_m has its usual meaning, σ_0 is the elastic cross section with neutrals, and

$$\sigma_+ \approx \frac{4\pi e^4}{m^2 v^4} = \frac{6.5 \times 10^{-14}}{W^2} \qquad (W \text{ in ev.})$$

This expression is obtained by applying the principle that the

scattering occurs at a radius at which potential energy equals kinetic energy, and that this radius determines a circular scattering area. The result is correct within small numerical factors and a possible multiplicative screening factor $\ln \Lambda$ of order 10.

The balance point between these cross sections is given in Fig. 40 as a function of electron energy and degree of ionization. It is apparent that all high power pulsed discharges begin under the influence of the neutral cross-section, but reach an equilibrium under the domination of the ionic cross-section.

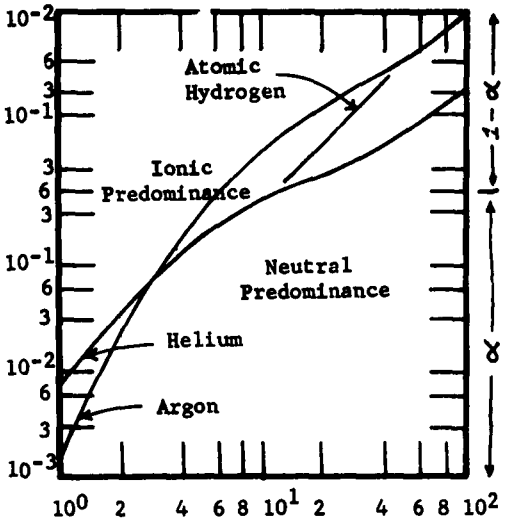

Fig. 40

The rate of change of electron temperature is given by the power equation of Chapter III. For this purpose it is necessary to modify the equation to include the Cravath factor (74), $(1 - T/T_e)$, where T is the temperature of the massive particles.

$$\frac{d\,T_e}{dt} = \frac{2e^2\,D_e}{3k^2\,T_e}\,E^2 - \frac{2m^2N}{3Mk}\left(1 - \frac{T}{T_e}\right)\left[(1-\alpha)\,\overline{\sigma_o\,v_e^3} + \alpha\,\overline{\sigma_+\,v_e^3}\right]$$

$$- (e\,V_i + 3/2\,k\,T_e)\,\overline{\sigma_i\,v_e}\,N$$

At initial time the gain term involving the field is arbitrarily large, and is certainly larger than the loss terms. In this interval, temperature rises in a time given by:

$$\tau_e = \frac{k^2\,T_e^2}{e^2\,D_e\,E^2}$$

If the equilibrium relation between T_e and E from Fig. 32A is now introduced to eliminate T_e, a time can be obtained which we will think of as the time to substantial equilibrium from zero temperature.

If in addition we inquire at the time τ_a required for the electron temperature to adjust itself to a new value when a change to a new value E is made, it follows that

$$\tau_a = \frac{k^2 (T_e^2 - T_{eo}^2)}{e^2 D_e E E_o}$$

For the direct heating of ions, a similar analysis applies. The equation for their temperature change, impeded by neutral molecules, will be

$$\frac{d T_+}{dt} = \frac{2 e^2 D_+ E^2}{3 k^2 T_+} - \frac{1}{2} (T_+ - T_o) \sigma_k N v_+$$

Here σ_k is the gas kinetic cross section to sufficient accuracy.

Again a time constant for the rising temperature can be found

$$\tau_+ = \frac{k^2 T_+^2}{e^2 D_+ E^2} ,$$

and the equilibrium temperature equation given by $(d T_+/dt) = 0$ can be used to eliminate T_+. Comparison of this with τ_e shows it to be a very slow process indeed.

Heating of ions (and neutrals) comes about by the indirect process of repetitive collision with electrons, which was given as the heating equation in Chapter III. No subscript will be used on T because it governs all heavy particles. T_o is the initial value of T.

$$\frac{dT}{dt} = +\frac{2m^2 N}{3M k} \left(1 - \frac{T}{T_e}\right) \left[(1 - \alpha) \overline{\sigma_o v_e^3} + \alpha \overline{\sigma_+ v_e^3} \right]$$

If T_e is maintained at a fixed or slowly varying level by action of an electric field, the heating process has a exponential time constant which is called the equilibration time, τ_q, and is given by

$$\tau_q = \frac{3kM T_e}{2m^2 N \left[(1 - \alpha) \overline{\sigma_e v_e^3} + \alpha \overline{\sigma_+ v_e^3} \right]}$$

τ_e, τ_+, and τ_q are all given as a function of E/p in Fig. 41.

When an electron plasma is removed mechanically from the electric field which maintained a distribution disparity, the equilibration is governed by a slightly different consideration. It is now necessary that any energy lost by the electrons be transferred to the ions at a constant total pressure. Thus

$$\frac{d\alpha T_e}{dt} + \frac{d\alpha T}{dt} + \frac{d\,(1-\alpha)\,T}{dt} = 0,$$

and integrating,

$$T_e + T = T_{eo} + T_o.$$

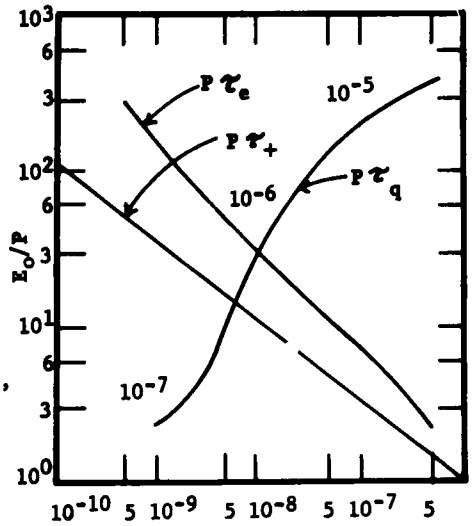

Fig. 41

When a cloud of non-equilibrium electrons interact with ions and neutrals by collision to attain a common equilibrium, although the cross-sections of these two systems differ, the energy transferred is a communal property of the massive particles, since they usually equilibrate between themselves much faster than they receive energy from the electrons. This is true if $\sqrt{(m_-/M_+)} \ll 1/4$, otherwise the energy (which enters the massive system through the process of larger cross-section) raises the temperature of one massive component over that of the other. The equilibration equation then becomes

$$\frac{dT}{dt} = +\frac{2m^2 N}{3MkT_e}\left[T_o + \alpha T_{eo} - (1+\alpha)\,T\right]\left[(1-\alpha)\,\overline{\sigma_e v_e^3} + \alpha\,\overline{\sigma_+ v_e^3}\right],$$

and the equilibration time constant depends in a new way upon the degree of ionization:

$$\tau_q = \frac{3k\alpha M T_e}{2m^2 N (1+\alpha)\left[(1-\alpha)\,\overline{\sigma_e v_e^3} + \alpha\,\overline{\sigma_+ v_e^3}\right]}.$$

In each of the four cases above, the equilibrium temperatures can of course be obtained by setting the time derivative equal to zero.

4-5 Theory of Electron Driven Shock Waves. A consideration of time constants in the previous section shows that the gas molecules do not have sufficient energy when the prompt shock wave is observed to account for this flow. Only the electrons possess the requisite energy at this time. If they are present even in relatively small concentrations, say 10%, their large non-equilibrium temperatures ($\sim 10^6$ °K) correspond to impressive mechanical pressures of the order of half of an atmosphere.

When electrons are in thermal equilibrium with the massive gas molecules, the unfavorable magnitude of their mass ensures that the direct mechanical contribution which they make to the collisional energy exchange problem in the gas is negligible. This fact makes it easy to overlook them as mechanical entities. However, if they are not in equilibrium, they have two excellent ways of making their energy felt mechanically. First, in diffusion away from a system, their coulomb fields become active and compel the positive ions to keep pace. Second, a non-equilibrium system at a higher temperature has an improved advantage in energy exchange during mixed collisions which can be interpreted as that of a fictitiously larger mass.

We inquire, therefore, what the fluid mechanics may be for interpenetrating clouds of non-equilibrium particles. As usual there will be present electrons, ions, and neutral molecules. First we write individual equations of continuity, limiting the analysis to the one dimensional case present in shock tubes.

$$\frac{\partial mn}{\partial t} + \frac{\partial mnv}{\partial x} = 0$$

$$\frac{\partial (M-m)N_+}{\partial t} + \frac{\partial (M-m)N_+V}{\partial x} = 0$$

$$\frac{\partial MN_o}{\partial t} + \frac{\partial MN_oV}{\partial x} = 0$$

Second we write two equations, one for electron momentum balance and the other for heavy particle momentum balance, with $M^* = M - m$.

$$\frac{\partial mnv}{\partial t} + \frac{\partial (mnv^2 + p)}{\partial x} = en \frac{\partial \varphi}{\partial x}$$

$$\frac{\partial (M^*N_+ + MN_o)V}{\partial t} + \frac{\partial \left[(M^*N_+ + MN_o)V^2 + P\right]}{\partial x} = - eN_+ \frac{\partial \varphi}{\partial x}$$

Third we write two equations for energy balance

$$\frac{\partial (\frac{1}{2} mnu^2 + w)}{\partial t} + \frac{\partial \left[\frac{1}{2} mnu^3 + (p + w)v + q\right]}{\partial x} = en \frac{\partial \varphi}{\partial x}$$

$$\frac{\partial}{\partial t}\left[\tfrac{1}{2}(M^*N_+ + MN_o)V^2 + W\right] + \frac{\partial}{\partial x}\left[\tfrac{1}{2}(M^*N_+ + MN_o)V^3 + (P+W)V\right] = -eN_+V \frac{\partial \varphi}{\partial x}.$$

Here in addition to symbols of usual meaning we have q as the heat transfer vector, and w and W as internal energies. These equations can easily be extended to ions of valence greater than unity, whether present in toto or as an admixture. They can also be enlarged to additional dimensions.

Two additional relations are required. Poisson's equation relating φ to any charge separations which may occur

$$\frac{\partial^2 \varphi}{\partial x^2} = 4\pi e\,(n - N_+)\ ;$$

and the principle of local neutrality, normally a condition of plasma behavior

$$n = N_+.$$

Plasmas with densities in the ranges encountered in shock tube practice will certainly fulfill this condition which is found to be valid for glow discharge concentrations as low as 10^{10} to 10^{12} charges per cc. This condition does not imply that the Poisson equation can be replaced by the Laplace equation, since deviations from equality of only a part per million can produce significant contributions to the space charge.

Adding the momentum equations, we consider the behavior of the right hand sides

$$e\,(n - N)\,\frac{\partial \varphi}{\partial x}$$

Introducing the Poisson equation here, we obtain

$$\frac{1}{4\pi}\,\frac{\partial \varphi}{\partial x}\,\frac{\partial^2 \varphi}{\partial x^2} = \frac{1}{8\pi}\,\frac{\partial}{\partial x}\left(\frac{\partial \varphi}{\partial x}\right)^2.$$

Transposing this to the left hand side we obtain the final momentum equation for the combined fluid (see below).

Adding the energy equations, we consider the right hand side again. It is

$$e\,\frac{\partial \varphi}{\partial x}\,(nv - N_+V)$$

If the first two continuity equations are subtracted from each other, they yield

$$\frac{\partial (nv - N_+V)}{\partial x} = \frac{\partial (N_+ - n)}{\partial t}$$

Introducing the Poisson equation and integrating once

$$nv - N_+V = -\,\frac{1}{4\pi e}\,\frac{\partial^2 \varphi}{\partial x\,\partial t} + f(t)$$

The arbitrary time function can be evaluated in some region of known and constant state. It is the electric current - i/e which

parallels the flow and will frequently be zero.

$$e\frac{\partial \varphi}{\partial x}\left[-\frac{i}{e}-\frac{1}{4\pi e}\frac{\partial^2 \varphi}{\partial x \partial t}\right]=-i\frac{\partial \varphi}{\partial x}-\frac{1}{8\pi}\frac{\partial}{\partial t}\left(\frac{\partial \varphi}{\partial x}\right)^2$$

This term can now be transposed to the left side of the total energy equation.

As yet we have not used the principle of local neutrality. Applying it first to the continuity equations we find that if $n \approx N_+$, then $v \approx V$. This allows us to write the final equations as

$$\frac{\partial \alpha N}{\partial t}+\frac{\partial \alpha NV}{\partial x}=0$$

$$\frac{\partial N}{\partial t}+\frac{\partial NV}{\partial x}=0$$

$$\frac{\partial MNV}{\partial t}+\frac{\partial}{\partial x}\left[MNV^2+p+P-\frac{1}{8\pi}\left(\frac{\partial \varphi}{\partial x}\right)^2\right]=0$$

$$\frac{\partial}{\partial t}\left[\tfrac{1}{2}MNV^2+w+W+\frac{1}{8\pi}\left(\frac{\partial \varphi}{\partial x}\right)^2\right]+$$

$$+\frac{\partial}{\partial x}\left[\tfrac{1}{2}MNV^3+(p+P+w+W)V+q+i\varphi\right]=0$$

where N is the total of heavy particles $N_o + N_+$. In addition to these equations we require the Poisson equation, the ideal gas laws $p = \alpha NkT_e$ and $P = NkT_o$, the definitions of internal energy per unit volume for an ideal gas $w = 3/2\ p + \alpha NeV_i$ and $W = 3/2\ P$, and some expression for the dependence or degree of ionization α either upon temperatures alone (Saha's equilibrium equation) or on previous history of temperatures and times (a suitable kinetic relation). We will refer to these equations as the equations of commingled flow.

Fowler and Fried (75) applied these equations in a much simplified form to the prompt shock waves of the electric shock tube. They assumed that $p \gg P$, $w \gg W$, $q \approx 0$, $i = 0$, and that $\partial/\partial x\ (\partial \varphi/\partial x)^2 = 0$ in regions of constant state. Then they obtained

$$\frac{\partial N}{\partial t}+\frac{\partial NV}{\partial x}=0$$

$$\frac{\partial MNV}{\partial t}+\frac{\partial}{\partial x}\left[MNV^2+p\right]=0$$

$$\partial\left[1/2\ MNV^2+3/2\ P\right]+\frac{\partial}{\partial x}\left[1/2\ MNV^3+5/2\ p\ V\right]=0$$

These are the equations of a single fluid whose density is governed by molecular mass but whose pressure is the electron pressure. We would therefore expect that all the processes characteristic of a simple fluid in a shock tube would be present here, a shock wave, a contact surface, and a rarefaction wave, joining four successive regions of constant state. The successive regions will be numbered 1-4 beginning in the undisturbed gas.

The differential equations are of course singular at the shock and contact discontinuities, and the adjacent regions must be pieced together by a flux integration of the equations over a slab bounding the discontinuity and moving with its speed of advance. Let these discontinuity speeds be designated U_s and U_c. Then integrating these equations first across the shock front in a steady state, Fowler and Fried obtained

$$N_1 U_s = N_2 (U_s - V_2)$$

$$MN_1 U_s^2 = MN_2 (U_s - V_2)^2 + \alpha_2 N_2 kT_2$$

$$1/2\, MN_1 U_s^3 = 1/2\, MN_2 (U_s - V_2)^3 + (5/2\, \alpha_2 N_2 kT_2 + \alpha_2 N_2 eVi)(U_s - V_2)$$

The solution of these equations for the velocities gives

$$U_s^2 = \frac{\alpha_2 kT_2}{M} \left\{ 5 + \frac{2eV_i}{k\,T_2} + \frac{1}{3 + \frac{2eV_i}{k\,T_2}} \right\}$$

$$(U_s - V_2)^2 = \frac{\alpha_2 kT_2}{M} \left\{ \frac{1}{3 + \frac{2eV_i}{k\,T_2}} \right\}$$

$$N_1 = \frac{(U_s - V_2)\, N_2}{U_s}$$

Integrating across the contact surface, one obtains

$$\alpha_3 N_3 T_3 = \alpha_2 N_2 T_2$$

$$(U_c - V_3) = U_c - V_2) = 0$$

It is not possible to apply flux integration across the rarefaction wave, because the separation of the bounding surfaces, if located in regions of constant state is not in general time independent. Solution of this phase of the problem requires a discussion of the simple waves which are consistent with the time dependent

equations concluding the terms in $(\partial\varphi/\partial x)^2$. Two extreme possibilities of easy solution arise, neither of which need describe an actual case. Either the charge separations are negligible in the wave, and $p >> (1/8\pi)(\partial\varphi/\partial x)^2$, or charge separations exert their maximum effect, and $p \simeq (1/8\pi)(\partial\varphi/\partial x)^2$. The first possibility was chosen by Fowler and Fried, to describe the expansion in terms identical with those of a conventional shock tube. The equations from which this discussion began are superior to those used by Fowler and Fried in that no advance assumption is made about the degree of ionization. They lead to a somewhat different result when followed out logically. Briefly reviewed they are

$$N_t + VN_x + NV_x = 0$$

$$(\alpha N)_t + V(\alpha N)_x + (\alpha N)V_x = 0$$

$$NMV_t + NMVV_x + p_x = 0$$

$$p_t + Vp_x + \alpha pV_x = 0$$

$$p = \alpha NkT$$

Combining the first and second equations gives

$$\alpha_t + V\alpha_x = 0$$

to replace the second equation. Combining this with the fourth, fifth and second gives the temperature equation

$$T_t + VT_x + (\gamma - 1)\,TV_x = 0$$

Adding and subtracting the third and fourth gives

$$p_t + (V + C)\,p_x + NMC\left[V_t + \left(V + \frac{\gamma p}{NMC}\right)V_x\right] = 0$$

$$p_t + (V - C)\,p_x - NMC\left[V_t + \left(V - \frac{\gamma p}{NMC}\right)V_x\right] = 0$$

If C is chosen as equal to $(\gamma p/NMC)$, these equations propagate along the characteristics $V \pm C$, and have the usual Riemann invariants along these characteristics

$$V \pm \int \frac{C\,dp}{\gamma p} = \text{const.}$$

Now from the temperature equation one can derive

$$C_t + VC_x + \frac{(\gamma - 1)}{2} CV_x = 0,$$

showing that acoustic speed squared propagates according to the same equation as temperature. Assuming that $C = Ap^n$, one finds that to be compatible with the equation for p and α, $n = (\gamma - 1)/2\gamma$, and A can be an arbitrary function of σ.

Whether or not α is invariant in the rarefaction is uncertain, but this seems an excellent assumption since the rarefaction is a cooling effect which should make the response time to adjustment of concentration longer than the stabilizing value which existed prior to expansion. In other words, ionization is frozen into the expanding gas. If so, the integration of the Riemann invariant gives as usual

$$V \pm \frac{2\,C}{\gamma - 1}$$

and we obtain

$$V_3 = \frac{2}{\gamma - 1}\sqrt{\frac{\gamma \alpha_4 kT_4}{M}}\left[1 - \frac{A_3}{A_4}\left(\frac{\alpha_3 N_3 T_3}{\alpha_4 N_4 T_4}\right)^{\frac{\gamma - 1}{2\gamma}}\right]$$

On assuming that $\alpha_2 = \alpha_3 = \alpha_4 = 1$ from which $A_3 = A_4$ follows, and applying the relations $N_4 = N_1$ and $U_s - V_2 = U_c = V_3$ one obtains the result given by Fowler and Fried.

$$U_s = y\sqrt{\frac{5kT_4}{3M}}$$

where y is the solution of the equation

$$y = 3/\beta\left[1 - \left(\frac{5\beta y^2}{3}\right)^{1/5}\right]$$

in which $\beta = (1/8)\left[3 + (32\,Z + 9)^{1/2}\right]$ and $Z = (eV_1/MN^2) < 1/2$. The condition $Z < 1/2$ requires that the kinetic energy of an incoming particle be greater than the ionization energy. Otherwise there is no solution. The quantity y as a function of Z is given in Table VI

TABLE VII

Z	0	.05	.10	.15	.20	.30	.40	.50	∞
y	0.600	0.548	0.518	0.495	0.467	0.450	0.428	0.405	0.405

Using the revised equations presented here it is no longer necessary to make specializations concerning α, except the reasonable one that $\alpha_3 = \alpha_4$, and hence $A_3 = A_4$. Then one obtains in place of the Fowler-Fried relations the following:

$$U_s = \sqrt{\frac{\alpha_4 kT_4}{M}} \left[\frac{16 + 8\beta + \beta^2}{\theta\,(3+\beta)}\right]^{1/2}$$

where $\beta = 2eV_i/kT_2$, and $\theta = \alpha_4 T_4/\alpha_2 T_2$ are related by the equating of V_3 at the foot of the rarefaction wave to V_2 on the subsonic side of the shock wave, i.e., θ is the solution of the equation:

$$\theta^{1/2} - \theta^{3/10}\,(16 + 8\beta + \beta^2)^{1/10} \frac{\sqrt{16 + 8\beta + \beta^2} - 1}{\sqrt{15\,(3+\beta)}} = 0$$

It then follows that

$$U_s = y\sqrt{\frac{\gamma\,\alpha_4 kT_4}{M}}$$

when θ and the quantity y are given in Table VIII.

TABLE VIII

β	0	0.01	0.1	1.0	10.0	100.0	1000.0	∞
y	0.600	0.596	0.591	0.572	0.542	0.464	0.476	0.491
θ	8.85	8.89	9.29	11.42	30.67	292.	2580	2.48β

It is interesting that this exact solution shows very little dependence on the ionizing conditions present in the shock front as Weymann remarks (76), even less in fact than the original Fowler - Fried theory. This is in good agreement with the experimental behavior of the shock tube.

Although these assumptions were successful in accounting for the available data (Fig. 42), the adiabatic simple wave structure implied for the rarefaction process may not be correct for several reasons. (Parenthetically it should be stated that regardless of the process involved, the consequences will be only a minor change in the magnitude and structure of the function y, and that this change can probably always be absorbed in the somewhat unknown relation between T_e and E which is used to reconcile the data.) The first objection is that local heating by the electric field in the driver region, and the large heat conduction coefficient of the electrons may act to make the expansion isothermal rather than adiabatic.

The second objection is that the electron expansion if freely

possible could generate double layers of such intensity that $(1/8\pi)(\partial\varphi/\partial x)^2 \approx p$, and the tendency may instead be to develop a rearward facing shock wave of the type originally suggested by Atkinson (Section 4-2).

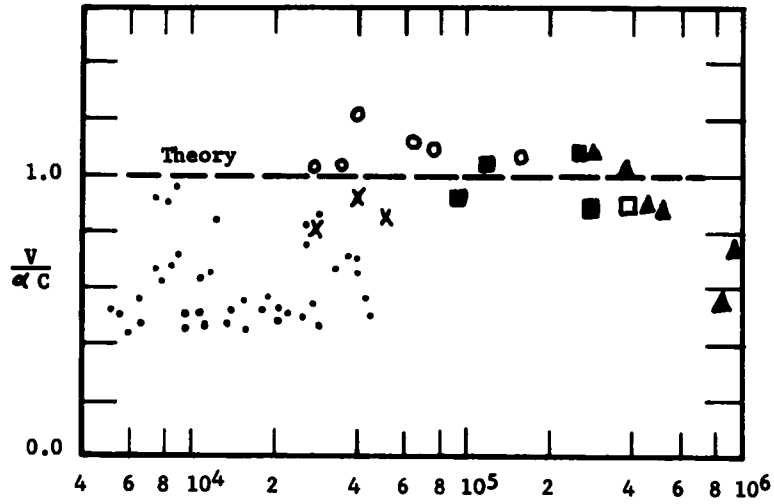

Fig. 42

Jeffries (77) has made a study of the behavior of an isothermal rarefaction wave in a equilibrated driver, a situation which definitely might come to pass during the propagation of the delayed shock wave. He finds that the Mach numbers of isothermally driven shocks will always be less under corresponding conditions than those of adiabatically driven shocks (Fig. 43).

4-6 Theory of the Delayed Flow. If we assume that the delayed flow differs from the prompt flow only in that it is an equilibrated flow, the numerical results of Table VIII can be applied if a new interpretation is given to β and θ.

$$\beta = \frac{2\alpha_2 eV_i}{(1+\alpha_2)kT_2} \qquad \theta = \frac{(1+\alpha_4)T_4}{(1+\alpha_2)T_2}$$

Then shock speed is given by

$$U_s = y\, C_4.$$

where

$$C_4 = \sqrt{\frac{\gamma(1 + \alpha_4)kT_4}{M}}.$$

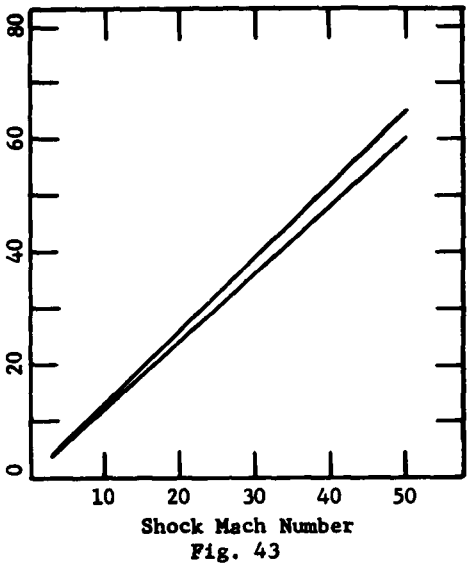

Fig. 43

4-7 Blast Wave Theory. Harris (64) has given an approximate treatment of the problem of abrupt energy delivery to a small finite region which subsequently expands into one, two, or three dimensions with the expanding mass concentrated at the front. He finds that if W_1 is the energy input per unit area of plane front and ρ_o the initial mass density, then

$$\frac{W_1}{\rho_o} = \left(\frac{2}{\gamma + 1}\right)^2 \dot{R}^2 \,(2R)$$

is the equation of motion of the wave in one dimension. In two dimensions

$$\frac{W_2}{\rho_o} = \left(\frac{2}{\gamma + 1}\right)^2 \dot{R}^2 \,(\pi R^2)$$

where W_2 is the energy input per unit length of cylindrical front, is the equation; and

$$\frac{W_3}{\rho_o} = \left(\frac{2}{\gamma + 1}\right)^2 \dot{R}^2 \,(4/3\pi R^3)$$

where W_3 is the energy input is the equation in three dimensions. These integrate respectively into

$$R = \left(\frac{3}{2}\right)^{2/3} \left(\frac{\gamma + 1}{2}\right)^{2/3} \left(\frac{W}{2\rho_o}\right)^{1/3} t^{2/3}$$

$$R = \frac{2^{1/3}}{1/4} \left(\frac{\gamma + 1}{2}\right)^{1/2} \left(\frac{W}{\rho_o}\right)^{1/4} t^{1/3}$$

$$R = \left(\frac{5}{2}\right)^{3/5} \left(\frac{3}{4\pi}\right)^{1/5} \left(\frac{\gamma + 1}{2}\right)^{2/5} \left(\frac{W}{\rho_o}\right)^{1/5}$$

4-8 Electron Driven Expansion of Planetary Nebulae. The known data concerning the Crab nebula are highly compatible with the hypothesis that an electron drive is active. According to Burbidge (78) the average electron energies which radio emission indicates are in the neighborhood of 30 Mev. Presuming gas of an average atomic weight of about 5, this would indicate wave velocities of 2×10^4 km/sec on the above model, a figure in close accord with the data of Baade on the so called "wisps" in this nebula. Reasoning in reverse from the average velocity of expansion of 1.1×10^3 km/sec measured by Myall, the overall average of electron energy indicated in the nebula would be much lower, about 0.03 Mev.

This difference can be understood when it is noted that only 3×10^{49} electrons have the higher energy, while perhaps 10^{58} have this lower energy, assuming as is commonly done that the overall electron concentration is about 10^3/cc. The more populous electrons of lower energy furnish a background of mechanical motion without entering into radiation processes.

A second essential point is that this major component of electron gas need not have cooled appreciably since the original explosion. It is not radiating rapidly enough by synchrotron radiation or by bremstrahlung, and its elastic collision equilibration time with the heavy gas ions is over 3000 years.

The process suggested here is closely related to the ideas of Pikel'ner (79) about electron pressure as a factor in nebular equilibrium.

The great paradox of the planetary nebulae, that the lines of Ne V show in general lower (doppler effect) expansion velocities than the lines of Ne I, also yields to the mechanism of acceleration by an electrical double layer. To explain all of its features the problem should be analyzed in more detail than will be given here. We presume that in the second, or rarefaction double layer, momentum balance is established between two or three proponderant species: electrons and perhaps a mixture of hydrogen and helium ions. Energy balance between these species then determines the potential difference across the double layer. Minor concentrations of impurity species such as neon are now accelerated across a potential difference which is unaffected by their concentrations, and their velocity is then governed by the equation

$$u_2^2 = u_1^2 - \frac{ZeV}{M}$$

in the rest frame of the foot of the wave, where u_2 is the velocity at the foot, u_1 is the velocity at the head (in this same frame), V is the potential difference. Shifting to the frame of external observation, with velocities denoted by v, $v_2 = u_2 + u_1$ and $v_1 = 0$. Then

$$v_2 = u_1 + \sqrt{u_1^2 - \frac{ZeV}{M}} \approx 2u_1 - \frac{ZeV}{2u_1 M} .$$

Here u_1 is now recognized as the wave speed of the retreating double layer. We see that the increase of Z decreases the velocity of advance v_2 of highly ionized species of constant mass M, but the species of variable mass and roughly similar Z/M have nearly the same flow speeds (e.g. H and O III).

We conclude that the shock waves presumed to exist in planetary nebula may not be of the ordinary thermal character, but may result from the presence of fast electrons, presumably originating in β processes. In fact, such processes may occur in many situations where nuclear reactions release large numbers of electrons.

4-9 Rarefaction Shocks. Since the acceleration of electric fields by charge separation, and since the potential differences across these fields will be limited by the internal energy of the electrons ($e\Delta\varphi \approx kT_e$), it is entirely possible that the condition that $p \approx (1/8\pi)(\partial\varphi/\partial x)^2$ is met in the region of the rarefaction. If so, we are dealing with a system which has an equivalent pressure

$$p^* = P - \frac{1}{8\pi}\left(\frac{\partial\varphi}{\partial x}\right)^2$$

From this we can derive the following speculative equation of state, where u is gas volume and A is the area of the shock front:

$$p^* = \alpha NkT_e - \frac{1}{8\pi}\left(\frac{kT_e}{e}\right)^2 \frac{A^2}{u^2}$$

This equation of state has the properties necessary for the existence of rarefaction shocks, i.e., $(\partial^2 p/\partial u^2)$ can be negative.

The development of such shocks arises because coulomb forces will not permit charge separations to build up over long distances. On a microscopic scale this implies Debye shielding, with the development of a Debye layer instead of an extended space charge zone. Thiemer (80) has supplied us with an equation of state for full ionization derived on microscopic considerations of Debye shielding. It possesses the same mathematical properties as the previous equation and is:

$$P^* = NkT_e\left[1 - Z^3e^3\left(\frac{8\pi N}{9k^3T^3}\right)^{\frac{1}{2}}\right] .$$

This is expected to be valid for $N < 10^{18}$ cm^{-1} and $T_e > 10^4$ °K.

CHAPTER V

BREAKDOWN WAVES, PRECURSORS AND ELECTRON FLUID DYNAMICS

5-1 Breakdown Waves. It was mentioned in Chapter I that breakdown waves with speeds of 2×10^7 cm/sec were observed in the discharge chamber very early in the course of this research, and that these were categorized as akin to the waves noted by Wheatstone, Thomson, and Beams and others in the laboratory, and by observers such as Schonland (81) in natural lightning.

Thomson (4) observed that the luminosity front may travel at a speed as high as one half the speed of light. Beams (5) studied luminosity fronts in air and hydrogen and reported that the breakdown wave always moves from the electrode to which the potential is applied toward the electrode at ground potential, regardless of the polarity of the applied voltage. Von Zahn (3) showed that there is no Doppler shift in the spectral lines which implies that the luminosity front does not result from motion of the particles emitting the observed radiation. Schonland (81) has made extensive studies of the lightning discharge measuring the velocity of propagation of the luminosity front traveling into undisturbed gas, sometimes called a pilot streamer, and the propagation velocity of the secondary front which travels down the partially ionized channel left by an earlier pilot streamer. Schonland has also made some predictions of the minimum propagation velocity which he obtains from qualitative energy considerations.

Luminosity studies of spark breakdown by Loeb (82) have indicated that potential waves are present during this phenomenon. Loeb terms the dendritic luminosity fronts observed in spark breakdown "streamers". Westberg (83) recently published a rather complete study of potential waves present in the transition of a glow discharge to an arc. Fowler and Hood (84) have observed luminosity fronts propagating into a field free region. We shall subsequently see that there are probably three or four modes by which energy can be supplied to waves of this fast moving family, and this fact offers a criterion for classification.

Paxton and Fowler (85) have recently presented a hydrodynamical theory of potential wave propagation with particular emphasis on waves propagating into non-ionized regions, based on an extension of the theory of Chapter IV. The model presented treats the potential wave front as an electron shock wave in an electron gas. An electron shock wave will be called a breakdown wave if the source of its energy is an electrostatic field in a charge free region. It will be called a striation if its energy comes from a current

and a field in a charge-bearing region. It will be called a heat-conduction wave if the source of its energy is a cloud of electrons maintained at a high temperature elsewhere than the front. It will be called a streamer if the source of energy is reabsorbed photons generated at or near the front. This choice of language is not intended to imply that all these processes have been established categorically, but rather that there seems to be considerable evidence for these distinctions. There remains the possibility of subclasses of waves depending on the ionization process in the front. The two important ionization processes active in this model are photoionization and electron impact ionization. In the case of molecular gases, both ionization processes are active to various degrees depending on the gas and ambient conditions. In the case of atomic gases where photoionization of the gas by its own photons is not possible, either electron impact ionization or a combination of electron impact and photoionization must be the active process.

We turn our attention to the breakdown wave and presume that, near that electrode at which the potential gradient in the gas is greatest, ionization of a small quantity of gas occurs and the electrons produced are given kinetic energy by the electric field. This localized high temperature electron gas expands, producing an electron shock wave which propagates into the undisturbed gas, partially ionizing the overrun neutral gas molecules. The energy necessary for driving the shock wave is given directly to the electrons in the shock zone by the external electric field. The electron shock is followed by a rarefaction wave, but the analysis of the rarefaction wave presents the usual uncertainties and will not be included here.

As in Chapter IV we begin with a three-fluid, hydrodynamical model which is applied to a three-component system in which the electron gas has achieved a steady state, but the heavy particles, due to their large inertia, are in a transient state. The time constants associated with the motion of the heavy particles are large enough that there is only a slight change in the kinetic energy of these particles during their brief interaction with the electron shock wave.

The steady state equations of mass, momentum, and energy transfer for continuous media are those given in Chapter IV. For the case where the electron pressure is much greater than the partial pressures of the other species, where there is no electrical current, where there is negligible heat flow, and where inelastic energy losses can be neglected, the transfer equations differ only in that the term in $E^2 = (\partial\varphi/\partial x)^2$ must be carried to the end.

In the rest frame of the shock wave, cold neutral atoms enter the shock zone from the front side and a partially ionized gas leaves the rear side of the shock zone. Under the quasi-steady state conditions present, the flow velocities of the massive particles whether ions or neutrals are originally equal and are not altered by the passing of the shock wave. Thus

$$V_+ = V_o = V_1 = V_2$$

The condition of zero electrical current implies

$$nv = N_+V_+.$$

Substituting these results into the continuity equations gives

$$N_+ = N - N_o = \alpha N$$

Substituting these relations into the momentum transfer equations these relations give

$$m\alpha N_1V_1^2 = mnv^2 + nkT_2 + \frac{1}{8\pi}(E_1^2 - E_2^2),$$

and substituting these same restrictions into the energy transfer equation, gives

$$m\alpha N_1V_1^3 = mnv^3 + 5nvkT_2.$$

Solving these two equations for the velocity of the electron shock wave as a function of the remaining variables yields

$$V_1^2 = \frac{B + \left[B^2 + 4W^2\,(15\,k^2T_2^2 - 10\,kT_eW)\right]^{\frac{1}{2}}}{\left[2m(3\,kT_2 - 2W)\right]}$$

where $$B = 16\,k^2T_2^2 - 10\,kT_2W - W^2$$

and $$W = \frac{(E_1^2 - E_2^2)}{8\pi\alpha N}.$$

The quantity W is unknown because the electric field behind the shock zone and the degree of ionization of the gas behind the shock wave have not been determined. To include the explicit determination of these quantities requires additional equations related to the collision processes and the rarefaction wave as well as an integration of Poisson's equation. However, experimental evidence (5) has shown that the potential wave propagation is of the same general character regardless of the polarity of the applied potential which indicates a secondary dependence of the propagation velocity on the direct effect of the electric field. The cited experiments give a slightly greater velocity for a negative applied voltage than for a positive voltage. Considering these experimental results, the expression for wave velocity is here tentatively simplified by assuming W negligible; however, later a qualitative

dependence of propagation velocity on W will be noted.

With the assumptions discussed, the wave speed reduces in first approximation to

$$U_s^2 = V_1^2 = \frac{16\ kT_2}{3m} .$$

With this equation and the modified transfer equations, the electron density in the region behind the shock wave can be determined to be

$$n = 4\ N_+ = 4\ \alpha N.$$

There is very little available data giving both the propagation velocity and the applied field for breakdown waves moving into a non-ionized gas. Such data as are available are given in Table IX. The streamer velocity of 3.5×10^5 m/sec listed in the table for atmospheric hydrogen is only a lower bound because it is the velocity of a secondary streamer which was propagating down the partially ionized channel left by an earlier, faster pilot streamer. The data for streamers in argon were taken from Loeb, Westberg, and Huang. There have been considerable experimental data taken on lightning discharges, but the electric fields are largely unknown in these cases. Rough guesses of these fields give suggestive agreement also.

TABLE IX
Propagation Velocity of Breakdown Waves in H_2 and A Gases With Different Pressures and Field Strengths

Applied Field volts/m	Gas	Pressure mm Hg	Experimental Velocity m/sec	Theoretical Velocity m/sec	Source
1×10^4	H_2	.2	4.9×10^7	2×10^7	Beams(5)
1×10^4	H_2	.5	4.5×10^7	1.7×10^7	Beams(5)
1×10^4	H_2	1.5	4.0×10^7	1.4×10^7	Beams(5)
1×10^6	H_2	760	3.5×10^5	1.5×10^6	White(86)
2×10^5	A	300	1.0×10^6	2.7×10^6	Loeb, et.al.(87)

Considering present uncertainties in regard to the electron temperatures and fields only qualitative agreement between the theory and experimental results can be expected. From Table IX we see that such agreement exists for the available data.

As mentioned above, experimental evidence indicates that potential wave velocities are slightly greater for electron layers moving toward the anode than for such layers moving toward cathode. Poisson's equation demands a dependence of the electric field around such a layer as shown pictorially in Fig. 44. In the case of an anode-to-

cathode impulse, E is less than E_o which makes W positive. For a cathode-to-anode wave, E is greater than E_o and W becomes negative.

Taking $W \approx kT_e$ gives for positive W

$$V_o^2 = 5.8 \frac{kT_e}{m}$$

and for negative W

$$V_o^2 = 5.2 \frac{kT_e}{m} .$$

Therefore, theory confirms that the breakdown waves propagating away from the negative electrode should in fact be the faster.

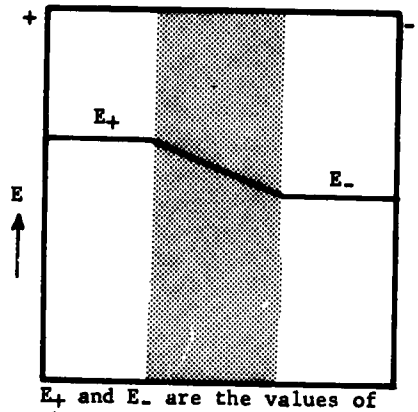

E_+ and E_- are the values of the field on the positive and negative sides of the charge zone. Fig. 44

5-2 Heat Conduction Waves and Precursors. Many investigators beside ourselves have been confronted with precursor luminosities in the expansion chamber of electric shock tubes. Although their presence has often led to speculation about the thermal state of the gas into which the subsequent plasma-acoustic shock moves, little has been written about them, and they are generally ignored in this respect. One of the most generally advanced explanations has been Rayleigh and resonance scattering from the gas. While this may well be present also, even as bright a source as the shock tube would scatter only enough light to allow a exposure of about 10^{-6} erg/cm^2, whereas 10^{-3} erg/cm^2 is a typical threshhold for photographic materials.

Recently we have observed a front of this type under conditions which make it a very prominent feature of the experiment. An improved design of the linear electron driven shock tube was constructed, and will be described in Chapter IX. It generated a column of driver gas 1 meter long at an electron temperature sufficient to produce Mach 40 electron driven plasma acoustic shocks at capacitor potentials of only 10 KV, in a tube 50 mm in diameter. Expansion was made into a collinear chamber which was also a meter in length. It was tested in hydrogen and argon, and found to produce powerful precursor fronts in addition to the normal electron driven wave phenomena (Fig. 45).

The new front appeared at first sight to coincide with gas breakdown and to move instantaneously along the expansion chamber, owing to the slowness of the wave speed cameras in use. On careful comparison with a fiducial pattern, however, it was later found to have a speed of about 2.0×10^8 cm/sec in argon at 100μ Hg.

Although as usual it was at first regarded as a scattered light front, observations of decidedly anomalous behavior in the recombination afterglow from a weak preionization discharge which had been present intentionally in the expansion chamber, gave an unexpected clue to its nature. The fast front reduced the luminosity of this afterglow in a narrow zone just in advance of its leading edge. This result has led us to consider the front as an electron hydrodynamic wave akin to the breakdown waves since the electric field which must exist in an electron hydrodynamic wave would stop the recombination processes responsible for the afterglow light from the preionization.

Fig. 45 Precursor Wave and Plasma Shock

The following additional observations concerning the fronts were than made with a faster mirror. The wave velocities lie in the electron hydrodynamic range. Corresponding wave velocities of the fronts were slightly greater in argon than in hydrogen; they were independent of gas pressure at pressures below 500 μHg but decreased with pressure at higher values; they were not affected by the presence or absence of the preionization; they were not influenced by an axial magnetic field of as much as 1000 gauss. These fronts were perhaps affected in brilliance, but not perceptibly in speed, by a short zone of transverse magnetic field of about the same magnitude. They were much less brilliant in hydrogen than argon. They were unaffected by moving toward a grounded electrode at the far end of the shock tube, or with the electrode unconnected, into a space free of electric fields (except for a very weak residual field escaping from the driver of less than 30 volts per meter). An increase in wave speed with increasing E/p in the driver chamber was found to exist and is shown by the data in Fig. 46. The data seem to indicate therefore that the speed controlling factor is the electron temperature in the driver chamber.

The precursor waves were found to maintain a constant ratio to the plasma acoustic waves of $\sqrt{M/m}$. The data were 285 $\pm$ 55 for twelve measurements in argon, and 55 $\pm$ 10 for the measurements in hydrogen, compared with theoretical values of 283, and 43 or 61 depending on whether hydrogen should be treated as a mono or diatomic gas for these purposes. v

The wave takes the form of a zone of strong luminosity at low pressures and large driver fields, but becomes quite diffuse with weak fields, and changes in form to a step of luminosity at high pressures.

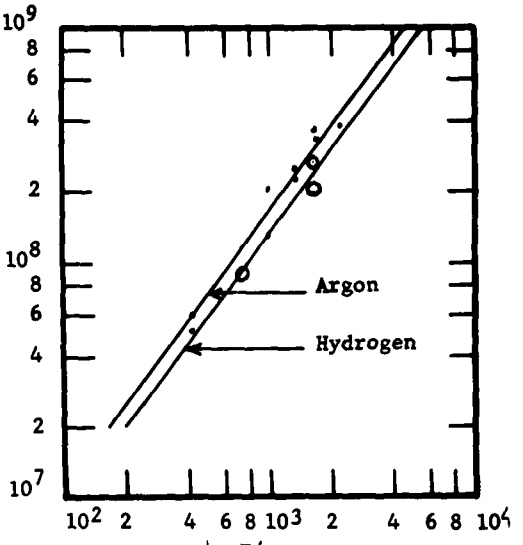

Fig. 46

Since waves of the electron hydrodynamic class are insensitive to the mechanism which serves to transport energy to the wave front, we have suggested that these precursors are of electron hydrodynamic character but use some other energy source than an electrostatic field. Two possibilities suggest themselves for the mode of energy transport to this front. Either the walls of the expansion chamber act as a light pipe for the intense radiation from the driver, or else the energy of the driver is delivered to the front by heat conduction processes. It seems most likely to be the latter, because of observed dependence on electric field in the driver which implies in turn a concomitant dependence upon electron temperature in that region.

Energetically speaking, heat conduction is a sufficient mechanism. If it be assumed that the wave ionizes the gas to a fraction α, then the waves observed would require a power flux density to the front of about 2 α megawatts/cm^2. In a neutral gas the electron heat conduction coefficient would be 10^{-4} α megawatts/cm^2/unit gradient. In a fully ionized gas it would be 2 x 10^{-3} α. Thus a temperature gradient of at most about 10^3 to 10^4 $^\circ$K/cm is all that is needed to deliver the power required. Beginning with an electron gas at 10^6 $^\circ$K in the driver, the required gradient need hardly be noticeable in a flight of 100 cm. The flow would therefore proceed at driver electron temperature, as is roughly observed.

Transmission of the required energy by photon absorption at the front in the neutral gas, would require that photons be converted into ionization and fast electrons by reactions such as the binary reaction

$$M^* + M^* \rightarrow M^+ + e + \text{K.E.},$$

or the dissociation reaction

$$h\nu + M \rightarrow M^{+} + e + K.E.$$

These electrons might then further augment the ionization by impact upon metastable and blockaded resonance states. The suggested reactions are only two of several possible electron-energizing photon-induced reactions. If the photon theory is correct, one would estimate that the electron temperature in the wave is closely related to the residual energy of the reaction. Energies of order 10 ev are easily possible, consistent with flow velocities 2×10^8 cm/sec, but should be chiefly characteristic of the gas under study. It is difficult, but not impossible, to make this model consistent with a dependence of velocity on driver chamber field, and we regard it as an unlikely explanation of this front.

Hales and Josephson (71) have observed potential variations on electrostatic probes as this front passes. From their reported data it is possible to derive some additional information about the structure of this front. Wave thicknesses turn out to be unexpectedly large ($\sim$ 30 cm) and electron concentrations small ($\sim 10^6$ cm). The parabolic shape of the potential wave observed is exactly what one would expect from a slab of electrons of nearly uniform concentration.

Similar thicknesses are observed for the luminous zone in the segmented shock tube, but the much greater luminosity present in the latter case implies larger electron concentrations, perhaps by a factor of 10^3. Rough estimates of the exposure to be expected from these waves place it at 10^{-8} n ergs/cm^2. This is in agreement with the fact that the waves seen by Hales and Josephson were barely detectable on a photograph (as noted before the photographic threshhold is in the vicinity of 10^{-3} erg/cm^2).

Clotfelter (61) also noticed the precursor waves as an instantaneously arriving induction signal in his magnetic measurements (Chapter X). He noted that it always had the character of an outwardly moving cloud of negative charge, but presumed at the time that it was of optical origin, and termed it a "photoelectric" signal.

CHAPTER VI

RADIATION STUDIES

6-1 General Observations. Since the various phenomena of the electric shock tube are largely marked by variations of the luminosity emitted, and since these variations are a direct indication of the processes taking place locally, the goal of the study should be a complete space and time resolved spectral analysis in frequency and absolute intensity of the entire emitted radiation. We have only been able to make the most cursory of efforts toward this goal.

Spectroscopy of these radiations can supply a well-known arsenal of tools for investigation. Qualitative observations show the atomic and molecular species responsible for the radiation; absolute intensities of lines and continua can give electron temperatures and process cross-sections for exotic processes; half-widths of lines can give measures of interparticle interactions, especially ion concentrations.

The electric shock tube is a useful tool for self-study because of the radiation processes occurring in it, but at the same time is an equally good tool for study of the processes themselves because they occur under conditions which are potentially well controlled and well defined. Some of these results will be given below.

6-2 Qualitative Spectral Observations. Zanstra (8) had proposed that the radiation from the Rayleigh phenomenon came from recombination of effusing ions produced in the electrodeless discharge. Although all subsequent work has tended to verify the importance of various recombination processes in these fronts (owing to the high levels of ionization encountered) the picture of passive effusion is generally inconsistent with the data, even for the flow of the driver gas behind the contact surface, and a considerable measure of active ion production in situ must be included. Careful work by Compton (11) demonstrated that there was luminosity from the shocked gas which could of course only be developed locally.

Clotfelter (88) conducted an early spectroscopic examination of the flow which showed that the Balmer series broke off at H_θ and an intense continuum existed beyond this point, terminating at around 2300 A°. In an attempt to show that the necessary conditions for recombination were present, rotating mirrorgrams were taken with two filters placed over adjacent portions of the

expansion chamber. One filter transmitted only the continuum and the other transmitted only the line series. No displacement of the luminous front was observed on the mirrorgram at the point where the front crossed the dividing line between filters, showing that the continuous light was emitted within 10^{-7} seconds of the quantized light. This would be a requirement if the quantized transitions had each been preceded by the unquantized transitions which would accompany radiative recombination. It was hence concluded that a fast recombination could be an active process in producing the radiation from the fronts.

Observations concerning the washing out of the higher members of the Balmer series, coupled with the great broadening of the remaining members suggested the work of von Traubenberg, and Finkelberg, and the Holtsmark method was subsequently applied to determine ion concentrations.

Luminosity at the shock front in the electric shock tube is not as difficult to explain as in conventional shock tubes. The problem in the conventional case is that the cross sections for inelastic collision by neutral atoms are known to be so small at the energies present in the front, that no elatation would be expected in the times available. Only electrons encounter sufficient cross sections to produce the radiation, but they are not available to the shock through atom-atom ionization. In the electric shock tube, the electron precursor wave generates ample electrons for use in the shock proper when the latter possesses sufficient strength to be an ionizing shock. In the conventional shock tube, part of the problem of brilliant shock luminosity in comparatively weak shocks was removed by the observation (89) that the spectra were those of low threshhold substances such as sodium and calcium. Additional apparatus cleanliness eliminated this effect. Even so, the spectra of noble gases can be excited (29), and the question where the initial electrons come from remains. Once present, however, they are self regenerating. In explosive driven shock tubes (90) there is the possibility of precursor wave electrons from the chemical reaction if the propellent is detonated in direct contact with the shocked gas.

The numerous impurity lines found in our early versions of the shock tube furnished a rough estimate of the electron temperatures and probably the overall temperatures present in the expanding driver at times rather late in its history. These impurities came from decomposition of the tube wall and volatilization of the electrodes. Their spectra showed that excited systems having energies 170 ev above the ground state can be present some distance down the expansion chamber. Silicon IV lines were graded in intensity, all lines being most intense at the head of the expansion chamber and becoming unobservable 5 cm down the expansion chamber. Silicon III lines had a slight intensity gradation and were visible throughout the entire 14-cm region investigated and had a maximum intensity 6 cm down the side tube. The lines of

Silicon I were not present at all near the head of the expansion chamber, but were found throughout the lower 9 cm of the 14-cm region investigated. The ionized forms of oxygen showed analogous behavior. This gradation was made the basis of the estimate of temperature, using the Milne-Fowler color-temperature theory commonly employed in astrophysical work. Table X (from the Handbuch der Astrophysik) gives the temperatures at which various levels of excitation, in thermal equilibrium, would reach their maximum radiated intensity.

TABLE X

SiI	7,000°	H	10,000°
SiII	10,000°	CII	16,500°
SiIII	17,500°	OII	17,500°
SiIV	25,000°	CIII	25,000°
HeI	16,500°	OIII	26,000°
HeII	35,000°	CIV	40,000°

Locating the position of the maximum of each of these stages of excitation then gave an index of temperature in the discharge at that point. Table XI is based on this sort of estimate.

TABLE XI
DISCHARGE TEMPERATURE DISTRIBUTION IN H_2 AT
3500 V, 0.3 mm Hg, T-TUBE CONFIGURATION

Distance from head of tube	Temperature	Gas
-1 cm	26,000	OIII
-1 cm	25,000	SiIV
1-2 cm	17,500	SiIII
3-4 cm	17,500	OII
5 cm	10,500	SiII
9-10 cm	10,000	H
12 cm	7,000	SiI

DISCHARGE TEMPERATURE DISTRIBUTION IN H_2 AT
4500 V, 3 mm Hg, LINEAR SHOCK TUBE CONFIGURATION

- 8	10,000	H
- 7	10,500	SiI
0	26,000	OIII
6	10,000	H
15	7,000	SiI

The method is capable of refinement, but is probably not as good as either the method of black body reversal, or the use of

absolute line intensities, both of which are now being employed (91) with great success and precision.

The large ion concentrations present were found by Teska (92) to ameliorate the selection rules in helium, and permit radiation of a variety of forbidden lines. Fig. 47 is a spectrum of an expanding helium discharge.

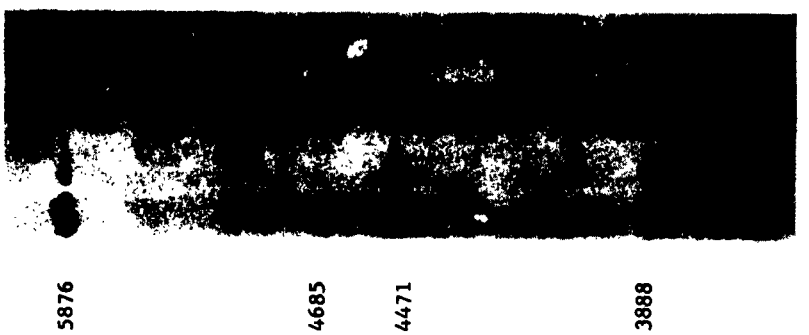

Fig. 47 Helium Broadening and Forbidden Transitions

6-3 Half-Widths and Ion Concentrations. Spectral lines always have a finite breadth determined largely by the average environment of the radiators. Beginning with an intrinsic line width which depends upon the structure of the atom, one may have broadening which depends upon thermal motion, upon close collisions, and upon mean local fields of surrounding neighbors. It is somewhat difficult to draw a line between the latter causes, but limiting theories can be derived for all causes of broadening. Because of a general doubt that a given observation of broadening should be interpreted by one theory rather than another, the use of broadening as a laboratory tool was somewhat slow in developing although a detailed theory had been advanced as far back as 1919 by Holtsmark (93). In 1930 von Traubenberg (94) noted that the Balmer lines of large n can be so greatly broadened that they are indistinguishible from a continuum. In 1931, Finkelnberg (95) used this fact to make semi-quantitative estimates of ion concentrations in laboratory discharges in hydrogen at super-atmospheric pressures. In 1936, Verweij (96) applied the Holtsmark statistical analysis of Stark splittings to the estimation of ion concentration in the chromosphere of the sun using Balmer line broadening. Craggs and Hopwood (12) in 1947 studied the growth of ion concentration in time and space in spark channels in hydrogen using half-widths of the Balmer lines. They pointed out that one could trust the

Stark effect interpretation of the broadenings observed because of the peculiar pointed shapes of the odd members of the series resulting from the presence of an undeviated component in the Stark array. In 1952 three independent applications of the method were reported. Jurgens (97) examined the water stabilized carbon arc at atmospheric pressure, and found Balmer broadenings from which ion concentrations could be inferred. Olsen and Huxford (98) introduced hydrogen as a probe gas in argon and neon flash lamps and determined ion concentrations by broadening. Atkinson (99) used half widths to determine ion concentrations in expanding hydrogen plasmas from the electric shock tube. He noted that the origin of the broadening could not be from temperature or pressure because of the unreasonable values required, but was positively indicated to be Stark broadening not only because of the peaking of the odd numbered Balmer lines, but also because the even members of the series were seen to be split at high ion concentrations, owing to the lack of an undeviated component. His work, together with that of Marks (100) and Rose (101) cast doubt upon the adequacy of the simple Holtsmark theory. The broadening seemed to be strongly sensitive to temperature as well as ion concentration. Griem (102) in 1954 greatly improved the analysis of the stabilized arc experiments, showing the importance of electron collision corrections to the Holtsmark theory. Spitzer (103) called attention to the importance of electron collision broadening. Ecker, (104) and Thiemer (105) in 1957 considered the Debye shielding of the positive ions by the electron cloud as a means of explaining some of the discrepancies found by Atkinson. Turner (106) in 1958 applied Stark broadening to the conventional shock tube, noting quantitative discrepancies. Kolb and Griem (107) have completed a definitive analysis of the problem, combining the enhancing efforts of electron collision with the diminishing effects of electron shielding of the ions to obtain working curves for interpretation of ion broadening in general. The rather interesting practical conclusion has been reached that if all precautions are taken ion concentrations can now be measured to better than 10% accuracy using line profiles, but that because of the generally offsetting character of the two electron corrections to the Holtsmark theory, even the crude half-width theory does not deviate excessively for the range of experimental conditions usually found in plasmas, and often is much better.

No further work has been done on broadening at the University of Oklahoma since doubt concerning the theory arose. A review of the earlier work, and a report of some not previously reported will conclude this section. Most of the discrepancies found before can now be rationalized in the light of better understanding of electric shock tube operation.

In presenting these results little effort will be made to improve on the half-width work originally reported, since the more accurate methods would demand a fitting of profiles, which are no longer available, and in any event, the data taken were averages over time at a given location in the expansion rather than the more

desirable time and space resolved data we would prefer. One adjustment has been made. Holtsmark first used his function with a smeared out distribution of line intensities for the several Stark components, by representing the intensity of the line as a step function between the splitting limits of the maximum pair of lines. This pair has a splitting factor of 14 for H_β. Atkinson altered the original Holtsmark method by noting that the far flung components of the Balmer lines were too weak in intensity to contribute substantially to the profile, and should be ignored in favor of the widest spread intense components. That is to say, in the expression

$$\Delta\nu = \frac{3h\left[n_1(n_1' - n_1'') - n_2(n_2' - n_2'')\right]}{8\pi^2 mec} E$$

the bracketed function of the electric quantum numbers n, n' and n'' was assigned the value 4 instead of 8 for the H_α line, 10 instead of 14 for the H_β line and 18 instead of 22 for the H_γ line. [In a recalculation of our data it seems more reasonable to ignore the information from H_α and H_γ entirely, because of the undeviated component which is only electron broadened.] Now the actual profile function $S(\alpha)$ of Griem et. al. shows that inclusion of the various corrections is, by the long arm of coincidence, equivalent to returning to the maximum quantum splitting factor of 14 originally used by Holtsmark. Accordingly our values have been adjusted back to this level, which amounts to using the formula

$$N = 3.55 \times 10^{14} (\Delta\lambda_{\frac{1}{2}})^{3/2}$$

where $\Delta\lambda_{\frac{1}{2}}$ is the full side-to-side half-width of H_β in Å. This corresponds to choosing a value of $\alpha_{\frac{1}{2}}$ of 0.080. A complete set of values of $\alpha_{\frac{1}{2}}$ is given in Table XII, computed from the $S(\alpha)$ functions of Griem. Under this approximation the correct maximum to take in the case of an H_β line broadened to the point that there is a dip in its center is the actual or wing maximum, not the central value.

TABLE XII
$\alpha_{\frac{1}{2}}$ FOR THE H_β LINE

Ion Concentration	TEMPERATURE 10^4	2×10^4	4×10^4
10^{15}/cc	.078	.080	.079
10^{16}	.080	.081	.084
10^{17}	.083	.078	.091

Since the use of the original Holtsmark function to sum the contributions of the various components shows that the location of the half-width of the total intensity function is very nearly the same as the half-width of the component for which the quantum

splitting factor is 6, the effect of all corrections is to reduce the ion concentrations that would have been obtained from an exact use of the Holtsmark theory alone by a factor 0.28.

The work of Atkinson was done in a T-tube configuration. His data were taken over a pressure range from 0.27 to 7.6 mm Hg and with capacitor potentials of 2000 to 4000 volts in a tube of 1.8 cm ID. It was observed that the ion concentration increased as the gas flowed down the expansion tube. All these data could be reduced to a common curve (Fig. 48) in terms of the time of flight to the point of observation, plotted against the fraction of ionization divided by the capacitor potential. The fraction of ionization is taken with respect to the initial particle density. This is not the true value, since it is necessary to correct for the hydrodynamical expansion or compression prevailing at the time and in the region of observation. Clearly this last fact (that the ion concentration was proportional to the capacitor potential) implies that the degree of ionization was far from complete, as the data in fact indicated. Rose (101) repeated this work in the linear shock tube configuration with substantially the same result, except that this tube was a more efficient producer of ionization, being somewhat smaller in diameter, and shorter; and that the time of maximum ion concentration occurred later in the linear tube. Rose also investigated the ion concentrations found in the driver (Fig. 49). Here it makes little sense to introduce a transformation from space to time, since the integrated intensities give a weighting to the longest duration concentrations prevailing, and most of the gas in the driver region (especially the rearward portion) is at rest during the time it is radiating most strongly.

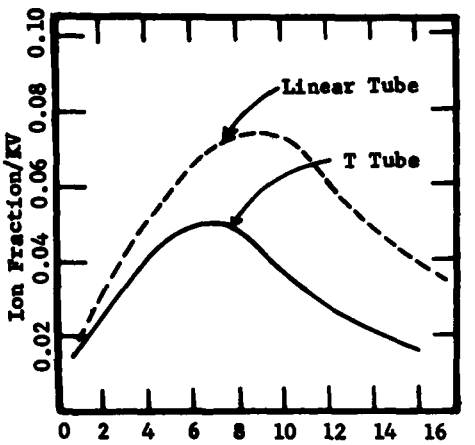

Fig. 48 Generalized Ionization in H_2

We have seen in Chapter III that the rise of ion concentration in the driver is geared intimately to the current in the driver. Since the peak value of this current, in the critically damped case generally used by these workers, is proportional to the initial capacitor potential, the ion concentration should have had the same proportionality, as was observed. The belated rise to a maximum in time must be ascribed to heat conduction throughout the driver which holds the ionization rate approximately the same everywhere, even outside the interelectrode zone containing the electric field. Olsen and Huxford (98) also observed this temporal behavior of ionization in their investigations of photoflash

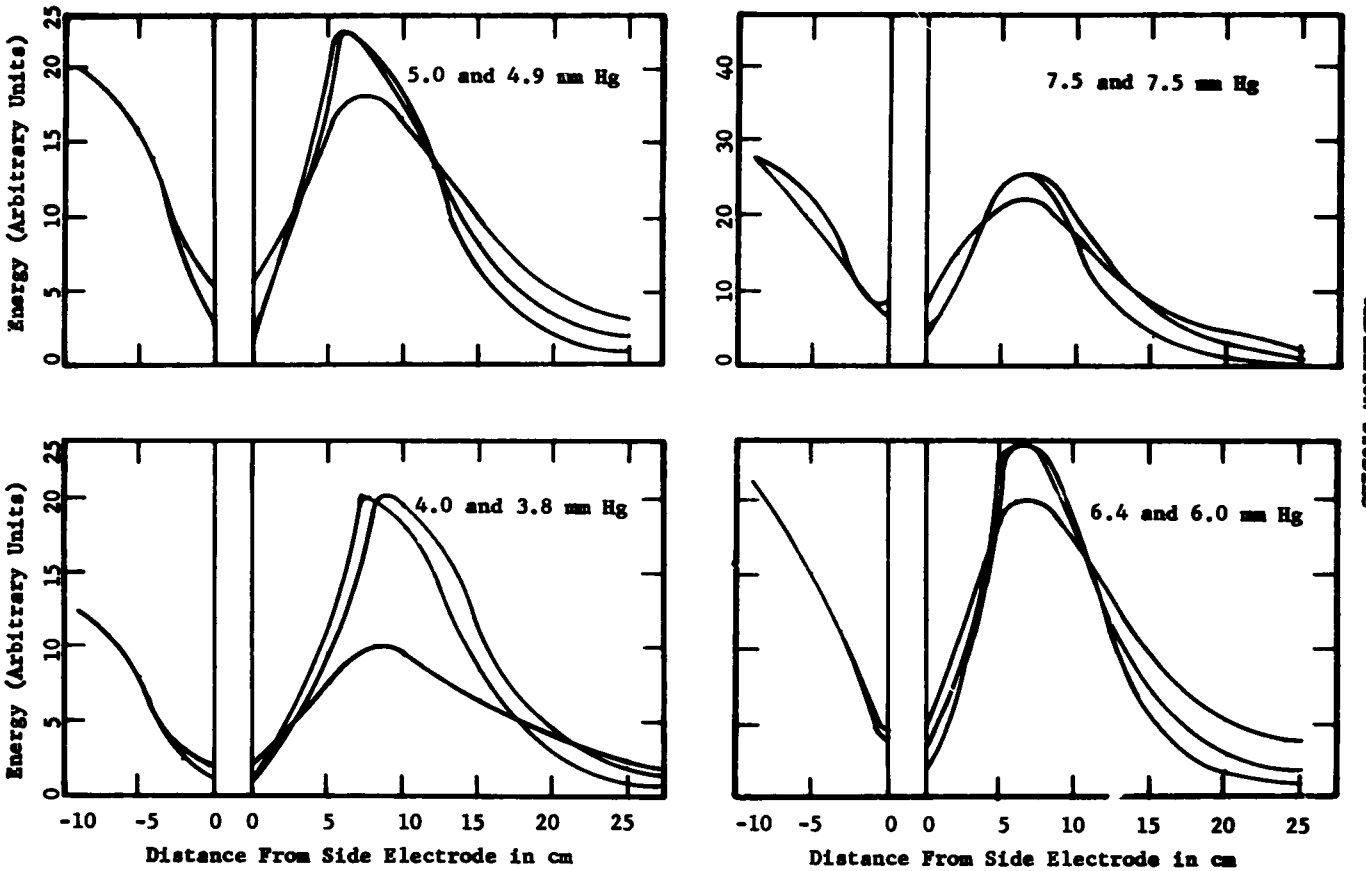
5.0 and 4.9 mm Hg
7.5 and 7.5 mm Hg
4.0 and 3.8 mm Hg
6.4 and 6.0 mm Hg
Energy (Arbitrary Units)
Energy (Arbitrary Units)
Distance From Side Electrode in cm
Distance From Side Electrode in cm

Fig. 49

discharges, which differ in only minute ways from the driver region of the electric shock tube.

Teska (92) investigated the state of ionization in helium along lines similar to those of Rose. It was expected that if the belated rise to a maximum was an artifact of the Holtsmark theory, the effect would be minimized in the broadening of the ionized helium lines. The nearly identical results obtained substantiate the explanation of the rise given above. Any differences can be assigned to the slower expansions of helium relative to hydrogen. The data are given in Fig. 50.

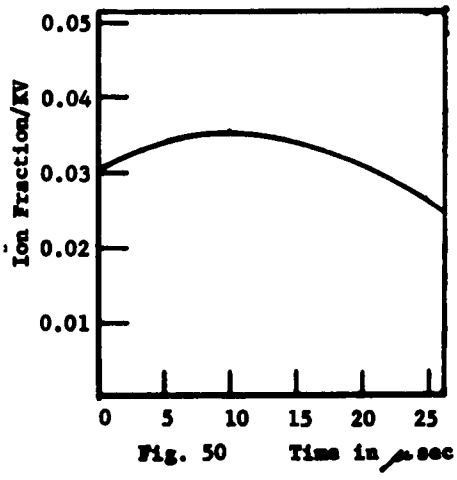

Fig. 50

6-4 Electron Recombination and the Radiation Law. Marks (100) examined the relation between ion concentration as determined by broadening, and the total integrated intensity of the H_β line. A logarithmic plot of these intensities against half-widths interpreted as concentrations is given in Fig. 51.

In actual fact, the quantity measured was not intensity, but exposure. Since the fronts at various pressures (and hence at different ion concentrations) pass the spectrograph's field of view in different time intervals because of their differing speeds, one would expect apriori that a velocity correction should be made on these exposures to give a quantity more nearly proportional to the intensity. To make this correction the exposures should all be multiplied by the velocities of advance of the luminosities. This correction was not made on the data of Fig. 51. To make such correction resulted in a much greater scatter of the experimental points, and introduced systematic differences between the points obtained with different capacitors. Whether or not the velocity corrections were made, the slope of the curve in Fig. 51 was very nearly two. Uncorrected it was 1.9. Corrected for velocity it was 1.8.

Little understanding of the fluid processes active was had at the time this research was completed. It is now apparent that the velocity correction should not have been applied, since the spatial extent of the various flows is largely fixed by the length of the driver section of the shock tube and the location of the point of observation. Hence the exposure would be the same for flows of whatever velocity was encountered. Barring the imperfection that the analysis is based on time integrated measurements, which does not seem to have hindered its validity much when one considers the reproducibility of the points shown in Fig. 51, the work of Marks

tends to establish the fact that the chief mechanism of quantized radiation production in the expansion chamber is recombination of the intensely ionized gas present there, since radiation from recombination should vary as the square of the ion concentration.

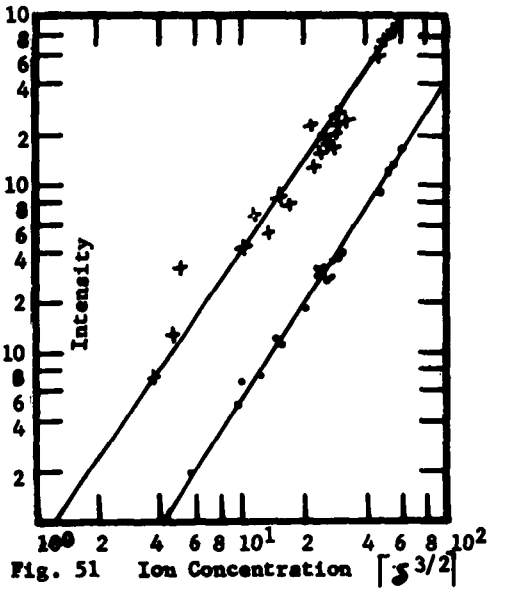

Fig. 51

Because the Marks research was conducted in the old T-configuration, Rose (101) also extended this study to the linear shock tube. He confirmed the earlier finding relative to the luminosity in the expansion chamber, but noted that in the driver chamber a linear law of relation existed between intensity and ion concentration (Fig. 49). This is much as would be expected in the very hot driver discharge where electron recombination should be inhibited by high electron temperatures, and hence dominated by excitation processes in the neutral gas.

In hydrogen discharges, and of particular interest, in the expansion from the electric shock tube, there is an intense continuum in the region between 2000 and 5000 Å. It is observed widely, in sparks in hydrogen, in arcs in hydrogen, and in hydrogen emission stars. It has been definitely distinguished from the molecular continuum (108) (109). It is in general believed to be the series limit continuum of the Balmer series, although it is understood that the increasing presence of Stark fields of local ions under conditions which are favorable to the continuum tends to enhance the series limit continuum by obliteration of the higher levels of the hydrogen atom. Even considering this, the continuum associated with the Balmer series remains anomalously intense, being far more intense than the corresponding Paschen continuum (Fig. 13).

An additional factor which was recognized by Lochte-Holtgreven (110), and independently by ourselves, is the negative hydrogen ion, which accounts for the opacity of certain stars, and on which much work has been done (111). This produces a continuum in exactly the right wave-length range to account for the preponderance of intensity of the Balmer associated continuum over the other hydrogen limit continua. It should however be linear in dependence on electron concentration, and decrease strongly with increasing electron temperature.

Still another factor in producing a continuum in the region could be bremstrahlung processes. Electron-ion bremstrahlung would vary as the square of the ion concentration. It should

increase strongly with electron temperature. There may also be ion-neutral bremstrahlung, a process for which there seems to be no theory available, but which must be closely related to the H^- affinity spectrum.

The problem of this continuum was of extra interest in our program because of the information it might convey about temperatures and possible ion concentrations in the transient states encountered in flowing ion clouds. Over and beyond this, the hydrogen continuum could be a valuable and much needed absolute standard continuous source of radiation if the theory of it could be placed on an only slightly firmer footing.

Equations for the wavelength dependence of these various processes have been obtained. Thus for the recombination continuum we have (in esu)

$$\mathcal{J}_\lambda = \frac{\pi e^4 h^2 V_i^2 n_+ n_e}{4 m \lambda^2} \left(\frac{2}{3\pi m kT}\right)^{3/2} e^{-\frac{h\lambda}{ckT}} e^{\frac{e V_i}{16 kT}}$$

as the power radiated per unit volume per unit solid angle per unit wave-length. For the electron-ion bremstrahlung, in the same units,

$$\mathcal{J}_\lambda = \frac{8 e^6 n_+ n_e}{3\pi m^2 \lambda c} \left(\frac{m}{2\pi kT}\right)^{1/2} \left[e^{-\frac{h\lambda}{ckT}} \ell n\, 4 - E_i(-h\lambda/ckT).\right]$$

Atkinson (112) measured the monochromatic radiant intensity of this continuum under one set of conditions, and the data were used to compute a rough recombination coefficient. A larger amount of data, however, gathered later over widely varying conditions, has shown that a simple explanation in terms of recombination is in error under high temperature conditions by as much as a factor of 10^2. These original data are given in Appendix 3, since we are not at present satisfied with our interpretation of them. To use them it is necessary to have the corresponding ion concentration and temperatures which are also given. The ion concentrations were those determined by Stark broadening, while the temperatures were taken to be those indicated by the accompanying shock speeds.

If one does in fact interpret the continuum as a recombination consequence, he obtains the array of recombination coefficients shown in Table XIII. In the limit of large concentrations where temperature is low the results tend to agree with the calculations of Cillie (53) for these supposed temperatures. However, the continuum at high temperatures is far too strong to be due to recombination alone. Electron bremstrahlung may perhaps account for the balance.

The limiting values of recombination coefficients fairly well agree with those of Olsen and Huxford (98) obtained by a study of

time variation of Stark broadening. However, their measurements were not made in a field-free region, but between the electrodes of a tube very similar to our shock discharge chamber, and this could account for any discrepancies. The effect of the field on rates of recombination is illustrated by experiments by Miller (113) in our laboratory (and older work by Kenty (114). When a voltage pulse is applied to the electrodes at variable intervals after the beginning of the discharge, it is found that, any time during the first ten microseconds the pulse makes the discharge more intense, so that production must exceed recombination in the discharge chamber.

TABLE XIII

THEORETICAL AND EXPERIMENTAL RECOMBINATION COEFFICIENTS*

Pressure mm Hg	2 kv	3 kv	4 kv	5 kv
0.45	1.15×10^{-15}	7×10^{-16} 6.2×10^{-13}	5.1×10^{-16} 1.0×10^{-12}	3.8×10^{-16} 1.1×10^{-12}
0.85	2.0×10^{-15}	1.4×10^{-15} 1.1×10^{-13}	1.1×10^{-16} 2.1×10^{-13}	8.0×10^{-16} 1.8×10^{-13}
1.95	4.1×10^{-15} 2.1×10^{-14}	3.0×10^{-15} 2.1×10^{-14}	2.4×10^{-15} 3.7×10^{-14}	1.9×10^{-15} 3.4×10^{-14}
3.20	6.4×10^{-15} 8.9×10^{-14}	4.5×10^{-15} 1.6×10^{-14}	3.5×10^{-15} 2.0×10^{-14}	3.0×10^{-15} 2.0×10^{-14}
5.20	9.3×10^{-15} 3.5×10^{-15}	7.0×10^{-15} 6.9×10^{-15}	5.1×10^{-15} 9.4×10^{-15}	4.5×10^{-15} 9.7×10^{-15}
8.0	1.3×10^{-14}	9.4×10^{-15} 3.5×10^{-15}	7.7×10^{-15} 5.0×10^{-15}	6.4×10^{-15} 5.2×10^{-15}
11.0		1.15×10^{-14} 1.4×10^{-15}	9.5×10^{-15} 2.7×10^{-15}	8.0×10^{-15} 2.0×10^{-15}

*Upper number theoretical, lower experimental, in each pair.

If a pulse is applied later, the intensity drops because the rate of recombination decreases owing to the increasing electron temperature. Thus the low values of recombination coefficient observed in "active" discharges can be a result of the continuing processes of production which maintain the ion concentration during a time interval in which it is presumed to be decaying freely. Clotfelter has analyzed this further (61). The recombination coefficient, α, is defined by the equation

$$dN/dt = -\alpha N^2,$$

in which N is the electron density, assumed equal to the density of positive ions. If, as a first approximation, production processes are neglected, the solution of this equation is

$$1/N = 1/N_0 + \alpha t,$$

if N_0 is the electron density at time t = 0. If 1/N is denoted by X and $1/N_0$ by X_0, this becomes

$$X = X_0 + \alpha t,$$

the equation of a straight line with slope α. This is the equation used by Olsen and Huxford to determine α from their measurements of ion concentrations as a function of time.

If production processes are included, the major ones may be included in an equation of this form:

$$dN/dt = -\alpha N^2 + \beta N(N_a - N) + \gamma N^2(N_a - N) + \delta N^3(N_a - N).$$

N_a is the number of atoms originally present in the gas, so that $(N_a - N)$ is the number of neutral atoms at any instant. These terms represent the following processes: The first term is simply recombination. The second term represents ionization by impact of electrons on neutral atoms, and hence is proportional to the number of electrons present and to the number of neutral atoms. The third term describes the process of photo-ionization. Since the production of radiation is proportional to N^2 if those atoms which are merely excited without being ionized are ignored, and the production of ions must be proportional to the number of neutral atoms present, the term has the form indicated. In a slightly ionized gas this coefficient would be small, but in a highly ionized gas, the ionic fields lower the ionizing potential sufficiently that photons of sufficient energy to raise the atom to a highly excited state may ionize it. Because of the intense high energy radiation present in such discharges, this effect may be quite significant. The last term describes the production of ions by photo-excitation (proportional to $N^2(N_a - N)$) followed by collision with an electron.

The equation may be rewritten as

$$dN/dt = N(\beta N_a) + N^2(\gamma N_a - \alpha - \beta) + N^3(\delta N_a - \gamma) - \delta N^4,$$

or

$$dN/dt = gN + hN^2 + jN^3 - \delta N^4.$$

If all terms containing N^3 and N^4 are neglected, the equation becomes

$$dN/dt = gN + hN^2,$$

whose solution is

$$1/g \log N/(g + hN) = t + C,$$

or

$$(g + hN)/N = C'e^{-gt}.$$

If N_o is the value of N at the time t = 0, that is, the initial ionization, and if X and X_o represent 1/N and $1/N_o$ respectively,

$$gX + h = (gX_o + h)e^{-gt},$$

and if g is quite small and only a small interval of time is considered, this may be approximated by

$$gX = gX_o - g(gX_o + h)t$$

or

$$X = X_o - (gX_o + h)t.$$

If g and h are replaced by their values, this becomes

$$X = X_o - (\beta N_a X_o + \gamma N_a - \alpha - \beta)t.$$

This, too, is the equation of a straight line, having the same intercept as the line obtained when production is ignored, but having a smaller slope.

6-5 Opacity of Hydrogen Discharges. If the continua studied in Section 6-4 are to be used for calculation of volume processes, or for a radiation standard it is necessary to know that the plasma is transparent to its own radiation. Gardner (115) investigated the opacity of the luminous flow by placing a mirror behind a shock tube of square cross section and reflecting the radiation back through the flow. Repeated measurements showed that the gas was almost opaque, with a sudden onset of this opacity, below 2600 Å. Since the gas does in fact radiate reasonably well in the region below 2600 Å, it was inferred that the absorption was taking place in thin layers near the windows, so that only a single pass through one layer was needed for outgoing radiation, while three passes were needed by the reflected radiation.

Consideration of a variety of processes was made, but the point of onset of the absorption suggested most strongly the presence of H_2 molecules near the windows, and a dissociative absorption, plotting the data against a theory of the process given by Erkovich (116) gave the results of Fig. 52.

6-6 Dissociative Recombination. A peculiar phenomenon observed in noble gases at high pressures ($\sim$ 100 mm Hg) may have some bearing on the problem of dissociative recombination. A bright pulse of luminosity is present in the flow whose leading edge is the contact surface and whose trailing edge is remarkably well defined (Fig. 53). As yet no adequate explanation of the fluid dynamical processes which are present has been advanced.

The luminosity itself, however, was carefully investigated by Atkinson.

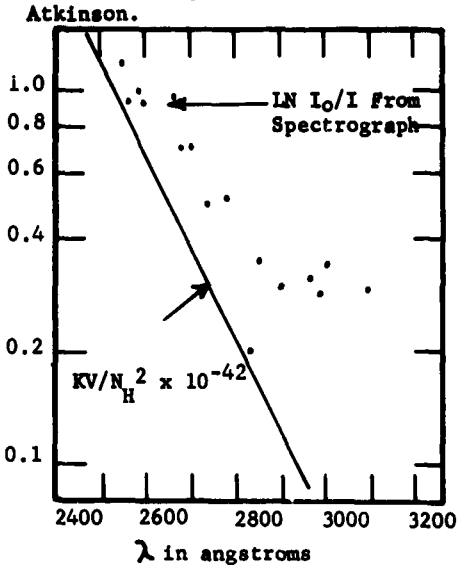

Fig. 52 Opacity Theory vs Experiment Fig. 53 Bright Pulse

A general survey of the mirrorgrams and Kerr-cell photographs that show the pulse-like distributions may be summarized in the following way: pulse like distributions of luminosity have been observed best in neon and helium; to a lesser extent xenon is also suitable; high initial pressures (200 mm of Hg), small capacitors (1 microfarad), large volume heating chambers (70 cm^3) and low capacitor potentials (3000 volts) tend to enhance the pulse like distributions. The pulse may be produced in T-shaped tubes in which the expansion chamber is connected midway between the electrodes of the heating chamber. However, the pulse is not as well developed in these T-shaped tubes as in straight tubes. The pulse will propagate through tubes having either conducting or non-conducting walls. Neither electrode polarity nor magnetic fields up to 15,000 gauss in the expansion chamber affect the pulse in any way. The leading edge of the pulse is preceded by a shock which, even though it is non-luminous, may be inferred directly from the mirrorgrams of a reflection process. The trailing edge of the pulse is not as well defined as the leading edge.

One of the simplest explanations that might be proposed for the pulse of luminosity would attribute the luminosity to easily excitable metal atoms evaporated from the ring electrode. These metallic atoms would tend to be localized in a thin layer immediately behind the contact surface because this layer in the early stages of the expansion was located near the ring electrode. The observation of pulses from T-shaped tubes discredited this explanation somewhat, but by far the most serious objection came from

the spectrograph. The Kerr-cell shutter and the rotating-mirror spectrograph combination made it possible to obtain a spectrum of the pulse alone without any of the light from the gases behind the pulse and to a lesser extent a spectrum of the post pulse luminosity alone. Except for a large intensity factor, both spectra appeared to be identical. The 5876, 5016, 4922, 4713, 4471, 4026 and 3889 Å lines of He I were the only lines found. The last two lines were found with the rotating-mirror spectrograph combination rather than the Kerr-cell shutter which would not transmit past 4471 Å.

When discharge conditions are suitable for the production of a luminous pulse (rather than a jet), stigmatic spectrograms of the shock tube are fairly well time resolved without the use of either shutter. That is, without the use of a shutter a spectrum of the brilliant luminous pulse at any time can be obtained without much interference from the dim, but long lasting, luminosity behind the pulse. The reciprocal problem of obtaining a spectrum of the post-pulse luminosity without interference from the pulse luminosity is obviously involuble without a shutter. Stigmatic spectrograms were made without any shutter for a sequence of pressures. The entire He I spectrum was found throughout the expansion and heating chambers for all pressures. The He II 4685 and 3203 A lines were present throughout the heating chamber, but only in an adjacent fraction of the expansion chamber. Under no circumstances did either line extend farther into the expansion chamber than the other. As the pressure was increased the length of the He II lines decreased until they were confined entirely to the heating chamber. For the particular circuit and tube used the critical pressure which marked the disappearance of the He II lines in the expansion chamber was about one half the pressure required for production of the pulse like luminosity distribution.

As would be expected after examining Fig. 36 the oscilloscope traces showing the time variation of the monochromatic intensity at a particular position were not very smooth and varied in height from flash to flash by as much as a factor of two. In the spectrograms this variation was averaged out because it was necessary to use many flashes to obtain a suitable exposure. With the photomultiplier and monochromator at least ten traces were allowed to fall on each frame of film so that an average trace could be constructed from the ten separate records. Table XIV gives the average relative intensities for various wave lengths, times, and positions. A 4 microfarad capacitor charged to 4700 volts was used to supply energy to He at 121 mm of Hg. Under these conditions the luminous pulse was well developed, and the recorded average relative intensities correspond to the most luminous portion of the pulse. In Table XIV the relative intensities have been separately normalized for each wave length. Time origins and normalization factors used in the heating chamber differ from those used in the expansion chamber. Positive positions are measured from the ring electrode and lie in the expansion chamber.

TABLE XIV
RELATIVE INTENSITIES IN A SHOCK TUBE FOR TYPICAL LUMINOUS PULSE CONDITIONS

Position cm	Time Microseconds	Wavelength A	Relative Intensity
9.8	0	5876	10,000
14.9	48	5876	623
19.8	102	5876	36.3
24.7	174	5876	2.93
9.8	0	3889	10,000
14.9	51	3889	975
19.8	105	3889	19.4
24.7	176	3889	3.27
9.8	0	4170	10,000
14.9	51	4170	1,500
19.8	95.5	4170	34.7
24.7	164	4170	4.71

Whatever the explanation of the flow the character of the radiation processes in it are equally interesting. Two body recombination and three body recombination seem out of the question, and direct excitation would not be sufficient at the electron temperature of 1300°K which is consistent with the contact surface velocity of 1.03 km/sec. At this temperature, however, the mean particle energy of 0.15 ev is low enough to permit the existence of He_2^+ ions in copious quantities. Diffusion can be neglected at these pressures.

Two processes complete in the destruction of a He_2^+ molecule. First, atomic and electronic collisions energetic enough to furnish the 2.2 ev required to dissociate the molecule are not too rare. Secondly, the molecule can capture an electron and then radiate and dissociate into excited helium atoms. Let k be the rate at which He_2^+ is formed by collision between He^+ and He, $\overline{\sigma v}$ be the rate at which He_2^+ is destroyed by atomic collision, and $\overline{\sigma_e v_e}$ be the rate of destruction by electron collision, and α be the rate at which He_2^+ is destroyed by electron capture. Let n_2 and n_1 denote the particle density of the molecular and atomic ions respectively. Then if we consider no other destruction processes, we have,

$$\frac{d\,n_1}{dt} = -\,k\,n_1 + \overline{\sigma v}\,n_2\,N_o + \overline{\sigma_e v_e}\,n_e\,n_2$$

$$\frac{d\,n_e}{dt} = -\,\alpha\,n_e\,n_2$$

$$n_e = n_2 + n_1$$

Considering these equations, it seems unlikely that any solution except the basic recombination solution

$$\frac{d n_e}{dt} = - \alpha n_e^2$$

is reasonable. Following this, the intensity of the discharge intensity I would behave as

$$1 + \alpha n_o t = \sqrt{\frac{I_o}{I}} .$$

The data, plotted according to this expression (Fig. 54) gives a reasonable linearity, and if we estimate that at least one half of the power input not accounted for in thermal motion went into ionization, we place n_o at 2×10^{16}, and thus find an order of magnitude value of α of 2×10^{-11} cm^{-3} sec^{-1}.

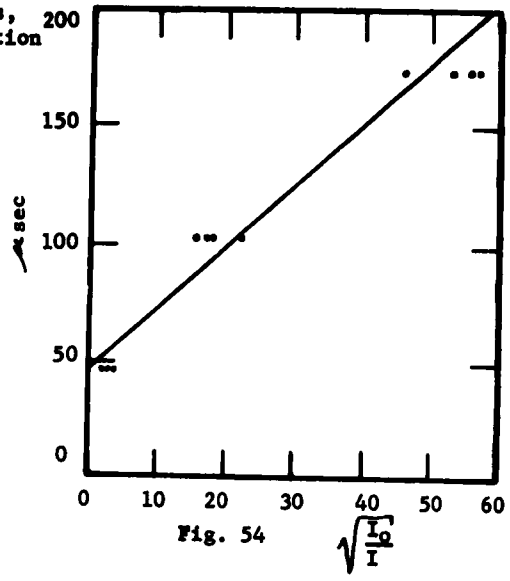

Fig. 54

CHAPTER VII

INTERACTIONS

7-1 Zone to Zone Transitions of Waves. When a wave moves out of one region of constant state into another, the crossing is commonly called an interaction. The term becomes a truly significant one when the "waves" are actually, themselves, discontinuities between regions of constant state. The electric shock tube is an especially effective device for the study of such interactions because they can be produced with various degrees of complexity, owing to the absence of diaphragms and the possibility of generating multiple shocks in a single apparatus.

Study of photographs has shown that the majority of the interactions between various recognizable supersonic flow fronts is in accord with the predictions of fluid mechanics. We have observed the four classified interactions which are listed below.

I. $S_{\rightarrow} C_{>}$ a shock front with particle flux from the right to the left (shown by the arrow subscript) overtaking from the left a contact surface which separates a region of high sound velocity on the left from a region of lower sound velocity on the right (shown by the inequality subscript).

II. $S_{\rightarrow} S_{\leftarrow}$ a shock with particle flux from right to left advancing to the right and colliding with a shock having a particle flux from left to right.

III. $C_{>} S_{\leftarrow}$ a contact surface between a region of high sound velocity on the left and a region of low sound speed on the right advancing to the right into a shock having particle flux from left to right.

IV. $S_{\leftarrow} S_{\leftarrow}$ a shock with particle flux from left overtaken by similar shock arriving from the right.

The expected flows resulting from these interactions are given by Courant and Friedrichs (117) as

I. $\underline{S}_{\rightarrow} C_{>}$ yields $\underline{R}_{\leftarrow} C_{>} \underline{S}_{\rightarrow}$,

II. $\underline{S}_{\rightarrow} \underline{S}_{\leftarrow}$ yields $\underline{S}_{\leftarrow} C \underline{S}_{\rightarrow}$,

III. $C_{>} \underline{S}_{\leftarrow}$ yields $\underline{S}_{\leftarrow} C_{>} \underline{S}_{\rightarrow}$,

IV. $\underline{S}_{\leftarrow} \underline{S}_{\leftarrow}$ yields $\underline{S}_{\leftarrow} C \underline{R}_{\rightarrow}$,

where $\underrightarrow{R}$ is a rarefaction wave with particle flux from the left, and $\underleftarrow{R}$ is a rarefaction wave with particle flux from the right.

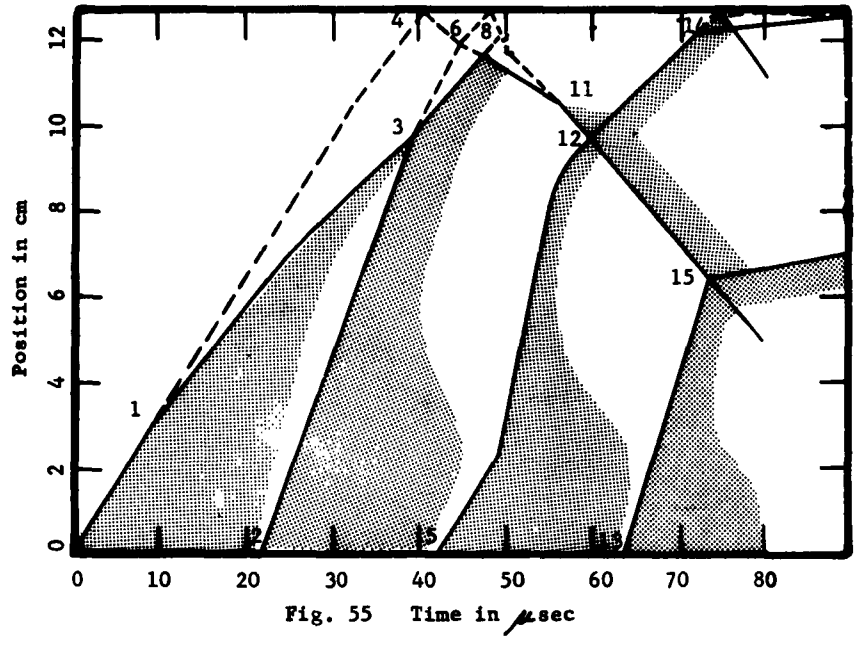

Fig. 55 Time in μsec

A description of Figure 55 will serve to illustrate the success we had in exhibiting experimentally the four types of shock interaction. Unfortunately all of the interactions present on the photographic negative are not visible on the print. Chronologically the negative showed the following interactions:

1. $\underrightarrow{\underrightarrow{S1}}$* and $\overrightarrow{C,1}$ separated, and both became visible.
2. $\underrightarrow{\underrightarrow{S2}}$ was then created at left end of tube.
3. $\underrightarrow{\underrightarrow{S2}}$ overtook $\overrightarrow{C,1}$ and accelerated it. This was an interaction of type I. No rarefaction wave was observed. $\underrightarrow{\underrightarrow{S3}}$ was formed.
4. $\underrightarrow{\underrightarrow{S1}}$ reflected from the right end of tube and formed $\underleftarrow{\underleftarrow{S4}}$.

*Shock 1 moving from left to right (upper arrow) with particle flux from right to left (lower arrow).

5. $\overrightarrow{S5}$ was then created at left end of tube.

6. $\overleftarrow{S4}$ met $\overrightarrow{S3}$ and produced $\overleftarrow{S6}$ and $\overrightarrow{S7}$. This was an interaction of type II. The predicted contact surface was not observed.

7. $\overleftarrow{S6}$ collided with $\overrightarrow{C,1}$ and produced $\overleftarrow{S8}$ and $\overrightarrow{S9}$. This was an interaction of type II.

8. $\overrightarrow{S7}$ reflected from right end of tube and formed $\overleftarrow{S10}$.

9. $\overleftarrow{S10}$ collided with $\overrightarrow{S9}$ and formed $\overleftarrow{S11}$. This was an interaction of type II. Neither the contact surface nor the other shock predicted by theory was visible.

10. $\overleftarrow{S11}$ collided with $\overrightarrow{C,1}$ and formed $\overleftarrow{S12}$. This was an interaction of type III. The other shock predicted by theory was not visible.

11. $\overleftarrow{S12}$ overtook and strengthened $\overleftarrow{S8}$ and formed $\overleftarrow{S13}$. This was an interaction of type IV. Neither the predicted contact surface nor the rarefaction wave was visible.

12. $\overleftarrow{S13}$ met $\overrightarrow{S3}$ and formed $\overleftarrow{S14}$ and $\overleftarrow{S15}$ interaction type II. The contact surface was not visible.

13. $\overrightarrow{S16}$ was then created at left end of tube.

14. $\overrightarrow{S15}$ reflected from right end of tube and formed $\overleftarrow{S17}$.

15. $\overleftarrow{S14}$ met $\overrightarrow{S16}$ and formed $\overleftarrow{S17}$ and $\overleftarrow{S18}$. The contact predicted for a type II interaction not observed.

The contact $\overrightarrow{C,2}$ associated with $\overrightarrow{S2}$ was also visible and interactions of the various shocks with it could be traced. A third contact C 3 of unknown origin was also visible.

We feel that in all the cases above the predicted flow fronts which were not observed were actually present but were not visible because there was no discontinuity of light intensity across them. On the other hand, the interaction in Figure 56 is different in appearance from any described in the literature. The reflected primary shock appears to be refracted before meeting the advancing contact surface. This may however be a consequence of the existence of a boundary layer, or of shock front curvature.

Fig. 56 Abnormal Interaction

No real effort has been made to exploit the possibility of multiple shock interactions in the electric tube to investigate such interactions quantitatively. In part this has been for lack of time, in part because it proved to be more difficult to generate the $S_{\leftarrow} S_{\leftarrow}$ and $\underline{S}_{\rightarrow} C_{\rightarrow}$ interactions under controlled conditions than was anticipated. The $\underline{S}_{\rightarrow} \underline{S}_{\rightarrow}$ and $C_{\rightarrow} \underline{S}_{\rightarrow}$ interactions can fairly easily be generated by using two shock drivers at opposite ends of an expansion chamber, but are an even more common feature of shock reflection by an obstacle, where, however, the interaction fronts are not independent in strength.

The qualitative effects shown in Fig. 55 were produced by an oscillatory underdamped discharge. Miller (113) attempted to create these successive discharges on a controlled basis by the use of two parallel capacitor banks switched through the driver chamber with a predetermined delay between switchings. The experiment was unsuccessful. When the interval between discharges was short the effect of the second bank was negligible. In retrospect, numerous misapprehensions contributed to the failure, the most disastrous one being the assumption that the problem was merely one of adding a rather small amount of energy to the driver. While this remains the goal, it can only be done by increasing the field in the driver, and our choice of circuit elements did not bring this about. Also, the use of the same electrodes for the two energy steps might have been less satisfactory than perhaps a segmented driver with each of the two capacitor banks connected to each of the segments and the back one operating at a higher potential than the front.

7-2 Reflected Shocks. Reflected shocks in the electric shock tube were first observed by Goldstein (10), and were investigated extensively by Compton (11). Subsequent application of Rankine-Hugoniot theory easily explained the great brilliance of the luminosity emitted by the gas piled up in front of the obstacle in terms of the high temperatures existing there.

It is of course incorrect to apply R-H theory naively to this situation. Once again the shock will be an electron-driven plasma shock, and the electron temperature behind it will be temporarily out of match with that of the heavy particles. This situation could be complicated further by the alternatives that the inflow to the shock may itself be either equilibrated or not, depending on the time of flight of the primary shock in reaching the obstacle.

In fact, however, expressed in terms of sound speed in the shocked flow, the solutions for the reflected shock are formally the same if the degree of ionization behind the reflected shock does not change significantly. Then in either case the reflected shock speed U_{sr} is given by

$$U_{sr} = \left(\frac{-g + \sqrt{4g^2 + 15}}{3} \right) \gamma^{-\frac{1}{2}} C_2$$

where as in Chapter IV,

$$C_2 = \sqrt{\frac{\gamma \alpha_2 kT_2}{M}} \quad \text{for non equilibrated flow,}$$

and

$$C_2 = \sqrt{\frac{\gamma(1+\alpha_2)kT_2}{M}} \quad \text{for equilibrated flow.}$$

The quantity g is

$$g = \sqrt{5 + \beta + \frac{1}{3+\beta}} - \sqrt{\frac{1}{3+\beta}}$$

where β is defined as in Chapter IV, and also differs for the two cases.

One finds now that the two interesting quantities, the shock speed ratio and the density ratio are given by the same formal expressions in terms of g, i.e., if the subscript 5 is applied to the region behind the reflected shock,

$$\frac{N_5}{N_2} = \frac{2g + \sqrt{4g^2 + 15}}{-g + \sqrt{4g^2 + 15}}$$

and

$$\frac{U_{sr}}{U_s} = \frac{-g + \sqrt{4g^2 + 15}}{3\sqrt{5 + \beta + \frac{1}{3+\beta}}}$$

The quantities g, N_5/N_2, and U_{sr}/U_s are tabulated as functions of β in Table XIV.

TABLE XIV

β	0	0.01	0.1	1.0	10	100	1000
N_5/N_2	2.50	2.50	2.52	2.68	3.37	3.91	7.06
U_{sr}/U_s	0.500	0.500	0.496	0.476	0.394	0.343	0.141

7-3 Boundary Layer Effects. Duff (118) has performed a thorough experimental analysis of the effect of boundary layers upon the thickness and true velocity of shock waves in conventional shock tubes. He finds that both primary shocks and reflected shocks invariably tend to be thinner and slower than theory expects. Hollyer (119) and Roshko (120), among others, have investigated the theory of growth of boundary layers in shock tubes and Roshko

finds that the ultimate thickness which the shock zone can acquire is given with reasonable accuracy by the expression

$$\ell = \frac{a^2}{10}\left(\frac{N_2}{N_w}\right)^2 \frac{M N_w V_2}{\mu_w} ,$$

and is reached in a time measured by

$$\tau = \frac{N_2 \ell}{N_1 V_2} .$$

The new quantities are represented as follows: a = tube radius, μ = viscosity, w subscripts apply to wall quantities in the layer.

We have found that in small tubes, Mach 3-10, shocks in argon seem to conform well to theoretical values of thickness and speed, but that shocks in hydrogen seem to fail of agreement rather noticeably. In Fig. 56, for example, the compression of the primary shock (Mach 7 in argon) is 4.3 and that of the reflected shock is 2.4. In these same small tubes ($\sim$15 mm dia.), in hydrogen, although the leading edge of luminosity moves fully into contact with the reflecting wall at low pressures as a shock should, and undergoes reflection well in front of the wall at high pressure, as a contact surface should, yet the transition from one behavior ot the other is a gradual one, and it is never possible to observe clear-cut $C_{\rightarrow} S_{\leftarrow}$ interactions at any stage. In 25 mm tubes in deuterium and 50 mm tubes in hydrogen the reflections do show the $C_{\rightarrow} S_{\leftarrow}$ interaction, and nearly normal values of the compression. Since the theory of Roshko would have predicted failure of these flows to agree with R-H theory, a modification is indicated. The probable modification required is one of replacing (when the gas is highly ionized) the equilibrated viscosity coefficient corresponding to the temperature presumed to be indicated by the shock speed by the non-equilibrated ambipolar viscosity which makes allowance for the sluggishness of the cold positive ions, and their restraining influence on the momentum-wasting electrons. When the degree of ionization behind the shock is small, the viscosity needed is probably the neutral particle viscosity at room temperature. Roughly these results imply an ℓ in the latter case of

$$\ell \approx 4\ a^2\ M_a\ p_o$$

where M_a is the apparent Mach number of the flow, the initial pressure p_o is in mm Hg. In the former case this length may require reduction by the factor T_+/T_e. The problem in the electric shock tube is worthy of a much more serious study, but even these tentative results suggest that the experimental observations are correct, and that boundary layers are not a serious problem in these shock tubes.

CHAPTER VIII

DIFFUSION, AND MAGNETIC INSULATION IN THE ELECTRICAL SHOCK TUBE

8-1 Diffusion Cooling. The effect of diffusion on the basically static driver plasma is adequately treated in Chapter III. Above a certain Δp there is no effect. Below this, diffusion rapidly becomes of major importance, and is governed by the ambipolar coefficient $T_e D_+ / T_+$.

In the expansion chamber, where flow occurs in the absence of an electric field, the equations change very little, but different questions can be asked. It is of interest, for example, how far the expanding driver plasma will move in an ionized condition, and what its profiles of ion concentration may be.

Let us assume that the expanding plasma is uniformly ionized across its section as it is extruded from the driver chamber. For simplicity we shall assume that the gas does not cool except by loss of ions, and is equilibrated (making the ambipolar coefficient $2D_+$). Then diffusion in a cylindrical tube is governed by the equation

$$\frac{\partial n}{\partial t} = 2D_+ \left(\frac{1}{r} \frac{\partial}{\partial r} r \frac{\partial n}{\partial r} + \frac{\partial^2 n}{\partial z^2} \right).$$

We shift to a moving coordinate system in which $z = V_2 t$. Then

$$\frac{1}{2D_+} \frac{\partial n}{\partial t} - \frac{1}{V_2^2} \frac{\partial^2 n}{\partial t^2} = \left(\frac{1}{r} \frac{\partial}{\partial r} r \frac{\partial n}{\partial r} \right).$$

separating variables

$$\frac{1}{r} \frac{d}{dr} r \frac{dR}{dr} = - \lambda^2 R$$

and

$$\frac{1}{2D_+} \frac{dT}{dt} - \frac{1}{V_2^2} \frac{d^2T}{dt^2} = - \lambda^2 T.$$

Then

$$R = J_o (\lambda r)$$

and

$$T = e^{\frac{V^2}{2D_+}t} \quad \text{or} \quad e^{-2\lambda^2 D_+ t},$$

because $V^2 >> 2D_+\lambda^2$ for all reasonable values of λ. The first T solution is equivalent to an inadmissable solution with $\lambda \equiv 0$. The whole class of solutions is then given by

$$n = \int A(\lambda)\, J_o(\lambda r)\, e^{-2\lambda^2 D_+ t}\, d\lambda ,$$

whence the desired solution, which at t = 0 has n uniform at a value n_o is

$$n = n_o\, a \int_0^\infty J_o(\lambda r)\, J_1(\lambda a)\, e^{-2\lambda^2 D_+ t}\, d\lambda$$

$$= \frac{n_o\, a^2}{8D_+ t} \sum_{s=1}^{\infty} \frac{\left(\frac{-a^2}{8D_+ t}\right)^s}{s!\,(s+1)}\; {}_2F_1\left(-s,-s,-s-1;\, 1;\, \frac{r^2}{a^2}\right)$$

$$= \frac{n_o\, a^2\, V_2}{8\, D_+\, z} \sum_{s=1}^{\infty} \frac{\left(\frac{-a^2\, V}{8D_+ z}\right)^s}{s!\,(s+1)}\; {}_2F_1\left(-s,-s,-s-1;1;\, \frac{r^2}{a^2}\right).$$

We see that basically the endurance of ion concentration in the flow is determined by the quantity $(a^2\, V_2)/8D_+ z$. Thus for tubes with a = 0.1 cm, p = 1 mm Hg, one would expect a duration of about 1 cm, as was observed, while for the segmented tube to be described in Chapter IX, one would expect durations of the order of meters, and the results also conform to this expectation.

Strictly speaking we have not dealt with the cooling of the gas, by the nature of our assumptions. However, the equation of cooling is largely composed of the diffusive loss, and requires chiefly the addition of a term for heat conduction by distributional transport. This amounts roughly to increasing the coefficient D somewhat and changing the dependent variable from n to nT.

8-2 Magnetic Insulation. Turner and Fowler (70) have investigated the advantages to be gained from introducing an axial magnetic field to insulate the electric shock tube against diffusion losses. They found: (1) that in a 1" diameter tube the initial velocity of the flow is only slightly increased by magnetic fields up to 7000 gauss, but that the attenuation of the flow is greatly reduced [Fig. (57)]; (2) that the effect of magnetic insulation is negligible at high pressures, but very significant at low pressures [Fig. (58)]; (3) that magnetic insulation suppresses the development of the delayed flow and enhances the prompt flow; (4) that proper ranges of magnetic insulation improve the planarity

of the shock front; (5) that the magnetic insulation becomes ineffective beyond a certain characteristic distance (time, probably) in the flow.

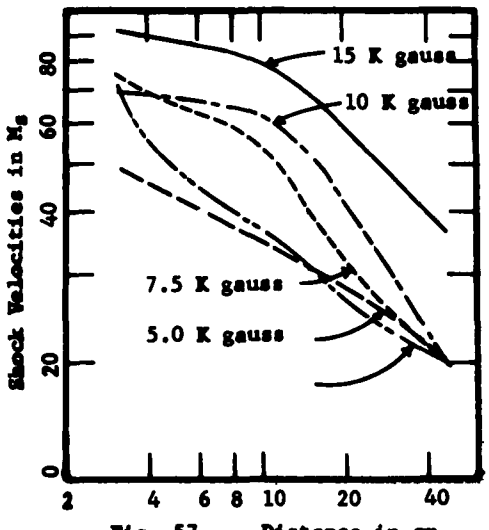

Fig. 57 Distance in cm

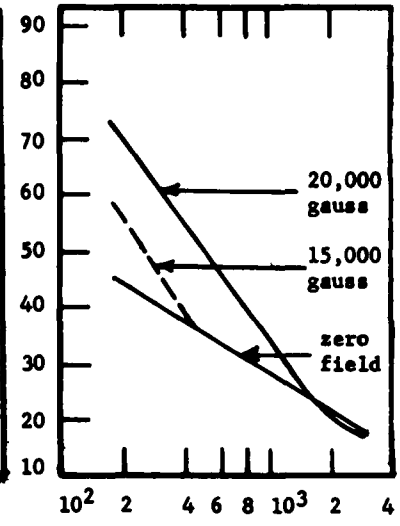

Fig. 58 λ in Microns

In establishing the operating range of the insulating effect it was observed that magnetic fields in the range of 5000 gauss actually reduced the flow speeds, while those in excess of 15,000 gauss produced spurious super-fast waves. The former effect was explained as an action in the driver, where pinching was suppressed, with a consequent decrease of the electric field, coupled probably with an increase in the wall loss rate which the pinching had partially inhibited. The latter effect is ascribed to an MHD extrusion of hairpin filaments of the driver current. It was accompanied by an observable spiralling pattern of the flow with the rotational sense required.

Subsequent tests with magnetic insulation on a 2 inch diameter shock tube have shown that it is obtained at much lower fields in this larger tube. In fact it seems probable that the operating range can be set roughly by the figure of 8,000 gauss inches-squared, although it is certainly variable in second approximation with the conditions used.

Based on equilibrated flow, magnetic insulation would not be expected to appear at fields as small as it does. Its observed behavior is therefore one of the strongest pieces of direct evidence for the picture of non-equilibrated flow. It would be inferred also (and earlier experiments with magnetic insulation in the driver alone tend to confirm this influence) that the chief site of action is the expansion chamber where otherwise the rate of cooling would be severe because of the excessive temperature

of the electron gas. It should be noted, however, that the magnetic field cannot be confined to the expansion chamber alone without causing channelling of the flow as it enters the fringing field that would exist in this arrangement.

Diffusion in a magnetic field is well known to be controlled by different coefficients in the transverse and longitudinal directions. In either case, however, it is the ambipolar coefficient which must be used. For the transverse ($\perp$) direction the individual diffusion coefficients are

$$D_{e\perp} = \frac{D_{eo}}{1 + (\omega_e \tau_e)^2} \quad \text{and} \quad D_+ = \frac{D_{+o}}{1 + (\omega_+ \tau_+)^2}$$

where ω is cyclotron frequency, and τ is collision interval. In the longitudinal direction the zero field coefficients apply. The ambipolar coefficients for non-equilibrated flow are thus

$$D_o = \frac{D_{eo}\, D_{+o}\, (T_e + T_+)}{D_{eo}\, T_+ + D_{+o}\, T_e} \approx \frac{T_e}{T_+}\, D_{+o}$$

and

$$D_\perp = \frac{D_{e\perp}\, D_{+\perp}\, (T_e + T_+)}{D_{e\perp}\, T_+ + D_{+\perp}\, T_e} \approx \frac{D_o}{1 + \frac{D_o}{D_{eo}} (\omega_e \tau_e)^2 + (\omega_+ \tau_+)^2} .$$

For equilibrated flow they are $D_o = 2\, D_{+o}$ and

$$D_\perp = \frac{2\, D_{+o}}{1 + \frac{D_{+o}}{D_{eo}} (\omega_e \tau_e)^2 + (\omega_+ \tau_+)^2} .$$

The only influence which these results have on the cooling profile of the tube is to exchange the coefficient $2D_+$ for the appropriate coefficient $D_\perp$; then the much smaller values of $D_\perp$ account for the greatly reduced attenuation.

When diffusion losses are minimized, the only perceptible change in the flow is a result of equilibration, following which all flow velocities drop by at least $\sqrt{2}$ because the energy of the system is now shared between at least twice as many particles. Observations on the segmented driver shock tube with magnetic insulation show this effect clearly. Flow velocities are observed to undergo a rather sudden change from one constant value to a lower one according to a ratio of $1.33 \pm .07$ in argon, and $1.77 \pm .23$ in hydrogen.

8-3 Reduction of Effective Degrees of Freedom. Turner observed that the shock reflection from an obstacle in the magnetically insulated tube was not what one would expect of an ideal gas, or even of an otherwise ideal gas to which one admitted ionization and dissociation processes.

Experimentally the reflected shock velocities, with a longitudinal magnetic field of 7500 gauss and higher, were somewhat higher than predicted by the real gas hydrodynamics of deuterium. For an ideal gas

$$\frac{M_R}{M_S} = 2\frac{\gamma - 1}{\gamma + 1} = \frac{2}{F + 1}$$

in the strong shock approximation, where F is the number of degrees of freedom. For a monatomic gas F = 3 so $M_R/M_S = \frac{1}{2}$. In some cases, however, $(M_R/M_S > \frac{1}{2})$ and for one case the ratio is almost 2/3 (see Table XV). Then, using the ideal gas theory, $\gamma = 2$ and F = 2. According to real gas hydrodynamics, however, the ratio M_R/M_S should only be 0.2 for $M_S = 20$, where ionization is included. The evidence indicates, therefore, that the effective γ of the gas is greater than 5/3 in the presence of a strong magnetic field, perhaps as much as 3.

TABLE XV

REFLECTED SHOCK VELOCITIES

Pressure μ Hg	B_z gauss	M_S at end	M_R	$\frac{M_R}{M_S}$
200	0	21.5	5.0	0.23
200	5,000	21.5	5.0	0.23
200	7,500	21.5	11.5	0.53
200	10,000	21.5	13.5	0.63
200	15,000	38.5	10.6	0.28
500	0	16	6.0	0.27
500	10,000	18	7.6	0.42
500	15,000	19	7.6	0.40
500	20,000	26	10.8	0.42
150[a]	0	19	6.6	0.35
150[a]	10,000	19	10.2	0.54
150[a]	15,000	22	11.8	0.54

[a]These shots were made at 6 kv in the Pyrex glass tube with the reflecting plug 40 cm from the ring electrode. All other shots were made at 8.25 kv in the alumina and Vycor tube with the reflecting plug 45 cm from the ring electrode.

A gas with a γ of 3 would need to have one-dimensional behavior. This is perhaps accounted for by the double layer deceleration process which is characteristic of a non-equilibrated gas.

8-4 Experimental Studies of Diffusion. Whether or not the diffusion equations with assumptions of local neutrality and ambipolarity are adequate to describe the plasma of the discharge column has never been adequately tested. In fact it is not clear that the mechanism of the constriction of the positive column at large gas densities is covered by the present equations, and a suggested modification has been offered (121). Since much of the operation of the electric shock tube is in the constricted domain, it was important to verify this suggested modification if possible.

Attempts to investigate the positive column of a gas discharge quantitatively are generally frustrated by the variations in composition which the gas undergoes in time owing to chemical reactions between electrical reaction products of the discharge. Even if a stable mixture of reaction products is obtained it is usually not amenable to comparison with experiment because the ionic species present are too numerous, and the ionization processes too complex. A new experimental approach to this problem has provided a wide variety of interesting information. There is a brief interval in the life of a discharge, just after it is turned on, when the column processes have completely established themselves, but the chemical reactions have not yet set in. This interval lies between about 10^{-4} and 10^{-2} seconds. By operating within this range, the species in the gas can be restricted to three: molecules, electrons, and ions of the parent molecule most of which are certainly singly ionized. The first application of the technique was to the constriction experiment. In the course of developing the new technique Jones (122) used at first a stigmatic image of a steady glow discharge tube on the slit of a spectrograph to give individual line information, and photometered across each tube image to provide a luminosity contour. On the assumption that the radiation was largely from excitation processes, the intensity at each point should have been proportional to the electron concentration. The experiment failed because stable configurations and spectral compositions could not be achieved, and no recognizable permanent point of constriction could be defined. Thus for example, a neon discharge constricted to a red filament by the abrupt addition of sufficient gas would change over a period of minutes to a much less constricted discharge with a bluish cast--both spectra being wholly due to neon. It was this temporal behavior which suggested the new approach, and indicated that the hastiness with which the certain earlier visual experiments (which had confirmed the constriction theory) had been made may in fact have been a virtue of them. Consequently a change was made to the pulsed discharge technique.

The apparatus consisted of a vacuum system, an electrical circuit, discharge tubes, and related optical systems. Spectrographic data was obtained using a Hilger E-1 quartz spectrograph, and photographic information was obtained with a long focal length f-10 camera. In both cases the data were recorded on either 103-D or panchromatic Kodak plates, and analyzed using a Knorr-Albers microphotometer.

A 7500 V variable power supply was used in conjunction with a repetitive, timed pulse generating circuit. A trigger pulse generated with 100 V fed through a R-C circuit determined the repetition rate of approximately one trigger pulse every eight seconds. This trigger pulse was applied to a 3C23 mercury thyratron which then delivered a 130 V pulse to a 5C22 hydrogen thyratron. The 5C22 was used as the switch for the tube discharge circuit which consisted of the 7500 V power supply in parallel with a 7500 V, 5 μfd pyranol capacitor. This latter capacitor then discharged through the tube with a time constant of about 3 millisec. This circuit provided the multiple exposures needed when operating at low light levels.

The time-current characteristics of the discharge were determined by photographing the trace with an oscilloscope.

The discharge tubes were designed to be viewed from a direction perpendicular to the axis of the tube. In order to eliminate the lens effect of cylindrical tubing, the center section of each tube was constructed from precision bore square tubing. The outside surfaces were ground and polished optically flat. The first tube was of 16.5 mm ID. Its electrodes were hollow nickel cylinders placed 27.0 cm apart.

A second tube was constructed from precision bore square tubing of a larger diameter (50 mm) in order to determine whether the constriction process is a function of pressure and diameter only, or if other variables were concerned. The nickel electrodes were flat discs 40 mm in diameter and 3.5 mm thick.

A simple, long focal length, f-10 camera was built to photograph the 3 millisec glow discharge. A step filter could be mounted on the emulsion side of the photographic plate to allow emulsion characteristic information to be obtained simultaneously with each exposure or at least once on each plate. The experiment was operated in a dark room and the camera was enclosed to prevent blackening from scattered light produced by the discharge.

The normalized intensity was plotted as a function of the cross section of the 50 mm tube from data obtained photographically in a neon discharge. The normalized intensity is defined as the ratio of the local intensity I to the central maximum I_o. The values for C and R were 5 μfd and 300 ohms respectively. The time-current characteristics of the discharge, determined at a pressure of 1.45 mm Hg were 4.8 missisec. and 17 amps. The results shown in Figure 59, clearly show that the constriction process sets in quite rapidly over the narrow pressure range of 0.75 to 1.0 mm Hg.

Theoretical considerations (121) predicted that the constriction of a column shown depend strongly on the electron temperature (T_e), the constriction occuring over a small range of T_e. Using von Engel and Steenbeck's theory (124) to estimate electron

temperature, the constriction in neon (large tube) occurred between 23,200 and 22,100 degrees Kelvin.

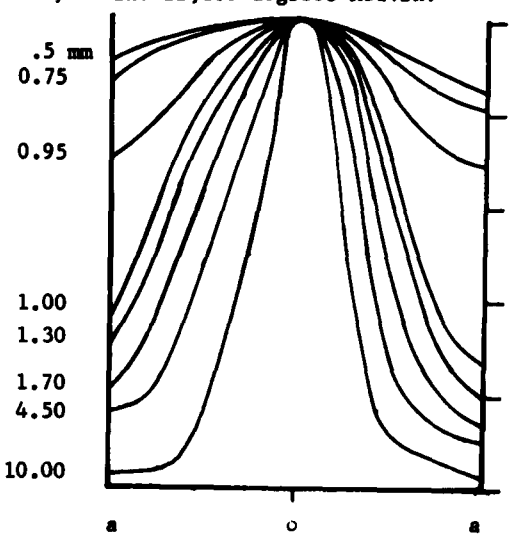

Fig. 59 Tube Width

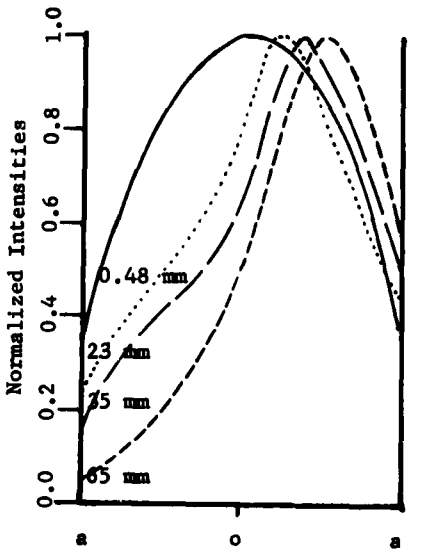

Fig. 60 Neon 50.0 mm Hg

At a pressure of 0.25 mm Hg the normalized distribution curve was the same as the 0.5 mm Hg curve (not shown in Fig. 59). It would appear that the intensity distribution does not change below 0.5 mm Hg; however, no data was obtained at pressures below 0.25 mm Hg. The firing potential below this pressure and at the 27 cm electrode spacing was beyond the capabilities of the discharge system.

On the basis of the information shown in Figure 59 the constriction onset takes place around 0.75 mm Hg, or at value of $\underline{ap}$ of 1.9 mm Hg - cm.

A second series of pressures was run using neon and the smaller diameter tube to determine of the constriction mechanism depended only on the values of $\underline{ap}$. The results, shown in Figure 60 were obtained using values of C and R of 0.5 μfd and 4000 ohms respectively. The time current factors for the discharge were 6 millisec. and 1.1 amps. In this case the intensity distribution curves were distorted, the center shifted progressively to one side as the gas density increased. The determination of the constriction point became difficult in this case. It is possible that the column remains centered until it becomes more or less wall-independent and then shifts preferentially to one side if the electrodes were not exactly parallel. The intensity distribution curve was not the same as for the larger tube. The general appearance of Figure 60 led us to suppose that the discharge was already partially constricted at 0.48 millimeters of mercury. However, if the form of the distribution is different in small tubes than large, the data

may well show that the constriction occurs at or near the same ap value as in the large tube.

Apparently there is a parameter or parameters in addition to the product of the tube pressure and radius which govern the constriction process. The charge densities were not equal in the two tubes nor were the electrodes of the same symmetry. It is felt that these factors should have been the same for both tubes and also the tube length to width ratio should have been constant, which was not the case.

To determine if the constriction mechanism is a function of tube current, three values of tube current were obtained by varying the values of R and C in the discharge circuit using the small diameter tube and a neon discharge.

The results, which are shown in Table XVI, did indicate that the constriction process sets in more rapidly at the lower tube currents over the current range of 140 milliamps to 17 amps.

TABLE XVI

ap (mm Hg-cm)	current (amps)
0.35	0.14
2.00	1.10
5.00	17.00

The values of ap were based on a visual approximation, directly from the photographs, of the point where the positive column had receded from the wall, Admittedly, the results are, at best, only semi-quantitative; but they indicate that a more accurate and detailed study of current effects is warranted.

At this stage the status of the suggested "constriction" term for the ambipolar equations is still in doubt. However, the method is extremely promising and is being pursued actively to elucidate this and other matters concerning the electric discharge at low pressures.

CHAPTER IX

IDEAL ELECTRICAL SHOCK TUBE DESIGN

9-1 Design Problems. Since the primary drive in the electric shock tube is from non-equilibrated electron pressure, the unique features of the device can best be brought out by arrangements which enhance this fundamental factor. High flow speeds generated by strong electric fields at low pressures in large tubes are the direction indicated by theory for exploitation. At large flow speeds and low pressures the equilibration transition can be postponed beyond the useful life of the flow. Strong fields rather than large potentials are desired, and although high potentials will produce strong fields, they can also be reached by close electrode spacings if potential is restricted by capacitor or switch considerations. Large tube diameters are desirable to reduce boundary layer effects, but they can also reduce diffusion losses to a tolerable level even without magnetic insulation.

One problem remains. As the tube diameter is increased, while the electrode spacing is shortened, the tube becomes more and more a blast tube and less and less a shock tube. This has now been overcome by making the shock tube driver in multiple segments, each with its own capacitor. Taking advantage of the fact that electron pressure depends on the magnitude of the electric field, the driver segments can be arranged in pairs with their capacitors charged in parallel but discharged back-to-back through the same switch as shown in Fig. 61. This basic unit pair combination can then be repeated as many times as necessary to obtain a driver of any given length.

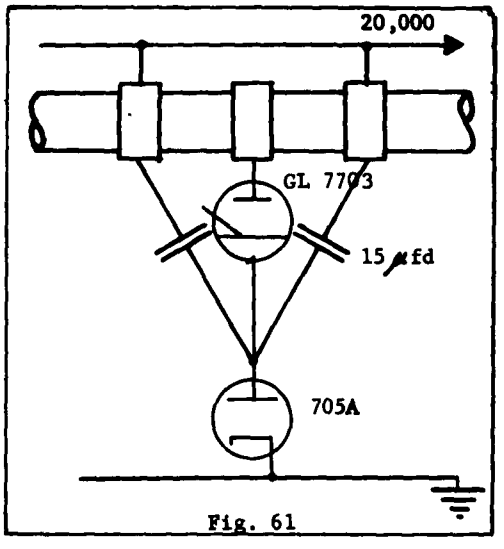

Fig. 61

9-2 Details of a Practical Segmented Shock Tube. Actual construction and testing has been completed on a two inch ID archetype with ten driver segments, each 10 cm long. Provision has been made for up to 10,000 gauss magnetic insulation, and preionization at currents up to 100 amperes. The capacitors used were 15 μfd units at 20 KV. Since the purpose of the construction was to test a

principle, expense was kept to a minimum by the use of steel electrodes and pyrex tubing. Research duplicates should employ some of the better materials mentioned in Chapter II.

Figure 62 is a block diagram of the elements which compose the complete system. It was necessary to include mirror camera synchronization in our equipment. To review the operation briefly, reiterated pulses from the mirror at each approach to synchronism await a favorable gating signal usually taken from a voltage indicator on the capacitors. In combination, these trigger a 300 μsec variable delay circuit which provides time for the mirror to rotate approximately 4^{o} into final position. This output triggers jointly the magnetic field capacitors and a 200 μsec delay leading to the magnetic field crowbar circuit, and a 140 μsec delay leading to the preionizing discharge. Output from the preionizing delay activates an additional 10 μsec delay which triggers the shock tube proper at the epoch when the mirror is correctly positioned, the magnetic field is at a maximum and holding, and the preionizing discharge has just ceased.

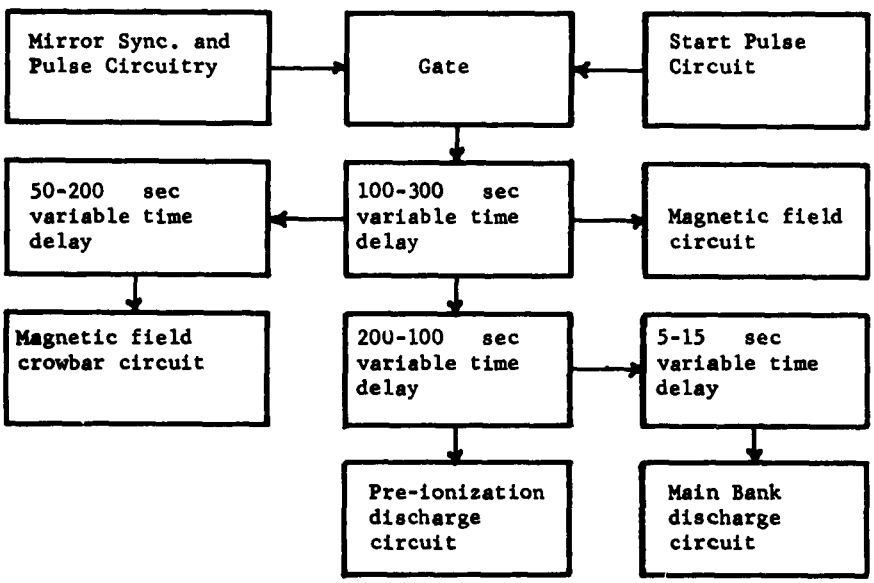

Electronic Synchronization Circuit

Fig. 62

Details of individual circuits are given in Fig. 10 and Figs. 63, 64, 65, and 66. No peculiar features are involved except in the voltage indicator circuit where a circuit has been devised to provide a sudden gating pulse when the capacitor voltage exceeds a given reference voltage.

It was necessary to reduce jitter to a minimum in the firing of each ignitron in the main discharge circuit since five ignitrons were used. To do this all igniter pulses were obtained from five individual secondaries on the same pulse transformer core. The primary was pulsed with a 10 μfd, 6000 volt capacitor bank through a 1907 hydrogen thyratron. The pulse applied to each igniter was approximately 4 KV. In future models it is now believed that a single common switch can successfully discharge all segments.

Some construction features of the tube should be noted. Epoxy resin was used to make the glass to metal seals. Extrusion voids were cut in the walls of each electrode to assure that no cement found its way inside the tube near the electrode. A special mandrel was used to align the electrodes and glass during construction. Each joint was cemented twice first to position the components and second to make a good vacuum seal. Since the tube is rigidly supported at each electrode, the electrode clamps were very carefully aligned by use of a dummy tube before the actual tube was installed. The order of assembly of the tube with a surrounding solenoid required that polyethylene or other heat sensitive dielectric material must be in place nearby before final soldered connections were made between straps attached to the capacitor terminals and the electrodes of the tube. This was accomplished successfully by use of Cerro de Pasco low temperature solders, which formed excellent bonds from copper to copper, and copper to steel. The present indications are that much useful information can be obtained without an insulating magnetic field, and the construction can then be simplified.

9-3 Design Considerations. In the driver, a maximal electric field is desired over the time it takes the wave to move twice the length of the expansion chamber. This suggests perhaps the need for a pulse network to produce a square pulse of field rather than the single capacitor damped discharge commonly used. Since the discharge tube as a load for a pulse forming network offers a variable impedance, it would be desirable to use a current-fed network to produce a square voltage pulse. Design of such networks has been dismissed as technically infeasible (125) and will not be discussed here, but might be worth more study.

The simple condenser discharge may not be too bad, however. The implication of the results of Chapter III were that during the pulse of rising current the ionization is increasing at a rate governed by the rise of current, and the driver electric field is relatively constant up until diffusion dominance sets in. If large capacitors are used, this condition may be maintained long enough with a single capacitor to provide a good drive.

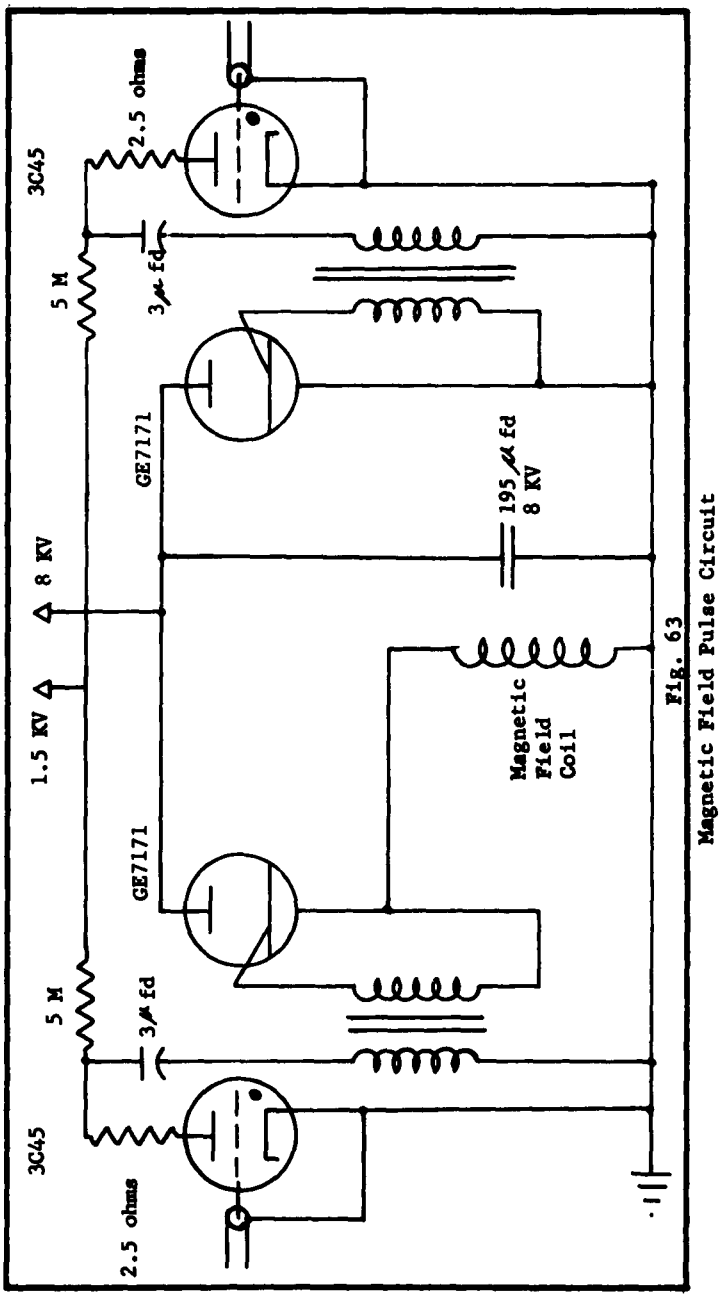

Fig. 63
Magnetic Field Pulse Circuit

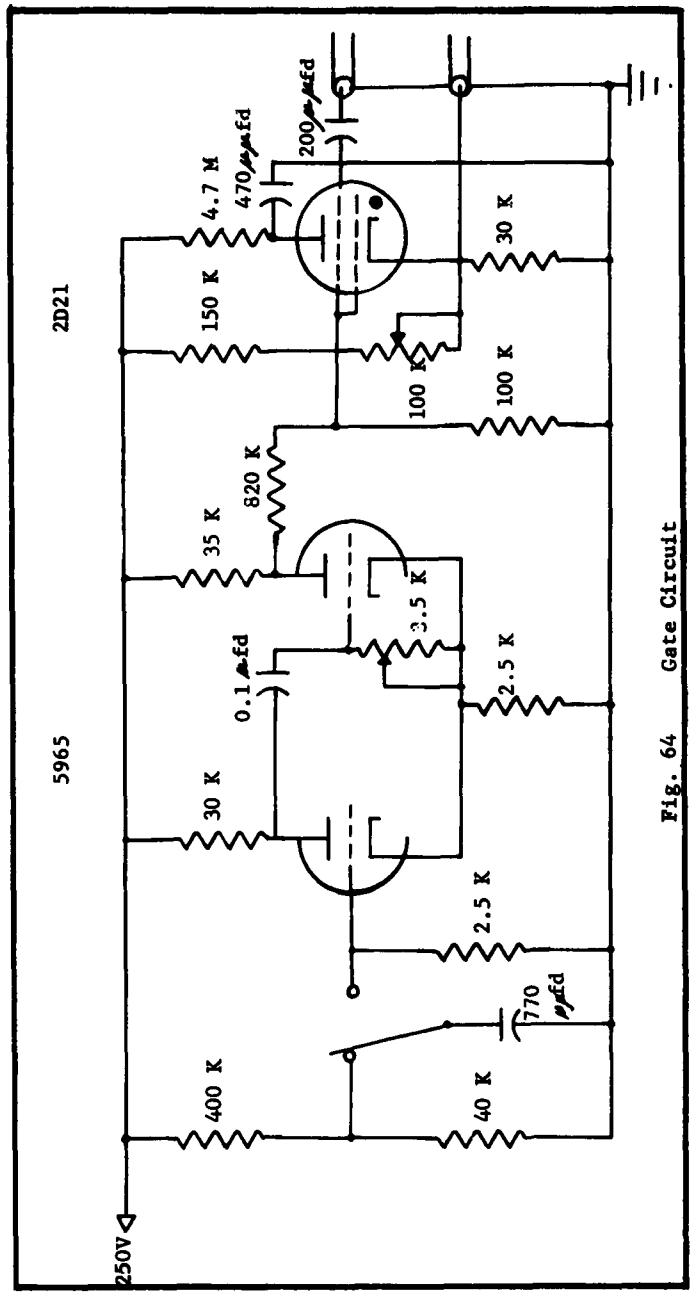

Fig. 64 Gate Circuit

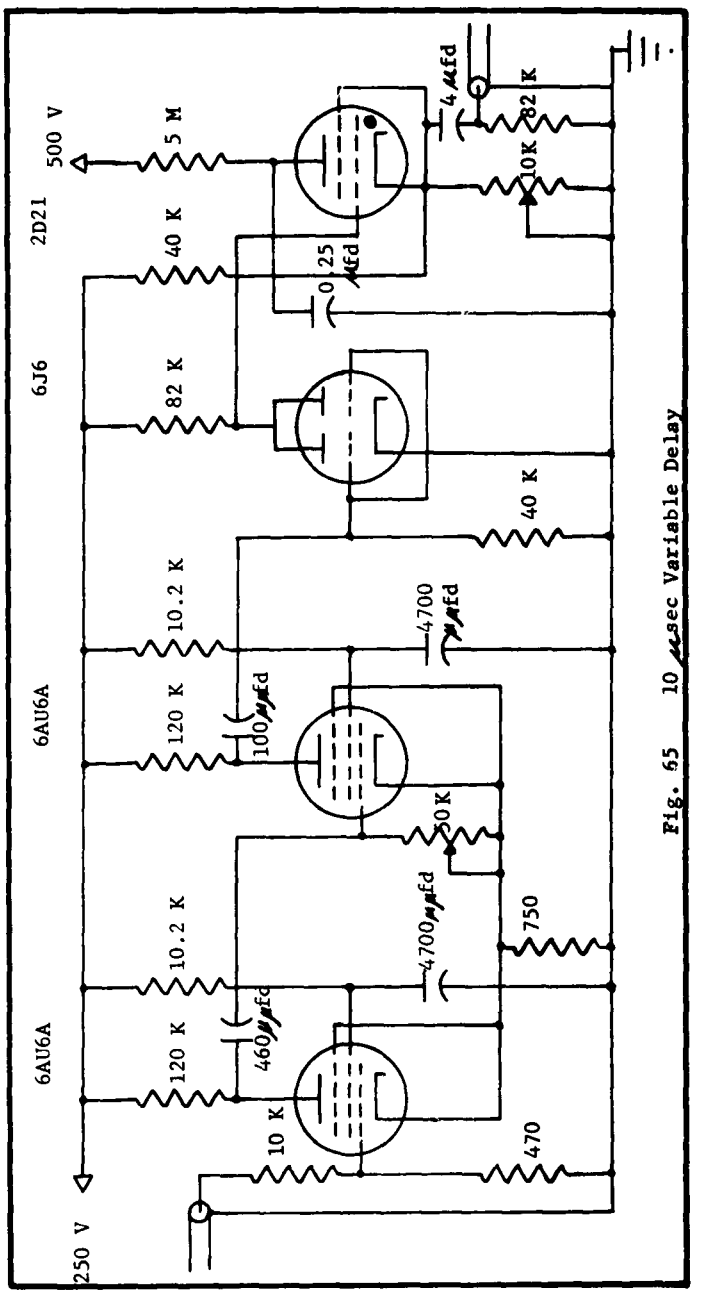

Fig. 65 10 μsec Variable Delay

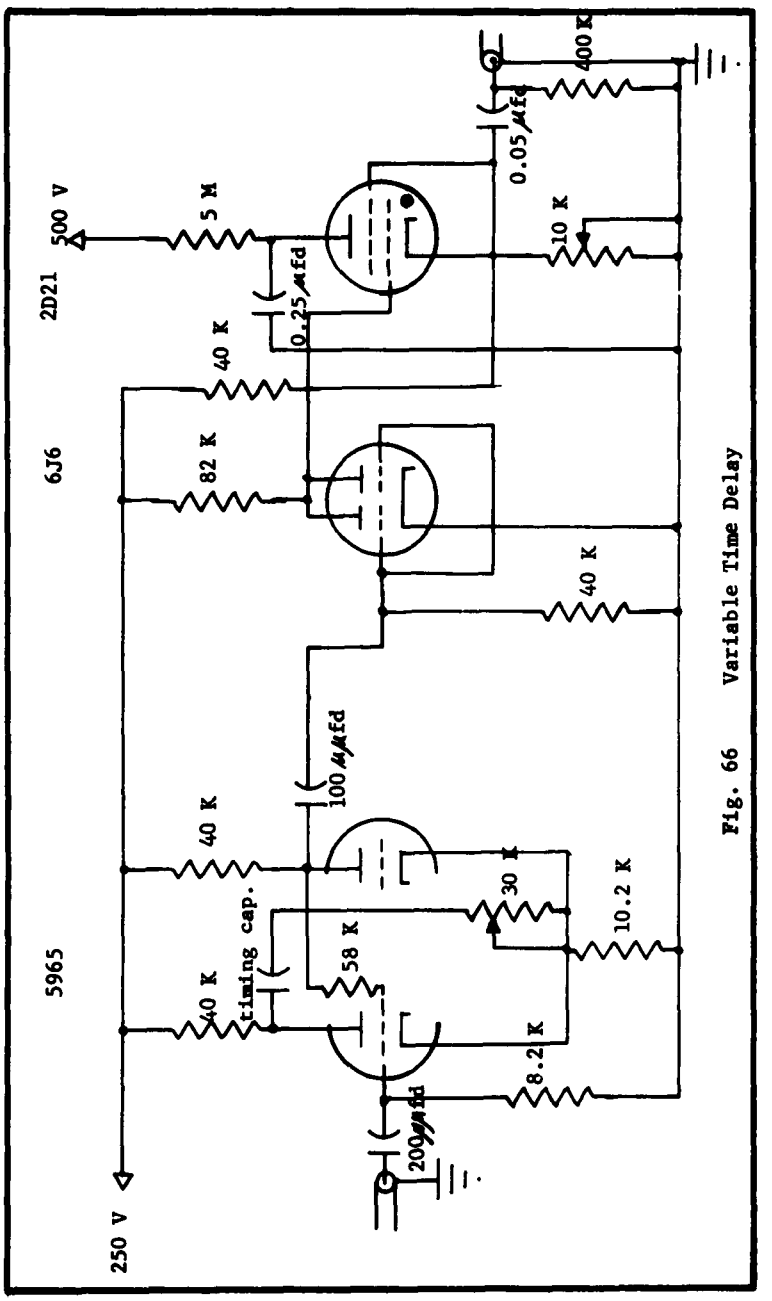

Fig. 66 Variable Time Delay

The time of duration of the discharge should be at least

$$\tau = \frac{2\ell}{U_s} .$$

The time of rise to a maximum in the capacitor discharge current, and hence the time interval to which the heating theory applies is less than (2L/R). Thus we may write

$$\frac{L}{R} > \frac{\ell}{U_s}$$

as the condition for optimal drive. If R_o is the circuit resistance used, this can be elaborated to

$$\frac{R_o + \frac{\ell_D}{15}\left(\frac{0.75}{r}\right)^2 p^{1/5}\,\gamma_o^{-1}}{L} < \frac{1}{\ell_E}\sqrt{\frac{kT_4}{M}}$$

where T_4 bears the relation to V_o found at the end of Section 3-2. It is only marginally possible to meet this condition, which again may be one of the reasons for attenuation of the electron driven shocks. ℓ_D equals driver length and ℓ_E equals expansion length.

9-4 Experimental Behavior. The segmented shock tube actually constructed was not tested for gas purity in the driver, and the only precaution taken in this direction was the frequent use of fresh gas. Care was taken however to ensure that the disadvantages imposed by the materials used were not aggravated by carelessness in vacuum technique. When completed the system was vacuum-tight and could be pumped to 10^{-5} mm Hg with ease. Hydrogen and argon were employed. It was found that the attenuation usually seen in electric shock tubes was noticeably reduced. The flow, even at 100 μ pressure, was remarkably free of the usual streaks of localized luminosity. Hydrogen, in which we had never before been able to develop a good reflected shock with a clear contact surface interaction gave excellent reflection patterns with a thickness of about 3.5 cm in an expansion run of about 30 cm. We attribute this improvement in behavior more to the size of the tube than anything else, leading to a more favorable ratio of boundary layer thickness to diameter.

Table XVII gives representative values of data obtained from wave speed measurements under several conditions. There seems to be no immediate limit in sight to the speeds attainable, except those set by switch gear.

TABLE XVII

SEGMENTED SHOCK TUBE VELOCITIES

Capacitor Potential in kv	Velocity in 10^5 cm/sec	Mach Number
5	5.1	15
6	6.5	21
7	7.7	23
8	7.6	22.5
9	8.4	25
10	10.0	30.0
11	9.3	27.0

All measurements in Argon at 0.1 mm Hg.

CHAPTER X

ELECTRICAL PROPERTIES OF THE FLOWING PLASMA

10-1 Experimental Observations on Conduction to Probes. The equipment details of the magnetic induction experiment of Clotfelter (61) have been described in Chapter I. Sakuntala and von Engel (41) re-examined and extended the work of Clotfelter, continuing to use a weak magnetic field as an induced internal source of EMF. Clotfelter had shown, however, that an external EMF can produce comparable results in the absence of a magnetic field. The highly ionized plasma produced in a shock tube moves down the tube into a region across which a uniform magnetic field is applied. At a certain point in the field region, two cold electrostatic probes facing one another are inserted into the plasma. From the potential difference between the probes with various external resistances the internal resistance and hence the resistivity of the plasma can be derived as well as its flow velocity.

As the conducting plasma is swept through the uniform magnetic field an emf with respect to the laboratory frame is induced in the plasma between the probes whose maximum value is of magnitude

$$\varphi_o = 2\, V_2\, B\, a \times 10^{-8} \text{ (volts)},$$

where B is the magnetic induction in gauss, V_2 the maximum flow velocity in cm/sec and 2 a the separation between the probes in cm. The emf's so obtained are quite considerable. With $B = 10^2$ gauss, $V_2 = 10^6$ cm/sec and 2 a = 1 cm, the potential difference between the probes is 1 volt. (Ionization by collision even for the largest induced fields is negligible.) This equation holds only if no charge flows in the probe circuit. If, however, a charge flows through an external resistance r connected to the probes, the voltage φ between the probes will be smaller than φ_o. This reduction can have three causes: the plasma resistance, the reaction which the current has on the applied magnetic field, and possibly sheath voltages at the probes (not of the conventional kind since the electric field is induced in the plasma). The last two effects would depend on the magnitude of the current. Since the measurements have shown that the plasma resistance is constant with respect to changes in probe current, it follows that these effects are quantitatively insignificant and it is thus permissible to derive the plasma resistance R_p from φ_o, φ and r.

Unless great care was used the oscillograms of probe voltage were found to differ erratically. This was traced to voltages, induced by the large fluctuating discharge currents, in the cathode

follower circuits to which the two probes were connected. The disturbances were caused by the magnetic field of the current loop formed by the discharge path which runs radially from the center of the tube to the ring anode. Because of the large currents the discharge is constricted. During each current pulse the anode spot takes up a different position on the ring anode thereby inducing varying potentials in the probe circuit. By arranging symmetrical leads to the cathode follower, this disturbance was removed. Fig. 67 shows profiles of φ_0 as a function of time at various gas densities.

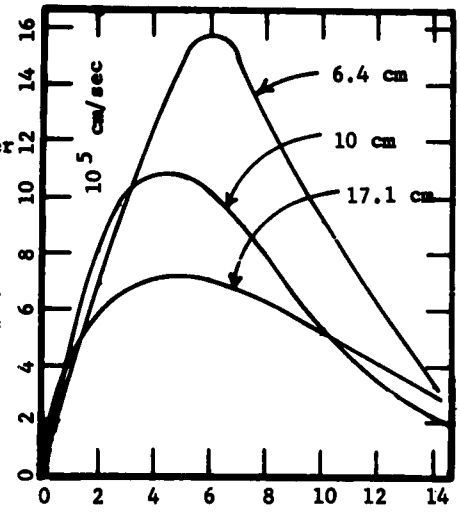

Fig. 67. Time in μsec

In earlier measurements (41) of the plasma resistance each probe was connected through a resistor to the ground. The results were unsatisfactory because of large parasitic pulses induced in this circuit. By using a symmetrical probe circuit with two equal resistances joining the two probes (one on each side of the expansion tube), and omitting any ground connection, traces free of parasitic voltages were obtained.

Figure 68 shows that R_p decreases first as i_{max} is increased and then seems to become constant. The rapid change of R_p with rising i_{max} may be thought to be caused by the variation of the degree of ionization of the plasma whereas the slow decrease of R_p at higher currents may be due to a slow rise of the plasma temperature. In another series of experiments by Sakuntale R_p was measured as a function of the gas pressure p (in hydrogen) between 0.5 and 5.0 mm Hg, while capacitor potential and magnetic field were kept constant. Figure 69 shows this for two values of the probe separation.

Similar data taken by Clotfelter are given in Table XVIII. Some doubt attaches to the absolute magnitude of these particular measurements, since they were taken with massive copper half cylinders as guard rings for the probes, and these may have short circuited the plasma in some ambiguous way. One remarkable result is obtained by comparing the resistances of the plasma in different gases under similar conditions. The resistance is found to vary roughly as the square root of the atomic mass.

Experiments in which the probe separation was changed raised a new problem. When the separation was 1.5 cm, the probes were in line with the walls of the glass tube; with 0.8 cm separation they were situated in the central region of the plasma. At first probe

potentials φ_o were observed to be independent of the separation and equal to the value obtained at 1.5 cm. This curious result suggested that since the stems of the probes were originally without insulating shield, the probes acquired the highest potential difference to which they were exposed in the moving ionized gas and this potential appeared along stems of the probes.

TABLE XVIII

PLASMA RESISTANCES

a = 0.8 cm, r = 0.1 cm

Gas	Pressure	Capacitor Voltage	Distance Along Flow	Resistance
He	2.8 mm Hg	4500 V	6.4 cm	25 r
"	"	"	14.1	400
A	"	4000 V	6.4	200
"	"	"	14.1	1800
H_2	"	4500 V	10.0	30
"	"	"	14.1	60
"	"	"	17.1	120
"	"	4000 V	6.4	10
"	"	"	10.0	20
"	"	"	14.1	50
"	"	"	17.1	150
"	"	3500 V	10.0	20
"	"	"	14.1	90
"	"	"	17.1	300
"	5.6 mm Hg	4000 V	6.4	35
"	"	"	10.0	60
"	"	"	14.1	280
"	"	"	17.1	500

In order to test this explanation the stems of the probes were painted with Glyptal and baked in an oven for about six hours at a temperature of 120°C. After testing the stems for perfect insulation the probes were inserted into the expansion chamber at a separation of 0.8 cm. The results were that with the stems insulated the voltage φ_o is proportional to the probe separation. If the probe distance was reduced to less than 0.5 cm erratic results were obtained which was believed due to aerodynamic effects of the probes on the flow of the gas.

In order to test whether a contamination of the probe surface affects the probe potential, observations were made before and after the probes were cleaned by sputtering. No difference could be detected.

From Fig. 68 we find that the R_p, the resistance of the plasma between the probes, at p = 1 mm Hg and i_{max} = 6700 amp, is 24 ohms

for a = 0.75 cm and 13.5 ohms for a = 0.4 cm. If the probe current in the plasma is assumed to be uniformly distributed over an area of constant cross section equal to that of a single probe surface (0.2 cm^2) this corresponds to a plasma resistivity ρ = 3.2 ohm cm and ρ = 3.4 ohm cm for a = 0.75 and 0.4 cm, respectively. On the other hand, if the probes are assumed to be facing against an infinite slab of conducting medium, the values of ρ would have been 14 and 10 ohm-cm.

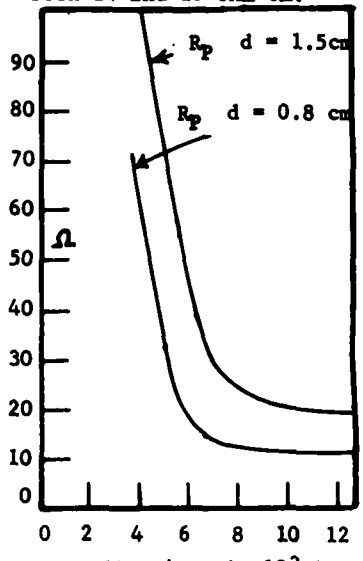

Fig. 68. i_{max} in 10^3 A

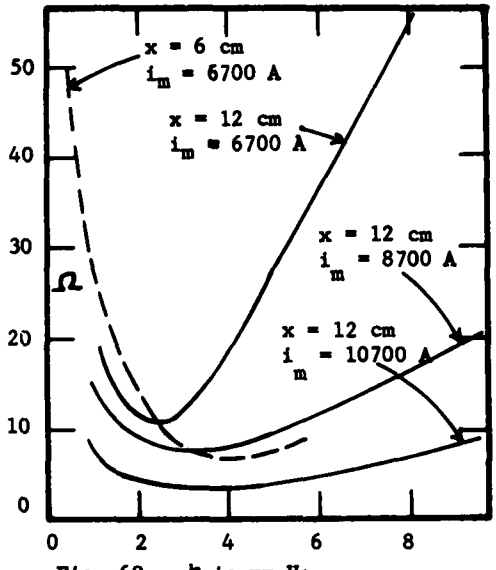

Fig. 69. ρ in mm Hg

Sakuntala and von Engel found further confirmation that the lines of current density are straight between the probes by measuring the plasma resistance with probes (of copper) and of different surface area. When the diameter of the disk of the probe was 0.12, 0.25, and 0.5 cm, R_p was found to be 300, 95, and 24 ohms at p = 1 mm Hg, 6700 amp and d = 1.5 cm. The resistance is thus inversely proportional to the collecting area. With 0.12 cm probes the collecting area is of course slightly larger than the face because the probe surface cannot be regarded any longer as a part of an infinite plane.

10-2 Concepts Involved in the Formulation of a Theory of Transient Conduction to Probes. Setting aside for the moment any further demonstration that neither boundary layers nor sheaths influence the observations, we shall take steps toward a theory of conduction in the volume of the medium. The problem of the conduction is simply this: as the plasma passes through the region between the probes it is subject to a brief impulsive electric field owing to the change in boundary conditions on the probe surfaces; its response to this field cannot be purely electric (i.e., sheath formation), since the electric forces continue to act equally on positive ions, or electrons, and therefore electrons,

because of larger mobility, would be required under all circumstances to leave the circuit at the probes faster than the positive ions do. This being manifestly impossible, there must also be a hydrodynamic contribution to the response in order to coerce the electrons to conform to the ion rate processes.

The first problem is whether the electrons and ions are decoupled in energy and momentum in this impulsive field. Decoupling in energy depends upon the relative values of the deviation of the impulsive field and the equilibration time for electron pressure. The former is $\sqrt{2r/V_2}$, where r is the probe radius. The latter is given in Chapter IV, and we modify it to allow for the fact that the plasma is not a hot one. Then for decoupling of the energy we have

$$\frac{2r}{V_2} \ll \frac{M}{4\alpha\, m\, N\, \overline{\sigma_e}\, v_e}$$

at 2 mm Hg in H_2, $\alpha \approx 0.25$, $\overline{\sigma_e}\, N_o \approx 25$ cm^{-1}, $\overline{v_e} \approx 10^7$ cm/sec, $V_2 \approx 10^6$, $r \approx 0.2$ cm, and we find that

$$4 \times 10^{-7} \ll 4 \times 10^{-6}.$$

Any gas heavier than hydrogen will give an even more favorable result.

Although the electrons may be decoupled in energy, they are not decoupled in the matter of momentum transfer. The rate of momentum transfer per unit volume from one sided collisions is

$$\frac{1}{8}\, m\, \overrightarrow{v_e}\ \sigma\ n_e\, N\, \overline{v_e}\ .$$

When the drift in the field is considered and the collisions from the opposite side are subtracted off, one obtains a net volume rate of transfer of

$$\frac{2e}{3}\left(\frac{V_2 \times B}{c} + E\right) n_e$$

where the factor 2/3 may reflect an oversimplification of the averaging processes, and will be replaced by $\eta \leq 1$ in what follows.

The hydrodynamical behavior of the plasma can be thought of as providing a transition between successive states of hydrostatic equilibrium, in particular one at points remote from the probes, and another on the center of symmetry of the probe system. If the momentum transfer between the three particle-systems is included, individual equations can be written for the behavior of the partial pressures of the components, assuming that electron-ion momentum transfer is negligible, and an isotropic pressure tensor exists.

$$(V_2 \cdot \nabla) j_e + \nabla p_e + e\, n_e \left(\frac{V_2 \times B}{c} + E \right) = \eta_e\, e\, n_e \left(\frac{V_2 \times B}{c} + E \right)$$

$$(V_2 \cdot \nabla) j_+ + \nabla p_+ - e\, n_e \left(\frac{V_2 \times B}{c} + E \right) = - \eta_+\, e\, n_e \left(\frac{V_2 \times B}{c} + E \right)$$

$$(V_2 \cdot \nabla) j_o + \nabla p_o = (- \eta_e\, e\, n_e + \eta_+\, e\, n_+) \left(\frac{V_2 \times E}{c} + E \right) .$$

[It is interesting to note that there is a hint from these equations that the Schottky local neutrality assumption may have a hydrodynamical basis, since $n_e = n_+$ is the simplest way to guarantee that total pressure is a constant under hydrostatic conditions]

The equations for the currents in the plasma are as usual

$$j_e = - D_e \left[\nabla n_e + \frac{e\, n_e}{k\, T_e} \left(\frac{V_2 \times B}{c} + E \right) \right]$$

$$j_+ = - D_+ \left[\nabla n_+ - \frac{e\, n_+}{k\, T} \left(\frac{V_2 \times B}{c} + E \right) \right]$$

$$j_o = - D_o\, \nabla n_o$$

If there is no production of ions, the divergences of all these currents are zero.

At remote distances from the probes, or everywhere for infinite probe impedance, the solution of this set of equations is given by a charge separation which makes

$$\frac{V_2 \times B}{c} + E = 0.$$

Then all pressures are constants, and the usual mode of linearized ambipolar analysis for j_e and j_+ can be pursued to a slightly different solution.

Near to the conducting probes the detailed solution has yet to be unravelled. The instinctive solution proposed is as follows: the dynamical contributions can be neglected to a first approximation, and the behavior treated as a succession of hydrostatic equilibrium conditions. Then the combination of the equations for pressure and current density in pairs, under the assumption that T does not vary but that T_e can, gives Δj_+ and Δj_e, the excess currents to the electrodes over and above the normal ambipolar current component:

$$\Delta j_+ = \frac{D_+ \eta_+ e n_+}{k T}\left(\frac{V_2 B}{c} + E\right)$$

and

$$\Delta j_e = -\frac{D_e}{(\eta_e - 1)}\left(\eta_e \frac{dn_e}{dx} + \frac{n_e}{T_e}\frac{d T_e}{dx}\right).$$

The gradient $(d T_e)/dx$ must then fulfill the requirement that $|\Delta j_+| = |\Delta j_e|$ which the cold electrodes impose, so that the total current density in the probe region is given by

$$i = e \Delta j_+ - e \Delta j_e = 2 e |\Delta j_+| = \frac{2 D_+ \eta_+ e^2 n_+}{k T}\left(\frac{V_2 B}{c} + E\right).$$

The concentration n_+ will be subject to two variations, one imposed by the basic ambipolar loss pattern, the other to fulfill the requirement of pressure constancy during the interval of probe passage. The former is probably the more significant one, being described by the usual function $J_o(\lambda r)$ in a cylindrical tube. Then the Kirchhoff 1st law requires that

$$\left(\frac{V_2 \times B}{c} + E\right)\nabla n_+ + n_+ \nabla \cdot E = 0.$$

Introducing a new set of coordinates, with x lying along the probe axis and y as a cylindrical radius around this axis, we can approximate this equation as

$$\frac{1}{y}\frac{\partial}{\partial y} y \frac{\partial \varphi}{\partial y} + \frac{\partial^2 \varphi}{\partial x^2} - \lambda^2 |x| \left(\frac{V_2 B}{c} + \frac{\partial \varphi}{\partial x}\right) = 0.$$

If $\varphi = -\frac{V_2 B}{c} + YX$, the equation separates into

$$Y = J_o(\mu y)$$

and

$$X'' - \lambda^2 |x| X' - \mu^2 X = 0$$

The solutions of this last must be divided into two regions and then matched at $x = 0$, to deal correctly with the function $|x|$. If $\lambda = 0$, the usual resistance solution for a slab conductor faced by circular probes is found

$$R = \frac{k T}{2 D_+ \eta_+ e^2 n_+}\left(\frac{1}{2r} - \frac{\ell n^2}{\pi a}\right)$$

where r is again probe radius, and a is tube radius. If $\lambda \neq 0$, the analysis has not yet been carried out.

10-3 Critique. The facts observed by Sakuntala and von Engel, and Clotfelter, were (1) Resistivity varies directly as the square root of the ionic mass. (2) Resistivity passes through a minimum as gas pressure increases at constant driving potential. (3) Resistivity varies roughly inversely as the 3/2 power of the capacitor potential. (4) Induced voltage varies as the square root of the capacitor potential for constant pressure. (5) Arrival times of signals varies inversely as the square root of the capacitor potential for constant pressure. (6) Unexpectedly large resistivity were observed, of order 1(ohm-cm) and more.

The resistivity predicted in section 10-2 is

$$\rho = \frac{k\, T_+}{2\, D_+\, \eta_+\, e^2\, n_+} .$$

Fact 1 is then a universal fact which can be deduced from the dependence on D_+, since D_+ varies inversely as the square root of the ionic mass. Fact 6 is also a direct consequence of the occurrence of D_+ instead of D_e as the factor governing resistivity. Facts 4 and 5 are explained by the electron shock mechanism, since $T_e \propto E_z \propto V_2^2$. The other facts require some study. It should be noted in passing that the observations of Sakuntala et. al. in connection with the dependence of resistance on probe spacing and area are not in accord with the theory advanced here, but the disagreements may not be real, considering the complexity of the actual experimental geometry.

Broadening experiments showed the gas in these experiments were partially ionized to about 25%. A number of experiments indicate a temperature of around 5000° at their conditions. Computation of the resistivity on the basis of a fixed cross section of the order of the first Bohr orbit gives $\rho \approx 2 \times 10^{-3}$ (ohm cm). Computation based on the potential energy V x 1.45 x $10^{-27}/r^2$ ergs from the $H + H^+$ calculations of Hylleras gives $\rho = 0.1$ (ohm cm) considering the repulsive orbit only, and would be increased considerably by including the attractive orbit and electron charge transfer processes. Computation on a strict coulomb repulsion model between the protons of the free H^+ and the bound H gives $\rho = 1$ (ohm cm). This last result is in excellent agreement with the experiments.

If we were to assume a fully ionized gas we should then calculate D_+ from ion-electron binary encounters. An approximate treatment is as follows: 90° scattering occurs if the particles approach within a distance b given by

$$\frac{e^2}{b} = 3\, k\, T_e$$

then

$$\sigma = \pi b^2 = \frac{\pi e^4}{9\, k^2\, T_e^2}$$

More exactly one must multiply by Spitzer's $\ell n \Lambda$ factor. Now

$$\rho = \frac{1}{e\, n\, \mu_+}$$

and Langevin finds, complete for persistence of velocity, that

$$\mu_+ = 3/4 \frac{e\lambda}{M\bar{V}_+} \left(1 + \frac{M}{m}\right)^{\frac{1}{2}}$$

with

$$\lambda = \frac{1}{\sigma N}$$

combining,

$$\rho = \frac{8\sqrt{2\pi}\, e^2 \sqrt{k\, T_+\, m}\; \ell n \Lambda}{27\, k^2\, T_e^2}$$

$$= \frac{T_+^{\frac{1}{2}}\, \ell n\, \Lambda}{3.4 \times 10^{-4}\, T_e^2} \text{ (ohm-cm)}$$

For our conditions this gives $\rho = 0.04$ (ohm cm), and it is difficult to imagine how the factors in this expression could be brought to values which would improve its agreement. We are led therefore, to select the H^+ into H theory.

Fact (3) now follows fairly readily from either of the latter two models for the cross section depending on what assumptions are made about the variation of ion concentration with temperature. Fact (2) also seems explicable on a basis of the variation of ion concentration with pressure.

Further experimental investigation with greater care seems likely to provide a valuable tool for establishing a number of properties of the plasma. Its use will depend, however, on accurate theoretical knowledge of the diffusion coefficient for H^+ into H, which these experiments may well check, and a solution for the conduction equation.

It should be again noted that this theory applies (as experiment demands) equally well to probes between which a potential is established by using an external EMF as with induction in a magnetic field.

10-4 Boundary Layer-Sheath Effects. To have been of any significance in the measurements of Clotfelter, and of Sakuntala and von Engel, boundary layers would have needed to form very quickly. Following the theory of flow past plates, we can assume that a layer of thickness δ develops in time t according to the equation

$$\delta = 5\sqrt{\nu t}$$

where ν is the kinematic viscosity.

Three effects are active. (1) Reduction in EMF from reduced velocities in the layer. (2) Increase in resistance from possible cooling in the layer. (3) Capacitative charging of the layer as a leaky capacitor paralleled by the resistance of the layer.

Analysis shows that the capacitative effects offset the resistive effects sufficiently over the short periods with which we are concerned to make the first effect (on the EMF) the only significant one. This leads order-of-magnitude-wise to the expression

$$E = \frac{2 V_2 B a}{c}\left(1 - \frac{3\sqrt{\nu t}}{2 a}\right)$$

where 2 a is the spacing between the probes.

The nature of the viscosity ν of a plasma has not yet been investigated adequately. Even if it is assumed to be wholly owing to the electrons the term $(3\sqrt{\nu t})/a$ would have been $\sim 1/10$ under the circumstances of the measurements. If, as is probably true, transverse viscosity in a plasma is an ambipolar transport phenomenon like diffusion, the term would have been $\sim 1/100$ or less.

When, however, we note that the principal effect of the boundary layer is upon the EMF, we see that this whole view point is not in accord with the basic fact that the induction in a magnetic field was observed to be equivalent to the action of an external battery, since the boundary layer can be active under the first conditions only. We therefore conclude that it plays no role at all.

10-5 Electrostatic Probes and the Shock. Hales and Josephson (71) have determined the magnitude of the potential step at the shock front as a function of shock speed using electrostatic probe stations. Their observation of the charge zone associated with the precursor was made at the same time and has been described in Chapter V. The results of their measurements are given in Fig. 70, and show that the potential step is explicitly determined by the temperature (presumably electron temperature) prevailing behind the

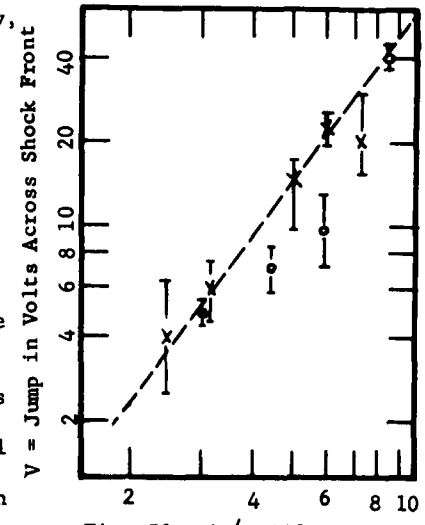

Fig. 70

the shock front. In fact $\Delta \varphi$ is very nearly equal to kT_e where

$$k\,T_e = \frac{9}{32}\left(\frac{M\,U_s^2}{e}\right)$$

is obtained from the shock conditions.

CHAPTER XI

MISCELLANEOUS OBSERVATIONS

11-1 MHD Studies. The electric shock tube provides an excellent means of studying interaction and penetration of magnetic fields and plasmas under controlled conditions.

Figure 71 shows single shot mirrorgrams of shock waves in a plasma created by discharging a condenser of 13 μf at 4.5 kv through hydrogen at 6 mm Hg. Figure 71 (a) is a photograph with zero magnetic field. Figure 71 (b) is taken with a field of $B = 10^4$ gauss applied transverse to the flow and extending between the edges of the pole pieces marked by the two narrow horizontal lines in the photographs. The axis of the shock tube is vertical in these pictures. The wide horizontal dark band separates the discharge chamber from the expansion chamber. The effect of the magnetic reflector is apparent from Fig. 71 (b). When the magnetic field is applied, a discontinuity in brilliance originates at the upstream edge of the pole piece and propagates upstream toward the discharge chamber. This discontinuity has been interpreted as a shock front. The whole luminous phenomenon recorded in the visual region lasts for about 40 μsec.

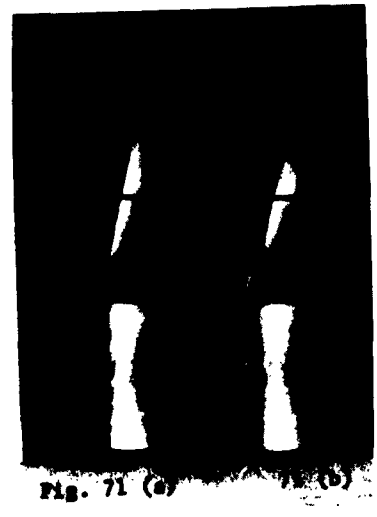

Fig. 71 (a) (b)

Tubes with metal and glass walls were employed in these experiments. It was found that the reflected pressure wave was more intense when metal tubes were used. From this it was concluded that one of the mechanisms responsible for the reflection of the plasma involved eddy currents flowing in the gas and completed through the walls. The deceleration of the plasma is then caused by the effect of the magnetic field on the charged particles which carry the current across the field. There is a second cause of retardation; as the plasma moves into the magnetic field the positive ions move along slightly curved paths. The component of the velocity in the flow direction is therefore reduced. This slowing down of the ion cloud is communicated to the main body of the gas

via collisions, and to the electrons. The back pressure thus produced augments the strength of the reflected wave. It should be noted that during the reflection process the gas flow continues to go in the forward direction. The reflected waves are discontinuities in luminosity moving opposite to the direction of the flow of the gas.

If the first cause of retardation alone is active an order of magnitude criterion for the appearance of the reflected wave may be derived by setting the magnetic pressure in the field equal to the kinetic energy of the moving gas. The same condition may also be stated by saying that flow speed into the field cannot exceed Alfven speed in the field. Hence

$$(B^2/8\pi)/(MNV_2^2/2) \approx 1.$$

From experimental data (Fig. 72) this relation seems to hold.

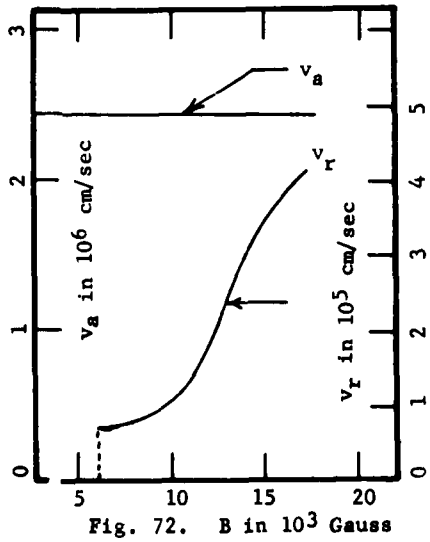

Fig. 72. B in 10^3 Gauss

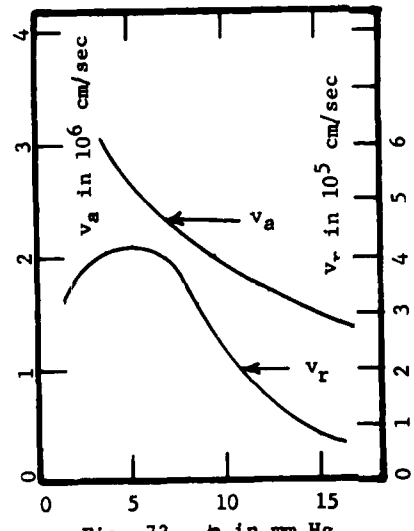

Fig. 73. p in mm Hg

If the second cause of deceleration were predominant the back pressure would be proportional to B^2 and inversely proportional to the ion mass and to a parameter which is a function of the gas pressure.

Figure 72 shows results obtained at constant initial pressure. The flow velocity V_2 in the shock wave produced in the discharge chamber and observed in the expansion chamber is found to be constant and independent of B as expected. The reflected wave velocity U_r is zero (wave is nonexistent) up to about 7000 gauss marked by the arrow, and rises as B is increased. In all cases considered U_r is found to be about an order of magnitude smaller than V_2.

Fig. 73 gives the observed dependence of V_2 and U_r on the

initial gas pressure p in the discharge chamber when a constant magnetic field of 13,000 gauss is applied. The variation of V_2 with p corresponds here to the usual relation $V_2^2 \cdot p$ = constant. As p is increased U_r passes a maximum. This perhaps can be understood by the simultaneous action of the two deceleration mechanisms mentioned before.

Since the results of the measurements given in Figs. 72 and 73 follow from the angles of the shock fronts shown in Fig. 71 (a) and (b), the accuracy of the observed values is marred by scattering. This is partly due to poor reproducibility of the high current pulse which was used to produce these flows, and partly to the weak contrast in the photographs, particularly in the reflected pressure wave.

11-2 Pinch Studies. Considerable attention was at one time given to developing a theory of the pinch for application to presumed effects in the early flow. Unlike the Rosenbluth theory (126) it was intended to apply to the partially ionized gas in an electric driver.

We presume that there is a purely magnetic driver with a pressure $B^2/8\pi$. The maximum value of this pressure occurs at the surface of the current carrying cylinder of plasma, whatever its current density pattern, and is $(I^2)/2\pi r^2$. Let this point be adopted as the face of a piston (contact surface) moving with speed V_2. A shock U_s will precede it; run to the center, and back to the piston. This point of intersection can then be taken as the compression minimum of the pinch.

Since the driver gas inside the pinch is continually heated by the field, the pinch will have difficulty even in developing beyond the stage of a weak shock. If p_o be the undisturbed pressure inside the pinch, the strength of the shock can be written as

$$\xi = \frac{2\pi p_o r^2}{I^2} .$$

But $kT_e = \eta(E/N_o)$, so that $p_o = \sigma \eta E$, where η is a coefficient to be evaluated by the methods of Chapter III. Then the rate of advance of the piston is given by a coordinate r_m.

$$-\frac{d r_m}{d t} = \frac{c_o (\mu - 1)}{\sqrt{\mu(\mu + 1)}} \frac{r_o}{r_m} \left(1 - \frac{r_m^2}{r_o^2}\right)$$

where $r_o = \sqrt{I^2/2\pi p_o}$, and for an ideal gas $\mu = 4$. Since when $t = 0$, $r_m = a$,

$$r_m^2 = r_o^2 + (a^2 - r_o^2)\, e^{\frac{2 c_o(\mu - 1)}{r_o \sqrt{\mu(\mu + 1)}} t} .$$

Changes of E and I in time have been neglected in this theory. If one objects to this, a very nice integral can be found in terms of the total charge Q which has passed through the tube. More serious objections are against the time integration of a shock theory which implies constant velocities in its derivation, and against the use of plane shock theory on a cylindrical wave.

The rate of advance of the shock front is given by a coordinate r_s

$$\frac{d\,r_s}{d\,t} = -\frac{r_o\,c_o}{r_m}\sqrt{\frac{\mu}{\mu+1}}$$

Since $r_s = a$ when $t = 0$, integration gives

$$r_s = a + c_o\,t\sqrt{\frac{\mu}{\mu+1}} + r_o\,\frac{\mu}{\mu-1}\,\ell n\,\frac{r_o + a}{r_o + r_m}\,.$$

The rate of return of the reflected shock is given by

$$\frac{d\,r_r}{dt} = \frac{r_o\,c_o\left[2 + (\mu-1)\,\frac{r_m^2}{r_o^2}\right]}{\sqrt{\mu(\mu+1)}\;r_m}\,.$$

Now when $r_s = 0$, then $r_r = 0$, and we shall call the value of r_m existing at this time r_c (c = critical). Hence

$$r_r = -\frac{r_o}{(\mu-1)}\,\ell n\,\frac{r_m^2 - r_o^2}{r_c^2 - r_o^2} + \frac{2\,r_o}{(\mu-1)}\,\ell n\,\frac{r_m + r_o}{r_c + r_o}$$

$$+\frac{r_o}{2}\,\ell n\,\frac{r_m - r_o}{r_m + r_o} - \frac{r_o}{2}\,\ell n\,\frac{r_c - r_o}{r_c + r_o} + (r_m - r_c).$$

The pinch radius condition is that $r_r = r_m$. Further solution involves much algebra. One approximation to the algebra gave the rather simple result that for fairly strong shocks, $r \approx a/\mu^2$.

11-3 Plasma Flow Around Models. Techniques of schlieren and shadow graphing of the flow around models can give important information about the thermodynamical state of the gas in the vicinity of the model. Holden (33) observed what appeared to be bow shocks in the plasma's own light around a wedge airfoil. Following this lead, extensive attempts were made by Holden and Sims (34) to produce an overriding synchronized illumination (Chapter II) which would permit shadowgraphing of these shocks. Carefully developed light sources and timing circuits which should have accomplished this failed to disclose any sign of density

discontinuities. It was concluded that these discontinuities were too small to be seen by this technique.

11-4 Exploding Wires. For completeness, reference should be made to the work of Bennett (and many others - see Chace (127)) on exploding wires (128). Using many remarkable techniques, and especially interferometry coupled with mirror scanning, he finds that a large part of the phenomena previously supposed to be intrinsic in the wire's explosion are actually associated with arcs taking place in the gas surrounding the wire. In particular he finds evidence of prompt shock waves which suggest an origin in electron pressure.

11-5 Electrode Driven Shocks. Frequently we have observed one or more shock waves which originate at the metal end electrode at some time subsequent to the breakdown, often so late that the luminosity in the driver has almost wholly died away. These waves propagate outward through the driver tube and on into the expansion tube, and can sometimes be seen to interact appropriately with reflected shocks (when there are any). We believe that this is evidence for the existence of the postulated strong potential double layer accompanying the rarefaction wave. Such a layer, on colliding with the electrode, could induce a massive electron flow by field emission, and this flow could then generate a new electron driven shock wave in the dark, yet hot, plasma.

ACKNOWLEDGEMENT

The author is indebted to the many young people who have allied their interests with his during the past 15 years in pursuit of the knowledge embraced in the foregoing. They have been cited severally in the text, but a listing here is appropriate. He is also grateful for the friendly support and continuing advice of many persons, among them B. D. Fried, formerly of Space Technology Laboratories, O. Laporte of the University of Michigan, L. B. Loeb of the University of California, A. Kantrowitz formerly of Cornell University, and A. von Engel of Oxford University. No acknowledgement would be complete however without a full and frank admission of the vital importance of the support of the U. S. Office of Naval Research and the sympathy of its many scientific officers, without whose help this research would in cold fact have been impossible.

Participants (chronologically arranged)

J. S. Goldstein
R. J. Lee
B. E. Clotfelter
R. J. Atkinson
W. D. Compton
L. W. Marks
A. Kleider
H. Rose
T. Coleman
G. Seay
J. T. Teska
W. B. Edwards
L. D. Flansburg
W. R. Holden
F. W. Miller
G. Simmons
R. Sims
H. G. Hughes
M. Sakuntala
G. W. Paxton
R. J. Jeffries
L. W. Jones
S. D. Gardner
J. D. Hood

BIBLIOGRAPHY

1. A. Toeppler, Pogg. Am. 127, 556 (1866).
2. H. Hertz, Wied, Am. 19, 78 (1883).
3. W. Von Zahn, Wied. Am. 8, 675 (1879).
4. J. J. Thomson, Recent Researches in Electricity and Magnetism, Oxford, p. 115 (1893).
5. J. W. Beams, Phys. Rev. 36, 997 (1930).
6. L. B. Snoddy, J. R. Dietrich and J. W. Beams, Phys. Rev. 50, 469 (1936); 52, 739 (1937).
7. R. J. Strutt, Proc. Roy. Sco. 183, 26 (1944).
8. H. Zanstra, Proc. Roy. Soc. 186, 26 (1944).
9. R. J. Lee and R. G. Fowler, Phys. Rev. 81, 457 (1951); R. J. Lee, Thesis (M.S.), University of Oklahoma (1948); R. J. Lee, Proc. Okla. Acad. Sci. p. 62 (1948).
10. R. G. Fowler, J. S. Goldstein, and B. E. Clotfelter, Phys. Rev. 82, 879 (1951); B. E. Clotfelter, Thesis (M.S.), University of Oklahoma (1949); J. S. Goldstein, Thesis (M.S.), University of Oklahoma (1948).
11. W. D. Compton, Thesis (M.S.), University of Oklahoma (1951); R. G. Fowler, W. R. Atkinson, W. D. Compton, and R. J. Lee, Phys. Rev. 88, 137 (1950).
12. J. D. Craggs and W. Hopwood, Proc. Phys. Soc. 59, 755 (1947).
13. A. Erdelyi, Higher Trancendental Functions, (McGraw Hill).
14. On deposit in University of Oklahoma Library.
15. E. B. Turner, Phys. Fluids 4, 544 (1961).
16. U. S. Patent 2,900,550 (1959).
17. See for example A. C. Kolb, Phys. Rev. 112, 291 (1958); E. H. Cullington, et.al., AFCRL-RT-55-227 (1955).
18. F. Llewellyn Jones, Vacuum 3, 116 (1953).
19. L. O. Heflinger and S. B. Leonard, Phys. Fluids 4, 406 (1961).
20. J. S. Goldstein, M.S. Thesis, University of Oklahoma (1948); Phys. Rev. 82, 879 (1951).
21. V. Josephson, J. Ap. Phys. 29, 30 (1958).
22. A. Kolb, Magnetohydrodynamics. Stanford (1957); D. B. Edwards, Nature 196, 833 (1962); M. Clopeau, C.R. Acad. Sci. Paris 254, 213 (1962).
23. D. Bloxom, J. Ap. Phys. 29, 1128 (1958).
24. W. Bostick, Phys. Rev. 104, 299 (1956).
25. N. Kemp and H. E. Petschek, Phys. Fluids 2, 599 (1959).
26. R. Patrick, Phys. Fluids 2, 599 (1959).
27. R. Meyer, Plasma Acceleration (ed. Kash) Stanford (1960).
28. L. O. Heflinger and S. L. Leonard, Phys. Fluids 4, 406 (1961).
29. H. E. Petschek, P. H. Rose, H. S. Glick, A. Kane, A. Kantrowitz, J. Ap. Phys. 26, 83 (1955).

30. C. E. K. Mees, Theory of Photographic Process, (MacMillan, 1944).
31. H. G. MacPherson, JOSA 30, 189 (1940).
32. R. A. Alpher and D. R. White, Phys. Fluids 1, 452 (1958); A. Klein, Aerospace Laboratories, Los Angeles (private communication).
33. W. R. Holden, M.S. Thesis, University of Oklahoma Library (1957).
34. R. Sims, M. S. Thesis, University of Oklahoma Library (1958).
35. T. Welch, M. S. Thesis, University of Oklahoma Library (1963).
36. M. C. Selby, NBS Circular 481 (1949).
37. W. Atkinson and W. R. Holden, ONR Report, Aug. 15, 1954.
38. S. C. Lin, E. L. Resler and A. Kantrowitz, J. Appl. Phys. 26, 95 (1955).
39. E. Turner, Space Technology Laboratories, Los Angeles (Private communication).
40. B. E. Clotfelter, Ph.D. Diss. 1953, University of Oklahoma Library.
41. M. Sakuntala, B. E. Clotfelter, W. B. Edwards and R. G. Fowler, J. Appl. Phys. 30, 1669 (1959); M. Sakuntala, A. von Engel, and R. G. Fowler, Phys. Rev. 118, 1459 (1960); M. Sakuntala and A. von Engel, J.Elect. Control.13, 13 (1962).
42. R. G. Fowler, and M. Sakuntala, J. Chem. Phys. 27, 824 (1957).
43. W. R. Atkinson, Ph.D. Diss, 1953, University of Oklahoma Library.
44. F. W. Geiger, C. W. Mautz, R. N. Hollyer and O. Laporte, University of Michigan Engineering Research Report Proj. M720-4 (1949).
45. Ieuan R. Jones, Report No. TDR-594(1208-01)TR-3, Physical Research Laboratory, Aerospace Corporation, Contract No. AF o4(647)-594, June 1961; R. M. Davies, "Stress Waves in Solids" Surveys in Mechanics. Eds. G. K. Batchelor and R. M. Davies. Cambridge: Cambridge University Press, 1956.
46. M. Knoll, Materials and Processes of Electron Devices, Springer (1959).
47. R. J. Lee, Phys. Rev. 100, 1234 (1955).
48. P. T. Smith, Phys. Rev. 36, 1193 (1930).
49. R. G. Fowler, Proc. Phys. Soc. Lond. 80, 620 (1962).
50. J. S. Townsend, Electrons in Gases, Hutchison (1947).
51. A. von Engel, Ionized Gases, p. 219, Oxford (1955).
52. R. J. Bickerton and A. von Engel, Proc. Phys. Soc. Lond. 69, 468 (1956).
53. G. Cillie, M.N.R.A.S. 92, 820 (1931/2).
54. L. D. Flansburg, M.S. Thesis, University of Oklahoma Library (1957).
55. S. C. Brown, Basic Data of Plasma Physics, MIT (USA).
56. M. L. Goldman, Report on file in University of Oklahoma Library (1962).
57. A. Kleider, M. S. Thesis, University of Oklahoma Library(1952).
58. T. Coleman, M.S. Thesis, University of Oklahoma Library (1952).
59. G. E. Seay, M. S. Thesis, University of Oklahoma Library(1953).
60. R. J. Lee, M.S. Thesis, University of Oklahoma Library (1949).
61. B. E. Clotfelter, Ph.D. Thesis, University of Oklahoma Library (1953).
62. R. J. Atkinson, Ph.D. Thesis, University of Oklahoma Library (1953).

63. R. G. Fowler, and G. E. Seay, Proc. Okla. Acad. Sci. 35, 111 (1954).
64. E. G. Harris, NNL Report ASTIA 1117 535 (1956).
65. L. D. Flansburg, M.S. Thesis, University of Oklahoma Library (1957).
66. G. W. Paxton, Private Communication.
67. H. G. Hughes, M. S. Thesis, University of Oklahoma Library(1933).
68. F. Clauser, Plasma Dynamics, p. 16, (Addison Wesley (1961)).
69. K. T. Compton, Phys. Rev. 22, 333 (1923).
70. E. B. Turner and R. G. Fowler, Phys. Fluids 4, 544 (1961).
71. V. Josephson and R. H. Hales, Phys. Fluids 4, 373 (1961).
72. L. O. Heflinger and S. L. Leonard, Phys. Fluids 4, 406 (1961).
73. L. Spitzer, Physics of Fully Ionized Gases, Interscience (1956).
74. A. M. Cravath, Phys. Rev. 36, 248 (1930).
75. R. G. Fowler and B. D. Fried, Phys. of Fluids 4, 767 (1961).
76. H. D. Weymann, Phys. Fluids 4, 1573 (1961).
77. R. A. Jeffries, Proc. Okla. Acad. Sci. 41, 127 (1961);R. A. Jeffries, (M.S.) Thesis, University of Oklahoma Library (1961).
78. G. R. Burbidge, Ap. J. 127, 49 (1958).
79. S. B. Pikel'ner, Astr. J. SSSR, 33, 785 (1956).
80. O. Theimer, (private communication).
81. V.F.J. Schonland, Handbuch der Physik, Vol. XXII, 576 (1956).
82. L. B. Loeb, Handbuch der Physik, Vol. XXII, 445 (1956).
83. R. G. Westberg, Phys. Rev. 114, 1 (1959).
84. R. G. Fowler and J. D. Hood, Phys. Rev. 128, 991 (1962).
85. G. W. Paxton, and R. G. Fowler, Phys. Rev. 128, 993 (1962).
86. H. J. White, Phys. Rev. 46, 99 (1934).
87. L.B. Loeb, R. G. Westberg, and H. C. Huang, Phys. Rev. 123, 43 (1961).
88. B. E. Clotfelter, M.S. Thesis, University of Oklahoma Library (1949).
89. R. Hollyer, A. Hunting, O. Laporte, E. Schwarcz, and E. Turner, Phys. Rev. 87, 911 (1952).
90. G. E. Seay, L. B. Seely and R. G. Fowler, J. Ap. Phys. 32, 2439 (1961).
91. G. Charatis, and T. R. Wilkerson, Phys. Fluids (1963).
92. P. Teska, M.S. Thesis, University of Oklahoma Library (1955).
93. J. Holtsmark, Phys. Zeits 20, 162 (1919); 25, 73 (1924).
94. H. Rausch von Traubenberg, Phys. Zeits, 31, 958 (1950).
95. W. Finkelnberg, Z. Physik 70, 375 (1931).
96. S. Verweij, Publ. Astr. Inst. Amsterdam 5, (1936).
97. G. Jurgens, Z. Physik 134, 21 (1952).
98. H. Olsen and W. Huxford, Phys. Rev. 87, 922 (1952).
99. W. R. Atkinson, M.S. Thesis, University of Oklahoma Library (1950).
100. L. W. Marks, M.S. Thesis, University of Oklahoma Library(1951).
101. H. C. Rose, M.S. Thesis, University of Oklahoma Library(1952).
102. H. Griem, Z. Physik 137, 280 (1954).
103. L. Spitzer, Phys. Rev. 55, 699(1939); 56, 39 (1939); 58, 348 (1940).
104. G. Ecker, Z. Physik 148, 593 (1957).
105. O. Thiemer and H. Hoffman, Ap. J. 127, 477 (1958).

106. E. B. Turner, Ph.D. Diss, University of Michigan (1956).
107. H. Griem, A. Kolb, and K. Shen, Phys. Rev. 116, 4 (1959).
108. W. Finkelberg, Kontinuierliche Spektra, Berlin. Springer 1938.
109. R. G. Fowler, W. R. Atkinson, and L. W. Marks, Phys. Rev. 87, 966 (1952).
110. W. Lochte-Holtgreven, Naturwiss Rundschau January, 13 (1954).
111. L. Aller, Astrophysics, New York: Ronald 1953.
112. W. R. Atkinson and R. G. Fowler, Bull. Amer. Phys. Soc. 1, 98 (1956).
113. F. L. Miller, M.S. Thesis, University of Oklahoma Library (1957).
114. C. Kenty, Phys. Rev. 32, 624 (1928).
115. S. D. Gardner, M. S. Thesis, University of Oklahoma Library (1962).
116. S. Erkovich, Opt. Spect. 8, 162 (1960).
117. R. Courant and K. O. Friedrichs, Supersonic Flow and Shock Waves, New York. Interscience (1948).
118. R. E. Duff, Phys. Fluids 1, 546 (1958); 2, 207 (1959).
119. R. N. Hollyer, Jr., Ph.D. Diss., University of Michigan (1953).
120. A. Roshko, Phys. Fluids 3, 835 (1960).
121. R. G. Fowler, Pro. Phys. Soc. 68, 130 (1955).
122. R. G. Fowler, and L. W. Jones, J. App. Phys. (1963).
124. A. von Engel, and M. Steenbeck, Elektrische Gasentladungen, Vol. II, Berlin: Julius Springer, 1934.
125. M.I.T. Radar Series (1962).
126. M. Rosenbluth, LASL Report LA-1850; Stanford Press (1957).
127. W. G. Chace, Exploding Wires, (New York: Plenum 1959).
128. F. Bennett, Sci. Amer. 206, 103 (1962); Phys. Fluids 5, 891 (1962).

APPENDIX I

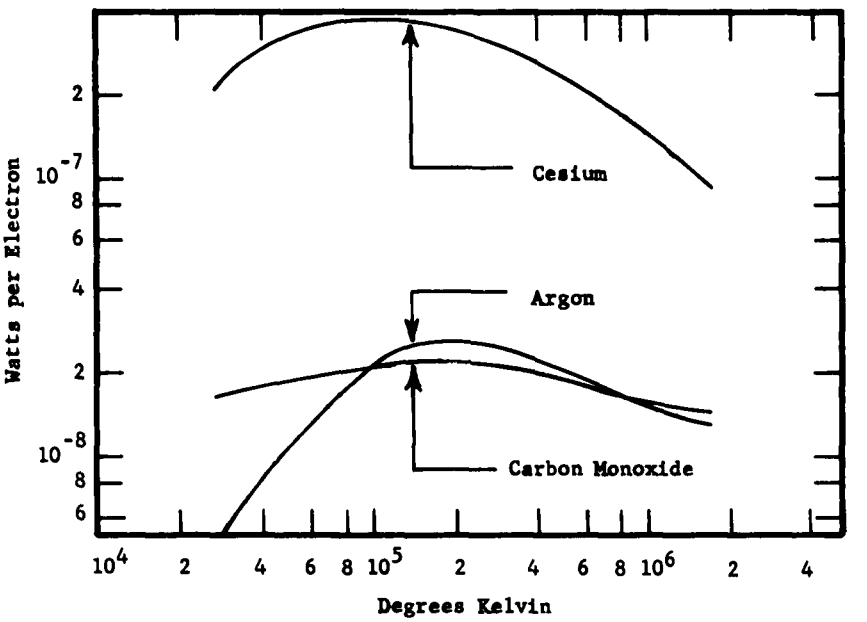
Watts per Electron
2
10^{-7}
8
6
4
2
10^{-8}
8
6
Cesium
Argon
Carbon Monoxide
10^4 2 4 6 8 10^5 2 4 6 8 10^6 2 4
Degrees Kelvin

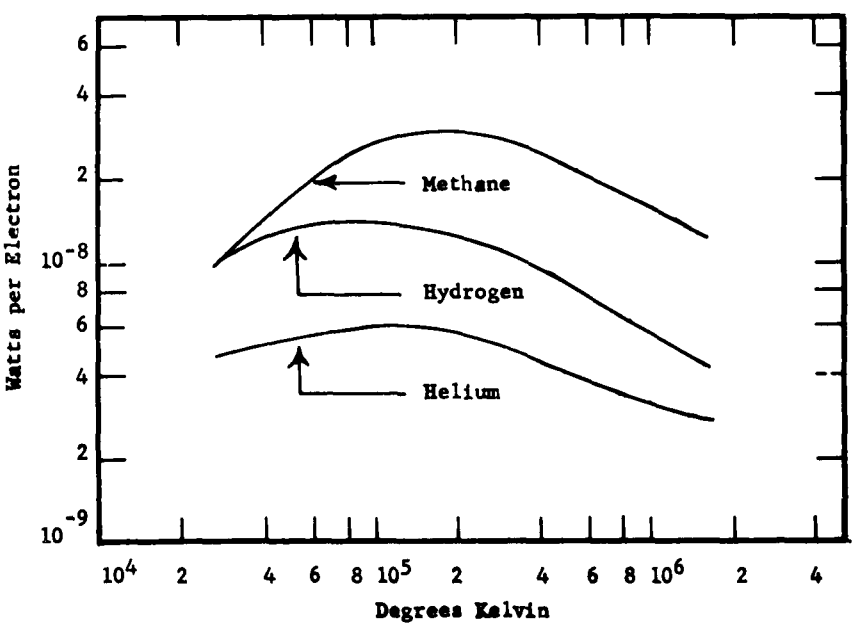
Watts per Electron
6
4
2
10^{-8}
8
6
4
2
10^{-9}
Methane
Hydrogen
Helium
10^4 2 4 6 8 10^5 2 4 6 8 10^6 2 4
Degrees Kelvin

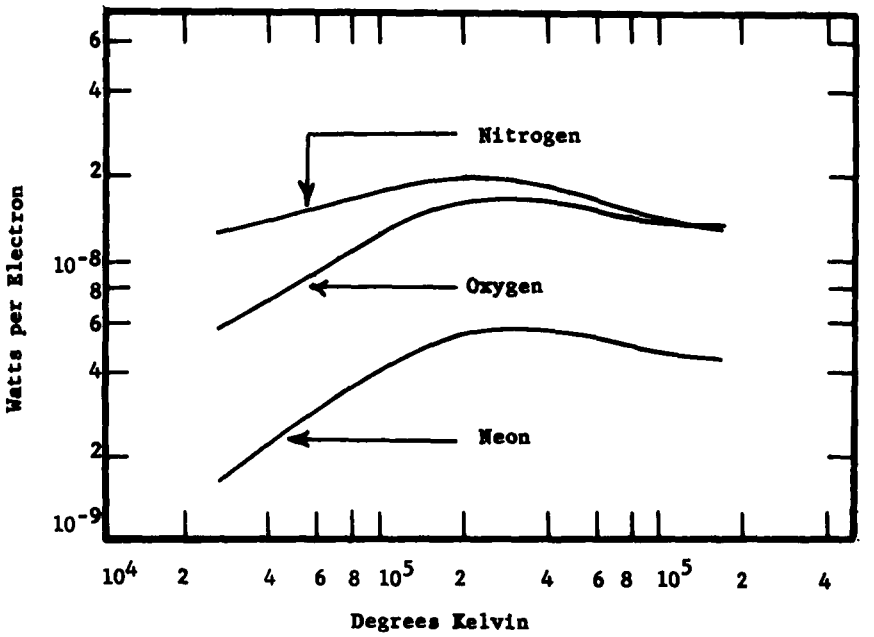
Nitrogen
Oxygen
Neon
Watts per Electron
Degrees Kelvin

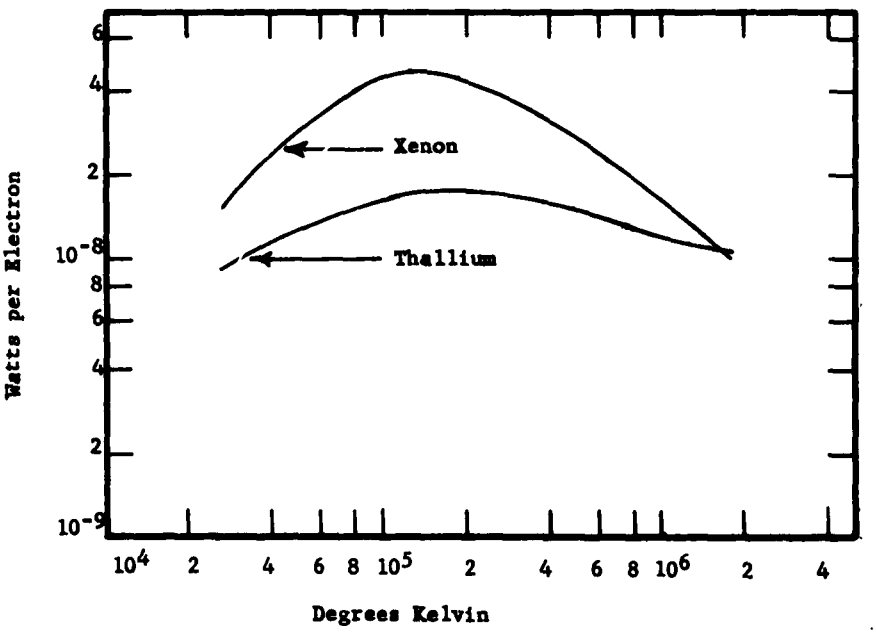
Xenon
Thallium
Watts per Electron
Degrees Kelvin

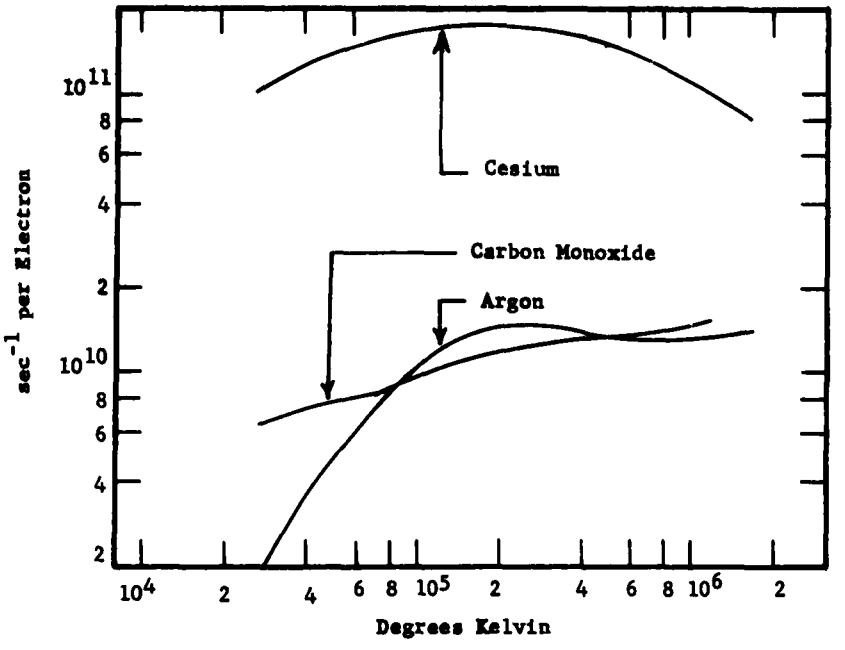
10^{11}
8
6
4
2
10^{10}
8
6
4
2
sec^{-1} per Electron
Cesium
Carbon Monoxide
Argon
10^4 2 4 6 8 10^5 2 4 6 8 10^6 2
Degrees Kelvin

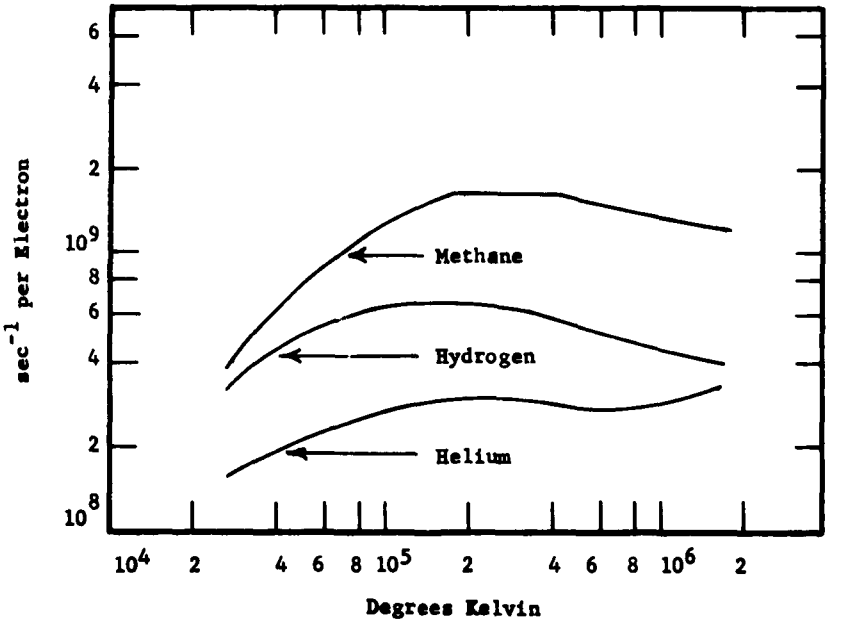
6
4
2
10^9
8
6
4
2
10^8
sec^{-1} per Electron
Methane
Hydrogen
Helium
10^4 2 4 6 8 10^5 2 4 6 8 10^6 2
Degrees Kelvin

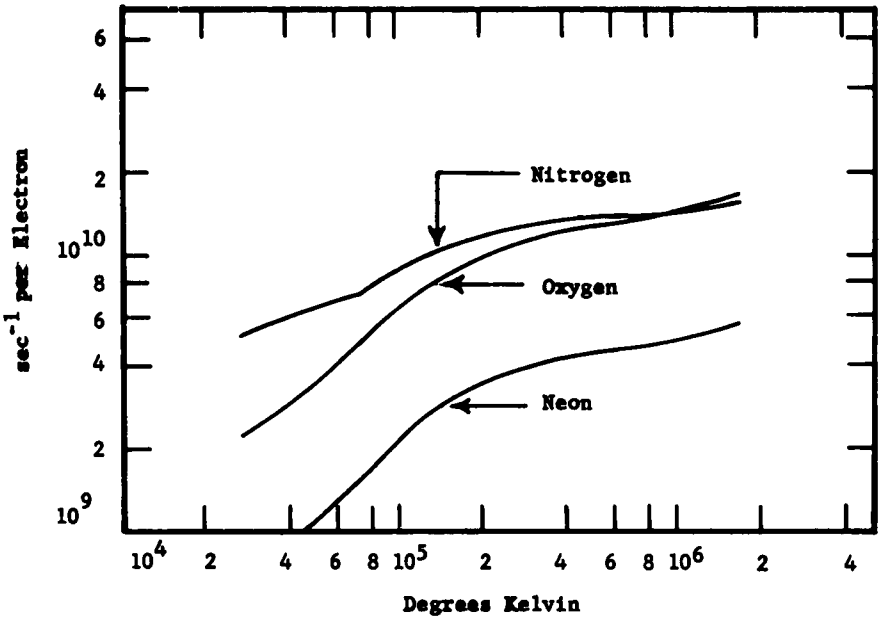
6
4
2
10^{10}
8
6
4
2
10^{9}
sec^{-1} per Electron
Nitrogen
Oxygen
Neon
10^4 2 4 6 8 10^5 2 4 6 8 10^6 2 4
Degrees Kelvin

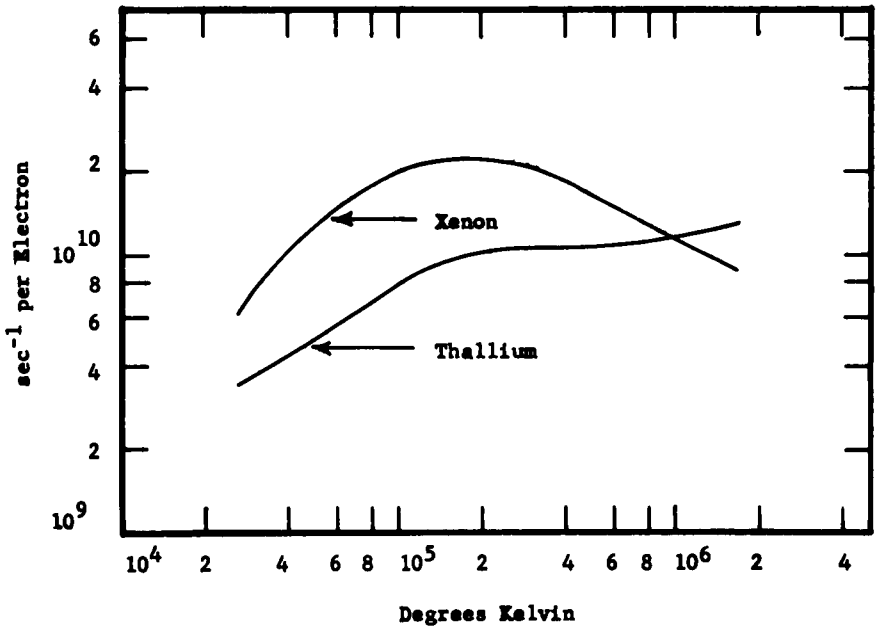
6
4
2
10^{10}
8
6
4
2
10^{9}
sec^{-1} per Electron
Xenon
Thallium
10^4 2 4 6 8 10^5 2 4 6 8 10^6 2 4
Degrees Kelvin

APPENDIX 2

LUMINOUS FRONT VELOCITIES u AND FLOW VELOCITIES u* IN HELIUM

Numbers in parenthesis beside the velocity u indicate either the position in cm at which measurement was made or the position range in cm over which average velocity was determined.

Pressure mm Hg	Potential Volts	u km/sec	u* km/sec
28.1	4680	2.8 (1.6-5.3)	2.2(10.1-11.5)	2.2
28.1	3020	2.1 (8.8)		1.8
28.1	1570	1.4 (3-11.5)		1.4
15.3	4680	3.6 (1.5-9.5)		3.4
15.3	4680	2.4 (9.5-18.5)		2.9
15.3	1420	2.0 (4.1)	1.4(8.8)	1.5
15.3	1710	2.1 (4.1)	1.6(8.8)	1.6
15.3	1990	2.2 (4.1)	1.7(8.8) 1.5(13.7)	1.6
15.3	2270	2.2 (4.1)	1.8(8.8) 1.6(13.7)	1.7
15.3	2570	2.3 (4.1)	1.9(8.8) 1.8(13.7)	1.8
15.3	2870	2.5 (4.1)	2.0(8.8) 1.9(13.7)	1.9
15.3	3170	2.6 (4.1)	2.1(8.8) 2.0(13.7)	2.1
15.3	3460	2.7 (4.1)	2.2(8.8) 2.1(13.7)	2.2
15.3	3780	2.9 (4.1)	2.3(8.8) 2.2(13.7)	2.3
15.3	4090	3.4 (4.1)	2.5(8.8) 2.3(13.7)	2.5
15.3	4390	3.7 (4.1)	2.8(8.8) 2.4(13.7)	2.7
15.3	4680	3.9 (4.1)	3.0(8.8) 2.5(13.7)	2.9
9.3	4680	4.5 (4.5-10.5)		4.5
9.3	4680	2.5 (6.5-14.5)		3.0
5.45	4680	5.0 (1.5-6.5)		3.7
1.6	4680	6.4 (2.5-6.5)	3.8(10.5-14.5)	4.4
1.6	3020	2.4 (7.5-10.5)		3.0
1.6	3020	4.0 (1.5-6.5)		3.8
7.6	565	1.5 (5.3)	1.1(14.9)	1.0
7.6	850	1.8 (5.3)	1.2(14.9)	1.3
7.6	1140	2.0 (5.3)	1.3(14.9)	1.5
7.6	1420	2.2 (5.3	1.5(14.9)	1.8
7.6	1710	2.4 (5.3)	1.6(14.9)	2.0
7.6	1990	2.6 (5.3	1.7(14.9)	2.2
7.6	2270	2.8 (5.3)	1.9(14.9)	2.5
7.6	2570	3.1 (5.3)	2.0(14.9)	2.7
7.6	2870	3.3 (5.3)	2.1(14.9)	2.9
7.6	3170	3.5 (5.3)	2.2(14.9)	3.1

Pressure mm Hg	Potential Volts	u km/sec		u* km/sec
7.6	3460 3.7 (5.3)	2.3(14.9)		3.3
7.6	3780 3.9 (5.3)	2.4(14.9)		3.5
7.6	4090 4.1 (5.3)	2.5(14.9)		3.8
7.6	4390 4.3 (5.3)	2.6(14.9)		4.0
7.6	4680 4.6 (5.3)	2.7(14.9)		4.2
7.6	4980 4.8 (5.3)	2.7(14.9)		4.4
29.5	4680 2.8 (4.1)	2.4(8.8)	2.1(13.7)	2.1
29.5	4180 2.4 (4.1)	2.2(8.8)	2.0(13.7)	2.0
29.5	3670 2.0 (4.1)	2.2(8.8)	2.0(13.7)	1.9
29.5	3060 1.8 (4.1)	2.1(8.8)	1.7(13.7)	1.7
29.5	2450 1.6 (4.1)	2.0(8.8)	1.5(13.7)	1.5
29.5	1860 1.6 (4.1)	1.7(8.8)	1.3(13.7)	1.4
29.5	1250 1.6 (4.1)	1.6(8.8)		1.2
51.3	3020 1.4 (15)			1.6
51.3	4680 1.6 (16.2)			1.9
61	3020 1.2 (15)			1.6
61	4680 1.6 (16.2)			1.8
91	4950 1.8 (4.1)	1.8(8.8)	1.7(13.7)	1.8
91	4390 1.8 (4.1)	1.9(8.8)	1.4(13.7)	1.7
91	3810 1.5 (4.1)	1.5(8.8)	1.3(13.7)	1.5
91	3160 1.4 (4.1)	1.5(8.8)	1.0(13.7)	1.4
91	2510 1.2 (4.1)	1.2(8.8)	.9(13.7)	.9

LUMINOUS FRONT VELOCITIES u AND FLOW VELOCITIES u* IN XENON

Numbers in parenthesis beside the velocity u indicate either the position in cm at which measurement was made or the position range in cm over which average velocity was determined.

Pressure mm Hg	Potential Volts	u km/sec	u* km/sec
19.5	3020	.33 (1.5-8.5)	.38
15.7	3020	.32 (8.5-11.5)	.37
9.2	3020	.43 (2.5-7.5)	.42
5.5	3020	.48 (1.5-9.5)	.48
2.9	3020	.57 (1.5-7.5)	.51
1.6	4630	.60 (3.5-8.5)	.68
3.2	4840	.67 (4.1)	.61
3.2	4300	.57 (4.1)	.59
3.2	3750	.61 (4.1)	.56
3.2	3070	.56 (4.1)	.53
3.2	2450	.56 (4.1)	.48
3.2	1850	.45 (4.1)	.42

Pressure mm Hg	Potential Volts	u km/sec		u* km/sec
1.3	4820	.88 (4.1)		.64
1.3	4270	.72 (4.1)		.60
1.3	3650	.71 (4.1)		.57
1.3	3050	.67 (4.1)		.53
1.3	2450	.66 (4.1)		.49
1.3	1850	.27 (4.1)		.44
1.3	1220	.47 (4.1)		.36
29.5	4950	.51 (4.1)	.53 (8.8)	.40
29.5	4450	.40 (4.1)	.43 (8.8)	.37
29.5	3840	.38 (4.1)	.32 (8.8)	.36
29.5	3160	.39 (4.1)	.32 (8.8)	.35
29.5	2540	.33 (4.1)	.32 (8.8)	.33

LUMINOUS FRONT VELOCITIES u AND FLOW VELOCITIES u^* IN NEON

Pressure mm Hg	Potential Volts	u in km/sec at 4.1 cm	8.8 cm	13.7 cm	u^* in km/sec
.94	4330	3.1	1.7		1.2
.94	3780	2.8	1.5		1.1
.94	3140	2.3	1.0		.93
.94	2520	1.7			.76
.94	1910	1.5			.58
2.0	4670		1.5	1.1	1.4
2.0	4270	1.8	1.4	1.0	1.3
2.0	3680	1.7	1.3		1.1
2.0	3050	1.6	1.1		1.0
2.0	2420	1.4			.90
5.35	4920	1.6	1.4	1.2	1.3
5.35	4320	1.5	1.3	1.1	1.2
5.35	3780	1.4	1.2	.92	1.1
5.35	3070	1.3	1.2	.85	1.1
5.35	2520	1.1	1.0		.91
5.35	1880	.91	.83		.75
5.35	1220	.81			.66
8.3	4770	1.5	1.4	1.1	1.3
8.3	4380	1.4	1.3	1.1	1.3
8.3	3780	1.3	1.2		1.1
8.3	3160	1.1	1.0	.81	1.0
8.3	2570	1.0	.75		.86
8.3	1990	.84			.74
12	4890	1.5	1.3	1.1	1.3
12	4370		1.2	1.0	1.2
12	3780	1.1	1.1		1.1

Pressure mm Hg	Potential Volts	u in km/sec at 4.1 cm	8.8 cm	13.7 cm	u* in km/sec
12	3140	.87	.79		.85
12	2490	.87	.72		.73
12	1880	.74	.53		.7
17.7	4950	1.2	1.1	.90	1.1
17.7	4420	1.1	1.1	.78	1.0
17.7	3840	.93	.86		.87
17.7	3160	.87	.70	.72	.79
17.7	2540	.80	.64		.70
17.7	1880	.67	.58		.63
17.7	1250	.72			.59
27.6	4770	1.0	.88	.81	.90
27.6	4330	1.0	.79		.85
27.6	3710	.88	.73		.79
27.6	3080	.83	.75		.73
27.6	2480	.74	.72		.67
27.6	1850	.63	.70		.60
52	4780	.90	.88		.80
52	4330	.80	.86		.76
52	3720	.73	.77		.71
52	3140	.67	.75		.67
52	2480	.64	.61		.63
52	1880	.55	.56		.59
92.5	4800	.80	.72		.70
92.5	4090	.71	.63		.66
92.5	3320	.64	.56		.60
92.5	2570	.58	.53		.54
92.5	2130	.53	.48		.49
92.5	1420	.38			.42
155.5	4930	.66	.62		.61
155.5	4380	.68	.63		.58
155.5	3750	.54	.54		.53
155.5	3110	.56	.52		.50
155.5	2500	.43			.45
155.5	1990	.32			.37

LUMINOUS FRONT VELOCITIES u AND FLOW VELOCITIES u* IN ARGON

Pressure mm Hg	Potential Volts	u in km/sec at 4.1 cm	8.8 cm	13.7 cm	u* in km/sec
1.1	4680	1.9	1.5		1.2
1.1	4090	1.7	1.2	1.1	1.1
1.1	3460	1.5	1.3		1.0
1.1	2860	1.3	1.0		.91
1.1	2270	1.0	1.0		.81

Pressure mm Hg	Potential Volts	u in km/sec at 4.1 cm	8.8 cm	13.7 cm	u^* in km/sec
1.1	1710	1.2			.66
3.1	4740	1.5	1.2	.93	1.2
3.1	4270	1.3	1.2	.86	1.1
3.1	3710	1.2	1.1	.86	1.0
3.1	3050	1.2	1.0	.75	.88
3.1	2450	1.0	.89		.78
3.1	1820	.81	.70		.66
8.7	4830	1.05	1.06	.95	.85
8.7	4390	.97	.99	.85	.82
8.7	3780	.82	.93	.71	.77
8.7	3130	.80	.74	.79	.72
8.7	2480	.76	.66		.64
8.7	1880	.76	.65		.57
8.7	1240	.69	.51		.50
8.7	940	.53			.47
28.4	4740	.82	.86	.58	.72
28.4	4330	.75	.76	.62	.70
28.4	3720	.71	.73	.52	.66
28.4	3080	.66	.66	.57	.61
28.4	2520	.69	.56	.61	.56
28.4	1880	.63	.41		.49

APPENDIX 3

BALMER CONTINUUM PHOTON EMISSION/CC/SEC/CM WAVELENGTH

(Multiply all tabulated values by 10^{23})

Voltage = 5 KV (Observation point 2 cm above electrode)

	Pressure						
λ	0.48 mm	0.85 mm	1.95 mm	3.2 mm	5.3 mm	8.0 mm	11.0 mm
5500	3.7	3.1	5.1	9.6	15	21	32
4600	6.1	6.4	11	5.0	16	21	25
4150	16	16	16	26	41	84	100
3700	31	30	23	35	55	100	80
3300	9.3	14	17	42	67	104	100
3000	18	8.6	16	29	53	80	72
2800	8.3	7.3	11	26	37	48	52
2600	5.5	4.6	6.2	8.0	22	25	24
2400	2.7	2.1	2.6	4.8	8.1	11	11

Voltage = 2 KV (Observation point 6 cm above electrode)

	Pressure						
λ	0.48 mm	0.85 mm	1.95 mm	3.2 mm	5.3 mm	8.0 mm	11.0 mm
5500			0.91	1.6	1.8		
4600			1.0	1.4	1.7		
4150			2.1	3.2	4.9		
3700			5.0	7.9	8.9		
3300			4.0	5.4	5.5		
3000			2.7	3.9	4.5		
2800			1.7	2.6	2.7		
2600			0.96	1.3	1.5		
2400			0.36	0.39	0.80		

Voltage = 3 KV (Observation point 6 cm above electrode)

	Pressure						
λ	0.48 mm	0.85 mm	1.95 mm	3.2 mm	5.3 mm	8.0 mm	11.0 mm
5500	1.1	1.9	3.4	5.4	6.6	8.8	7.2
4600	2.9	2.0	3.0	4.8	6.7	8.8	8.4
4150	3.0	2.7	7.6	13	23	33	29

Voltage = 3 KV (Observation point 6 cm above electrode)

	Pressure						
λ	0.48 mm	0.85 mm	1.95 mm	3.2 mm	5.3 mm	8.0 mm	11.0 mm
3700	4.0	5.1	14	21	32	38	40
3300	3.2	3.5	12	18	25	26	34
3000	3.6	3.2	8.2	13	16	23	17
2800	1.2	1.8	5.6	8.3	11	18	13
2600	0.80	1.1	2.5	4.1	5.5	6.4	7.2
2400	0.39	0.38	1.2	1.2	2.8	3.3	2.4

Voltage = 4 KV (Observation point 6 cm above electrode)

	Pressure						
λ	0.48 mm	0.85 mm	1.95 mm	3.2 mm	5.3 mm	8.0 mm	11.0 mm
5500	2.0	3.0	5.4	10	17	20	23
4600	11	8.5	5.6	11	15	22	28
4150	11	7.3	13	29	49	84	80
3700	12	11	21	42	62	120	92
3300	5.7	6.9	17	34	56	72	88
3000	6.5	7.1	13	26	40	60	56
2800	2.4	3.3	8.7	17	24	35	35
2600	1.2	2.0	4.9	9.0	12	17	24
2400	0.52	0.83	1.7	3.5	5.6	5.2	6

Voltage = 5 KV (Observation Point 6 cm above electrode)

	Pressure						
λ	0.48 mm	0.85 mm	1.95 mm	3.2 mm	5.3 mm	8.0 mm	11.0 mm
5500	2.2	3.9	6.3	16	27	30	35
4600	15	11	9.6	15	27	40	27
4150	17	8.3	17	43	70	120	139
3700	16	13	24	56	92	144	160
3300	9.2	9.2	21	51	85	128	136
3000	7.7	9.1	16	38	62	96	96
2800	3.2	4.6	11	25	49	68	56
2600	1.7	2.8	5.1	12	21	28	33
2400	0.63	1.2	2.3	3.8	7.6	12	12

ION FRACTION FOR USE WITH ABOVE TABLES

	For Observation Point 6 cm Above Electrode			
Pressure	2 KV	3 KV	4 KV	5 KV
0.45	0.084	0.112	0.144	0.170
0.85	0.105	0.135	0.165	0.200

APPENDIX 3

For Observation Point 6 cm Above Electrode				
Pressure	2 KV	3 KV	4 KV	5 KV
1.95	0.127	0.171	0.210	0.247
3.20	0.142	0.196	0.240	0.288
5.20	0.150	0.216	0.270	0.325
8.00	0.148	0.225	0.290	0.355
11.00	0.140	0.220	0.300	0.370

For Observation Point 2 cm Above Electrode				
Pressure	2 KV	3 KV	4 KV	5 KV
0.45	0.046	0.066	0.083	0.105
0.85	0.051	0.072	0.096	0.11
1.95	0.060	0.083	0.11	0.13
3.20	0.068	0.093	0.12	0.14
5.20	0.077	0.103	0.13	0.16
8.0	0.086	0.117	0.145	0.17
11.0	0.093	0.126	0.16	0.19

Shock Velocities				
Pressure	2 KV	3 KV	4 KV	5 KV
0.45	1.8×10^6	2.1×10^6	2.4×10^6	2.6×10^6
0.85	1.4×10^6	1.65×10^6	1.85×10^6	2.0×10^6
1.95	1.05×10^6	1.2×10^6	1.35×10^6	1.45×10^6
3.20	3.4×10^5	1.0×10^6	1.10×10^6	1.2×10^6
5.20	7.0×10^5	8.2×10^5	9.2×10^5	1.0×10^6
8.00	6.0×10^5	6.9×10^5	7.8×10^5	8.4×10^5
11.0	5.2×10^5	6.2×10^5	6.8×10^5	7.4×10^5

APPENDIX 4

ENERGY REQUIREMENTS OF GASES AT 1 MM HG

Gas	Energy for Full Ionization	Power Flux into a Fully Ionizing Mach 1 Shock**
A	0.09 joules/cc	2.8×10^3 watts/cm^2
He	0.14 "	1.35×10^4 "
H*	0.09 "	1.15×10^4 "
Ne	0.12 "	5.2×10^3 "
N*	0.11 "	3.7×10^3 "
O*	0.09 "	2.8×10^3 "
Xe	0.07 "	1.05×10^3 "

* ionization plus dissociation

** N.B. It is not implied that a Mach 1 shock will produce full ionization.